

**Theory of electromagnetic decay of nuclei and finding
lifetime of excited state using fast-timing technique**

MS-Thesis Report

submitted in partial fulfillment of the requirements
for the award of the dual degree of

Bachelor of Science-Master of Science

in

PHYSICS

submitted by

Sangram Keshari Patro

Roll no: P0191340

Under the Guidance of

Dr. Rudrajyoti Palit
(TIFR,Mumbai)

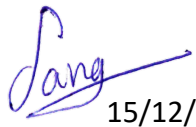


Department of Physical Sciences
Centre for Excellence in Basic Sciences
(UM-DAE-CBS) Mumbai-400 098
December 2023



Certificate

This is to certify that CEBS student **Sangram Keshari Patro** has undertaken project work from 15/06/23 to 15/12/23 under the guidance of **Dr. Rudrajyoti Palit** and affiliation: **Tata Institute of Fundamental Research, Mumbai**. This submitted project report titled **Theory of electromagnetic decay of nuclei and finding lifetime of excited state using fast-timing technique** is towards the academic requirements of the M.Sc. program's 9th Semester Project Course at UM-DAE CEBS.


15/12/23

Sangram Keshari Patro

Name & Signature of Student with Date



R. Palit 21/12/2023

Name & Signature of Advisor (s) with Date

Acknowledgment

I seize this moment to express my heartfelt gratitude to Prof. Rudrajyoti Palit, whose patient guidance has been instrumental in making this project an immensely enriching learning journey. I extend my sincere thanks to him for introducing me to this captivating field of study, sparking not only interest but also a profound shift in my perspective towards various other areas of interest.

In addition, I would like to acknowledge and appreciate the valuable contributions of Vishal Malik, Piku Dey, Dr. Ananya Kundu, and Biswajit Das, each of whom played a crucial role in different facets of the project. Their support and insights have been invaluable.

Lastly, my gratitude extends to all those who, directly or indirectly, contributed to the completion of this project. Your assistance and encouragement have been truly appreciated, and I am thankful for the collaborative effort that made this endeavor possible.

Abstract

The wave functions describing nuclear states are commonly defined as the eigenvectors of a Hamiltonian, assuming nuclear interactions. Electromagnetic and weak interactions are then treated as perturbations, leading to transitions between different states. Analyzing the rates of these transitions provides valuable insights into the properties of the atomic nucleus. Different types of bulk properties of nuclei are discussed. The theory of Multipole expansion of the electromagnetic fields is discussed with special focus on selection rules. Angular distribution of multipole radiation is also discussed. Dipole and quadrupole radiation patterns for pure (l, m) multipoles are explained.

The fundamental objective of nuclear spectroscopy is to detect and study excited states while quantifying their characteristics. Among these properties, the half-lives of excited nuclear states serve as a crucial metric, offering valuable information on transition probabilities. This, in turn, facilitates a direct understanding of nuclear structure and serves as a rigorous assessment of nuclear models. The work delves into various direct measurement techniques, addressing half-life ranges from picoseconds to microseconds. It involves a comprehensive comparison of the applicability, accuracy, and reliability of different experimental methods. The primary focus of this study is on the measurement of state lifetimes through fast-timing techniques utilizing gamma-ray detectors.

Contents

1	Introduction	5
2	Nuclear Transition Matrix Element	5
2.1	Transition probability and line width	5
2.2	Branching Ratio	6
2.3	Transition Matrix Element	7
3	Bulk Properties of Nuclei	8
3.1	Nuclear Shape and Electromagnetic Moments	8
3.1.1	Multipole expansion of charge density	8
3.1.2	Electric quadrupole and hexadecapole moments	9
3.1.3	Magnetic moments	9
3.2	Magnetic Dipole Moment of Odd Nuclei	11
3.2.1	Single-particle model	11
3.2.2	Schmidt value	12
3.2.3	Corrections to single-particle model	13
3.2.4	Ground State Spin and Isospin	13
4	Electromagnetic Transition	13
4.1	The spin of the photon	13
4.2	Coupling to electromagnetic fields	15
4.3	Multipole expansion of the electromagnetic fields	17
4.3.1	Selection rules	19
4.3.2	$E\lambda$ -transition	20
4.3.3	$M\lambda$ -transition	21
5	Angular Distribution of Multipole Radiation	23
5.1	Fields and Radiation of a Localized Oscillating Source	23
5.2	Multipole Expansion of the Electromagnetic Fields	26
5.3	Angular Distribution of Multipole Radiation	30
6	Lifetimes of excited states	32
6.1	Historical Background	33
6.2	Experimental Methods of Measuring Lifetimes of Isomeric States	34
6.3	Delayed Coincidence Techniques	35
6.3.1	Centroid Shift Method	35
6.3.2	Slope method	37
6.3.3	Moment relations	38
6.3.4	Numerical Convolution	39
6.3.5	Comparison and Applications	40
6.4	Delayed coincidence method	41
6.5	Experimental setup and Data acquisition system	43
7	Observations and Results	45
7.1	Lifetime Measurement	45
7.2	Common Timing Electronic Modules	49

8	Summary and Conclusion	50
A	Appendix	53
A.1	Transition Probability in Time-Dependent Perturbation Theory	53
A.2	Parity and Angular Momentum	55
A.3	Unitary Operator: symmetries and conservation laws	55
A.3.1	Rotational symmetry	55
A.4	Code to Fit the all the data points with a convoluted function of a exponential decay	57
A.5	Code to Fit the convoluted part with a exponential function by removing gaussian part data points	58

1 Introduction

We will study nuclear spectroscopic properties that can be extracted from experiments using electromagnetic probes. We assume here that the nucleus is already excited in some initial state and that it decays to a final state in the same nucleus through electromagnetic radiation by emitting a photon. In nuclear electromagnetic decays the radiation, and the photon itself, is called "**gamma**". The transition is caused by the interaction of the nucleus with an external electromagnetic field. We can consider the nucleons are point particles with a magnetic dipole moment. The charge distribution couples with the external field, causing "**electric**" transitions. And the magnetism generated by current loops due to proton orbital motion interacts with the intrinsic magnetism of each nucleon causing "**magnetic**" transitions. Electromagnetic transitions form the dominant mode of decay for low-lying excited states in nuclei, particularly for the light ones because nucleon emission is not possible until the excitation energy is above nucleon separation energies.

2 Nuclear Transition Matrix Element

2.1 Transition probability and line width

If we have a sample of N radioactive nuclei, the number of decays taking place in a given time interval is therefore proportional to $N(t)$.

$$\frac{dN}{dt} = -\mathcal{W}N(t) \implies N(t) = N_0 e^{-\mathcal{W}t}$$

Hence half-life, $T_{1/2} = \frac{\ln 2}{\mathcal{W}}$. The lifetime, or mean life, of an excited state is the average amount of time it takes for a radioactive nucleus to decay.

$$\langle T \rangle = \frac{\int_0^\infty t e^{-\mathcal{W}t} dt}{\int_0^\infty e^{-\mathcal{W}t} dt} = \frac{1}{\mathcal{W}} = \frac{T_{1/2}}{0.693} \implies T_{1/2} = 0.693 \times \langle T \rangle \quad (1)$$

It is impossible to predict whether the nucleus at higher excited state will decay or not. Hence, there is an uncertainty in time $\Delta t = \langle T \rangle$ associated with the existence of the excited state. Because of this we can't measure energy with infinite precision according to uncertainty principle. If we carry out the energy measurement for N nuclei in the same excited state having energy E_i then

$$\langle E \rangle = \frac{1}{N} \sum_{i=1}^n E_i \text{ and } \Gamma = \left\{ \frac{1}{N} \sum_{i=1}^n (E_i^2 - \langle E \rangle^2) \right\}^{\frac{1}{2}}$$

where Γ is known as the "**natural line width of a state**" and as we know

$$\Delta E \Delta t \sim \hbar \implies \Gamma \sim \frac{\hbar}{\langle T \rangle} = \hbar \mathcal{W} \text{ (from (1))} \quad (2)$$

Γ can be related to the probability of finding the excited state at a specific energy E . For a stationary state, the time-dependent wave function may be separated into a product of spatial and temporal parts,

$$(r, t) = \psi(r)e^{-iEt/\hbar}$$

The decay constant or the transition probability \mathcal{W} may be defined in the following way:

$$|\Psi(\mathbf{r}, t)|^2 = |\Psi(\mathbf{r}, t=0)|^2 e^{-\mathcal{W}t} \quad (3)$$

For decaying excited state to carry a separation we can change E to a complex quantity i.e. $E \rightarrow \langle E \rangle - \frac{1}{2}i\hbar\mathcal{W}$. So, the wave function becomes:

$$\Psi(\mathbf{r}, t) = \psi(\mathbf{r}) e^{-i\langle E \rangle t/\hbar - \mathcal{W}t/2} \quad (4)$$

It also satisfies (3). Now we write the wave function as a superposition of components having different energies (i.e. the energy spread around the excited energy level with energy E) as

$$\Psi(\mathbf{r}, t) = \psi(\mathbf{r}) \int a(E) e^{-iEt/\hbar} dE \quad (5)$$

where $a(E)$ is the probability amplitude for finding the state at energy E . Comparing (4) and (5) we have:

$$e^{-\mathcal{W}t/2} = \int a(E) e^{-i(E-\langle E \rangle)t/\hbar} dE \text{ (i.e. } e^{-\mathcal{W}t/2} \text{ is the Fourier transform of } a(E).)$$

By taking the inverse Fourier transform we have:

$$a(E) = \frac{1}{2\pi\hbar} \int_0^\infty e^{i(E-\langle E \rangle)/\hbar - W/2} dt = \frac{i}{2\pi} \frac{1}{(E - \langle E \rangle) + i\frac{1}{2}\hbar\mathcal{W}}$$

So, using (2), the probability for finding the excited state at energy E is given by the absolute square of the amplitude,

$$|a(E)|^2 = \frac{1}{4\pi^2} \frac{1}{(E - \langle E \rangle)^2 + (\frac{1}{2}\Gamma)^2} \quad (6)$$

The shape of such a distribution is **Lorentzian** and the width Γ may be interpreted as the full width at half maximum (FWHM) of such a distribution. There is no question of instrumental uncertainty occurring here. So, the width is the “**natural line width**” of the distribution in energy of the excited state.

2.2 Branching Ratio

A given excited state can decay to several final states. If the transition probability to the i th final state is $\mathcal{W}(i)$, the total transition probability for the initial state is the sum of the probabilities to all final states,

$$\mathcal{W} = \sum_i \mathcal{W}(i) \quad (7)$$

Similarly, the total width Γ is the sum of all the partial widths, $\Gamma = \sum_i \Gamma(i)$. From (1) and (7) we have:

$$\frac{1}{T_{1/2}} = \sum_i \frac{1}{T_{1/2}(i)} \quad (8)$$

The branching ratio gives the partial transition probability to a particular final state as a fraction of the total from a specific initial state.

$\pi^0 \rightarrow 2\gamma$	98.8%	$mass = 264m_e = 135.0 \text{ MeV} / c^2$
$\pi^0 \rightarrow e^- + e^+ + \gamma$	1.2%	

Figure 1: The mean lifetime of a π^0 -meson is 8.4×10^{-17} s and decays 98.8 of the time to two γ -rays, 1.2 of the time to a γ -ray together with an electron-positron pair.

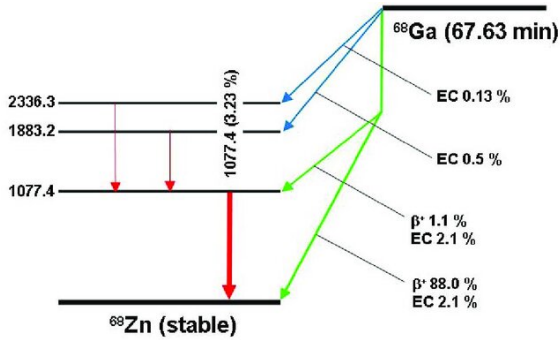


Figure 2: Decay scheme of ^{68}Ga to stable ^{68}Zn . Branching ratios of transition from ground state of ^{68}Ga to all states of ^{68}Zn is shown here.

2.3 Transition Matrix Element

The transition probability is proportional to the square of the nuclear matrix element,

$$\mathcal{M}_{fi}(M_f, M_i) = \langle J_f M_f \xi | O_{\lambda\mu} | J_i M_i \zeta \rangle \quad (9)$$

where $|J_i M_i \zeta\rangle$ and $|J_f M_f \xi\rangle$ denote initial and final wave function of the state. $O_{\lambda\mu}$ is the nuclear part of the transition operator. The labels ξ and ζ here denote quantum numbers that are required to specify the nuclear states uniquely. The initial and final states are not necessarily in the same nucleus as transition may also involve the emission of a particle such as an electron or a nucleon. M_f, M_i are the projection of the final and initial total angular momentum on the quantization axis, factored out using the Wigner-Eckart theorem,

$$\mathcal{M}_{fi}(M_f, M_i) = (-1)^{J_f - M_f} \begin{pmatrix} J_f & \lambda & J_i \\ -M_f & \mu & M_i \end{pmatrix} \langle J_f \xi \| O_\lambda \| J_i \zeta \rangle \quad (10)$$

where $\langle J_f \xi \| O_\lambda \| J_i \zeta \rangle$ is the reduced matrix element and $\begin{pmatrix} J_f & \lambda & J_i \\ -M_f & \mu & M_i \end{pmatrix}$ is the 3j-symbol. The angular momentum dependence of the matrix element is contained in the 3j-coefficients and is independent of the operator and the states involved, other than their angular momentum ranks. All the physical content of a matrix element is contained in the reduced matrix element. As a result, it may be compared with those of other quantities without being encumbered by dependence on the coordinate system used. Reduced matrix element is invariant under a rotation of the coordinate system.

3 Bulk Properties of Nuclei

3.1 Nuclear Shape and Electromagnetic Moments

3.1.1 Multipole expansion of charge density

As we know the potential due to a charge distribution $q(r')$ is

$$\phi(\mathbf{r}) = \left[\frac{1}{4\pi\epsilon_0} \right] \int \frac{q(\mathbf{r}')}{|\mathbf{r} - \mathbf{r}'|} dr' (\text{In CGS units } \left[\frac{1}{4\pi\epsilon_0} \right] = 1)$$

In the region $r > r'$, the potential can be expressed as an infinite series in terms of spherical harmonics,

$$\phi(\mathbf{r}) = \left[\frac{1}{4\pi\epsilon_0} \right] \sum_{\lambda\mu} \int \frac{4\pi \times q(\mathbf{r}') (r')^\lambda}{2\lambda + 1} Y_{\lambda\mu}^*(\theta', \phi') Y_{\lambda\mu}(\theta, \phi) dr' \quad (11)$$

For a charge distribution $\rho_{ch}(r')$ in a nucleus

$$\phi(\mathbf{r}) = \left[\frac{1}{4\pi\epsilon_0} \right] \sum_{\lambda\mu} \frac{4\pi Z}{2\lambda + 1} \frac{1}{r^{\lambda+1}} Q_{\lambda\mu} Y_{\lambda\mu}(\theta, \phi) \quad (12)$$

where the multipole coefficients are given by the distribution:

$$Q_{\lambda\mu} = \frac{1}{Z} \int e r'^\lambda Y_{\lambda\mu}^*(\theta', \phi') \rho_{ch}(\mathbf{r}') dr' \quad (13)$$

As $\cos\theta = 1$ along z-axis, As charge distribution is nearly spherical the importance of higher order terms decreases very rapidly with increasing λ . (12) can be written as

$$\phi(r) = \left[\frac{1}{4\pi\epsilon_0} \right] \frac{1}{r} \sum_{\lambda\mu} \sqrt{\frac{4\pi}{2\lambda + 1}} \frac{Q_{\lambda\mu}}{r^\lambda} \delta_{\mu 0} \quad (14)$$

The density distribution of a nucleus is given by, usually that for the ground state, $\rho(r) = |\psi(r)|^2$. For a nucleus with atomic number Z , it is more convenient to define the charge density distribution as

$$\rho_{ch}(r) = Z|\psi(r)|^2 \quad (15)$$

Using (15) the equation (13) can be written as

$$Q_{\lambda\mu} = \langle \Psi(\mathbf{r}) | e r^\lambda Y_{\lambda\mu}^*(\theta, \phi) | \Psi(r) \rangle$$

Hence we can identify the operator for the (λ, μ) electric multipole as

$$O_{\lambda\mu}(E) = e r^\lambda Y_{\lambda\mu}^*(\theta, \phi) \quad (16)$$

If we consider the nuclear wave function is made of products of single-particle wave functions we can write the operator as sum of operators, each one acting on an individual nucleon,

$$O_{\lambda\mu}(E) = e \sum_{\text{protons}} r_i^\lambda Y_{\lambda\mu}^*(\theta_i, \phi_i) = \sum_{i=1}^A e(i) r_i^\lambda Y_{\lambda\mu}^*(\theta_i, \phi_i) \quad (17)$$

$$\text{where } e(i) = \begin{cases} e & \text{for a proton} \\ 0 & \text{for a neutron} \end{cases}$$

If the charge distribution is spherical in shape, the contribution from the higher order terms decreases very rapidly with increasing λ as can be seen from (14). Hence to describe the electromagnetic properties of a nucleus, we mainly consider the lowest few multipoles, as the moments of these are the only ones that can be measured in practice. If the charge distribution is spherical in shape, $Q_{00} \neq 0$ but other higher multipole coefficients are vanishing which implies the Non-vanishing multipole coefficients are therefore measures of “**deformation**,” or departures from a spherical shape.

3.1.2 Electric quadrupole and hexadecapole moments

The existence of a nonvanishing electric quadrupole moment implies that the charge distribution of the state is deformed. Nuclei near closed shells are almost spherical and their quadrupole moment is less. The **quadrupole moment** is defined as the expectation value of the operator $r^\lambda Y_{\lambda\mu}^*(\theta, \phi)|_{\lambda=2}$ in the substate of $M = J$,

$$\begin{aligned} Q &= \sqrt{\frac{16\pi}{5}}e \langle J, M = J | r^2 Y_{20}(\theta, \phi) | J, M = J \rangle \\ &= e \langle J, M = J | (3z^2 - r^2) | J, M = J \rangle \end{aligned} \quad (18)$$

As for a spherical nucleus $\langle x^2 \rangle = \langle y^2 \rangle = \langle z^2 \rangle = \frac{1}{3}\langle r^2 \rangle$ which means quadrupole moment vanishes. The next higher order electric multipole is **hexadecapole**. Here, the spherical tensor rank of the operator is $\lambda = 4$. Multipole coefficients can also vanish for reasons of symmetry. For example, under an inversion of the spherical coordinate system as discussed in **Appendix**,

$$(r, \theta, \phi) \xrightarrow{P} (r, \pi - \theta, \pi + \phi)$$

Parity of $Y_{\lambda\mu}(\theta, \phi)$ is $(-1)^\lambda$ So, all the odd electric multipole coefficients vanish as otherwise it will violate symmetry under a parity inversion. This is observed experimentally too, for the case of neutron $Q_{00} = 0$ as it is a neutral particle. Experimentally we find upper limit of the electric dipole moment is $0.97 \times 10^{-25} \text{e-cm}$ close to zero.

Angular momentum coupling imposes a restriction on the highest order multipole coefficients a state can have. The multipole operator $r^\lambda Y_{\lambda\mu}(\theta, \phi)$ carries an angular momentum λ . Only multipole coefficients of $\lambda \leq 2J$ can be nonzero or in other words, the expectation value of such an operator vanishes for a state with spin J unless J, λ , and J can be coupled together to form a closed triangle.

3.1.3 Magnetic moments

Similar to electric moments a deformed nucleus can also have non spherical “magnetic charge” distribution. Magnetic moment of the nucleus is originated due to the intrinsic magnetic dipole moment of individual nucleons and the orbital motion of protons. We define a magnetic charge density $\rho_m(\mathbf{r})$ as the divergence of a magnetization density $\mathbf{M}(r)$,

$$\rho_m(\mathbf{r}) = -\nabla \cdot \mathbf{M}(r) \quad \mathcal{J}(r) = \frac{c}{|c|} \nabla \times \mathbf{M}(r) \quad (19)$$

For $\mathcal{J}(r)$, we can consider that nuclei are made of point nucleons having an intrinsic spin but no internal structure. A neutron is a particle with magnetic dipole moment $\frac{1}{2}g_n$ and proton with magnetic dipole moment $\frac{1}{2}g_p$. In a point particle picture the magnetization current density may be written as a sum of the contributions from all the nucleons in the nucleus in the following way:

$$\mathcal{J}(\mathbf{r}) = \sum_{i=1}^A \left\{ e g_\ell(i) \frac{p(i)}{M_N} + \frac{e\hbar}{2M_N} g_s(i) (\nabla \times s(i)) \right\} \delta(r - r(i)) \quad (20)$$

where, in units of nuclear magneton μ_N ,

$$g_\ell = \begin{cases} 1 & \text{for a proton} \\ 0 & \text{for a neutron} \end{cases} \quad g_s = \begin{cases} 5.586 & \text{for a proton} \\ -3.826 & \text{for a neutron} \end{cases}$$

and M_N is the mass of a nucleon. Magnetization density distribution in terms of multipole coefficients is given by the integral

$$\mathcal{M}_{\lambda\mu} = \int r^\lambda Y_{\lambda\mu}^*(\theta, \phi) \rho_m(\mathbf{r}) d\mathbf{r} = - \int r^\lambda Y_{\lambda\mu}^*(\theta, \phi) \nabla \cdot \mathbf{M}(\mathbf{r}) d\mathbf{r} \quad (21)$$

To find the parity of the multipole moment operator we can observe that it is $(-1)^{\lambda+1}$ as divergence will lead to one extra -1 for $(x, y, z) \rightarrow (-x, -y, -z)$. As a result, **even-order magnetic multipole moments vanish** otherwise it implies a breakdown of the symmetry under a parity inversion.

The lowest order nonvanishing magnetic multipole for a nucleus is the dipole. From (21), the magnetic dipole coefficient may be written as:

$$\mathcal{M}_{1\mu} = - \int r Y_{1\mu} \nabla \cdot \mathbf{M}(r) dr = \int \mathbf{M}_\mu(r) dr \text{ (using integration by parts)} \quad (22)$$

The operator for magnetic dipole $O_{1\mu}(M1)$ is given by the integrand of (22). Now we obtain the magnetic dipole operator in terms of orbital angular momentum $\mathbf{l}(i)$ and intrinsic spin $\mathbf{s}(i)$ of each nucleon,

- **Contribution from intrinsic spin part**

Compare (19) with the 2nd term of (20) to get $\mathbf{M}_\mu(r)$ in terms of $\mathbf{s}_\mu(i)$ as

$$\frac{c}{|c|} \mathbf{M}_\mu(r) = \frac{e\hbar}{2M_N} \sum_{t=1}^A g_s(i) \mathbf{s}_\mu(i) \implies \mathbf{M}_\mu(r) = O_{1\mu}(M1, s) = \frac{e\hbar|c|}{2M_N c} \sum_{t=1}^A g_s(i) \mathbf{s}_\mu(i) \quad (23)$$

- **Contribution from orbital angular momentum part**

For orbital motion, we note that,

$$\mathcal{M}_{1\mu}(\ell) \equiv \int \mathbf{M}_\mu(\ell) dr = \frac{1}{2} \int (r \times (\nabla \times \mathbf{M}(\ell)))_\mu dr = \frac{|c|}{2c} \int (\mathbf{r} \times \mathcal{J}(\ell))_\mu dr \text{ (using (19))}$$

We know that for a proton magnetization current $\mathcal{J}(\ell) = (\frac{e}{M_p})\mathbf{p}$, where \mathbf{p} is the momentum of the proton. So, the total momentum due to proton orbital motion is $\sum_{i=1}^A e g_\ell(i) \frac{\mathbf{p}_i}{M_N}$ and as we know $\mathbf{l}\hbar = \mathbf{r} \times \mathbf{p}$ we have:

$$\mathbf{O}_{1\mu}(M1, \ell) = \frac{|c|}{2c} \left(\mathbf{r} \times \sum_{i=1}^A e g_\ell(i) \frac{\mathbf{p}_i}{M_N} \right)_\mu = \frac{e\hbar|c|}{2M_N c} \sum_{i=1}^A g_\ell(i) \ell_\mu(i) \quad (24)$$

Hence the magnetic dipole operator becomes

$$\begin{aligned} O_{1\mu}(M1) &= O_{1\mu}(M1, \ell) + O_{1\mu}(M1, s) \\ &= \frac{e\hbar|c|}{2M_N c} \sum_{i=1}^A \{g_\ell(i)\ell_\mu(i) + g_s(i)s_\mu(i)\} \\ &= \mu_N \sum_{i=1}^A \{g_\ell(i)\ell_\mu(i) + g_s(i)s_\mu(i)\} \end{aligned} \quad (25)$$

Magnetic multipole operator of arbitrary order is given by[17]

$$\mathbf{O}_{\lambda\mu}(M\lambda) = \mu_N \sum_{i=1}^A \left\{ \frac{2}{\lambda+1} g_\ell(i)\ell(i) + g_s(i)s(i) \right\} \cdot \nabla_i \left(r_i^\lambda Y_{\lambda\mu}^*(\theta_i, \phi_i) \right) \quad (26)$$

3.2 Magnetic Dipole Moment of Odd Nuclei

The magnetic dipole moment μ is defined as the expectation value of $O_{1\mu}(M1)$ given by (25) in a state with $M = J$. In units of nuclear magnetons,

$$\mu = \langle J, M = J | O_{1\mu}(M1) | J, M = J \rangle = \sum_{i=1}^A \langle J, M = J | g_\ell(i)\ell_0(i) + g_s(i)s_0(i) | J, M = J \rangle \quad (27)$$

Since $O_{1\mu}(M1)$ carries one unit of angular momentum as $\lambda = 1$, $\lambda \leq 2J \implies J \geq \frac{1}{2}$. So, the expectation value vanishes in states with spin $J < \frac{1}{2}$.

3.2.1 Single-particle model

Pairs of identical nucleons in the ground state of a nucleus prefer to couple to angular momentum zero. For a zero-coupled pair of protons or a pair of neutrons, the total orbital angular momentum \mathbf{L} and intrinsic spin s must be either the combination $(L, S) = (0, 0)$ or $(L, S) = (1, 1)$ to satisfy the Pauli principle. $S = 0$ state implies the intrinsic spins of the two nucleons must be aligned anti parallel to each other and $L = 0$ implies two protons are moving in opposite directions. In the limit that pairing completely dominates the nuclear ground state, all pairs of neutrons and protons are coupled to $J = 0$.

In the case of even-even nuclei, the magnetic dipole moment vanishes due to the fact that the spin J must be zero which is verified experimentally for stable nuclei. For odd-mass nuclei, only one nucleon is outside zero-coupled pairs and Eq. (27) reduces to the expectation value of the unpaired nucleon alone i.e.

$$\mu_{\text{sp.}} = \mu_N \langle j, m = j | g_\ell\ell_0 + g_ss_0 | j, m = j \rangle \quad (28)$$

using Lande's formula we find that

$$\mu_{\text{sp.}} = \frac{1}{j(j+1)} \langle j, m=j | (\boldsymbol{\mu} \cdot \boldsymbol{j}) \boldsymbol{j}_0 | j, m=j \rangle \quad (29)$$

Magnetic dipole operator for a single nucleon is $\boldsymbol{\mu} = g_l \boldsymbol{l} + g_s \boldsymbol{s}$. so, the product $\boldsymbol{\mu} \cdot \boldsymbol{j}$ in Eq. (29) becomes

$$\boldsymbol{\mu} \cdot \boldsymbol{j} = (g_l \boldsymbol{l} + g_s \boldsymbol{s}) \cdot (\boldsymbol{l} + \boldsymbol{s}) = g_l \left(\boldsymbol{l}^2 + \frac{1}{2} (\boldsymbol{j}^2 - \boldsymbol{l}^2 - \boldsymbol{s}^2) \right) + g_s \left(\boldsymbol{s}^2 + \frac{1}{2} (\boldsymbol{j}^2 - \boldsymbol{l}^2 - \boldsymbol{s}^2) \right) \quad (30)$$

The expectation values of these operators are known so, from (29),(30) we get:

$$\mu_{\text{sp.}} = j \left(g_l \pm \frac{g_s - g_l}{2l+1} \right) \quad \text{for} \quad j = l \pm \frac{1}{2} \quad (31)$$

In this picture the magnetic dipole moment of the nucleus is completely determined by the unpaired nucleon.

3.2.2 Schmidt value

If all the nucleons except one are members of zero-coupled pairs, the spin of the state is also given by that of the unpaired nucleon. The two possible l -values for a given j are $l = j \pm \frac{1}{2}$. The parity of the state where a pair occupies single-particle orbits having the same l -value is $\pi = (-1)^l$. The spin and parity of the state along with whether the unpaired nucleon is a proton or a neutron is used to calculate dipole moment using (31).

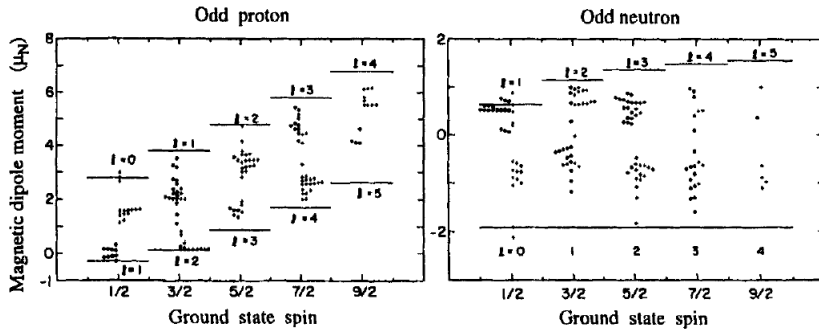


Figure 3: Magnetic dipole moment of odd-mass nuclei. The solid lines are calculated results using Eq. (31)

As we expect the l value should be between $j \pm \frac{1}{2}$ but in the above figure we can find that it is between the two Schmidt values for $l = j \pm 1$. This is because of the assumption that all the nucleons except one are tied in zero-coupled pairs. A more realistic ground state wave function includes other components as well. We can characterize them by the number of "broken" zero-coupled pairs, these non-zero-coupled pairs can contribute to the magnetic dipole moment of the nucleus which changes the dipole moment by substantial amount.

3.2.3 Corrections to single-particle model

The model should work best for nuclei with one nucleon away from a closed shell. Consider the closed shell nuclei 4He and ${}^{16}O$, if we remove one neutron or one proton we get 3He , ${}^{15}N$ or adding a nucleon gives ${}^{17}O$ and ${}^{17}F$. For all these cases also Corrections to the Schmidt values from nuclear structure considerations alone are found to be **much larger** than those required to account for the differences between the observed and Schmidt values. The reason for this is due to considering the nucleon to free in the nucleus. For example, the intrinsic magnetic dipole moment of a proton is taken to be $\frac{1}{2}g_p$ and that of a neutron is $\frac{1}{2}g_n$ but if charged mesons are exchanged between nucleons, their flow constitutes an electric current which may also contribute to the observed magnetic moments. Another assumption is also that we have made the naive assumption in Eq. (20) that nucleons in nuclei behave like point particles carrying the same charge and magnetic dipole moments as free nucleons.

3.2.4 Ground State Spin and Isospin

The ground state is the lowest one in energy for a nucleus. It is a special state of a system of N neutrons and Z protons by virtue of the fact that it is the most stable one. Since each nucleon has an intrinsic spin $s = \frac{1}{2}$ and an (integer) orbital angular momentum l , the total angular momentum or spin j carried by a nucleon is a half integer quantity. So, $J = \sum_{i=1}^A j_i$ and for isospin $T = \sum_{i=1}^A t_i$, where $t_i = \frac{1}{2}$ is the isospin of the i th nucleon. Since ground state spins of odd-odd nuclei are observed to be nonzero in general, we conclude further that pairing interaction is important only between two identical nucleons, two protons or two neutrons, but not between a neutron and a proton.

4 Electromagnetic Transition

Besides γ -ray emission, electromagnetic perturbation can also induce nuclear decay through internal conversion whereby one of the atomic electrons is ejected. This is usually more important for heavy nuclei, where the nuclear electromagnetic fields are strong and the orbits of the inner shell electrons are close to the nucleus. The decay can also proceed by creating an electron-positron pair but the probability is much smaller than that of the γ -ray emission. To discuss about electromagnetic transitions we need to establish a connection between the transition probability \mathcal{W} of (1) and the nuclear matrix element \mathcal{M}_{fi} of (9) using first-order time-dependent perturbation discussed in **appendix A**. The perturbation H' comes from the coupling between nuclear and electromagnetic fields, and the density of final states $\rho(E_f)$ is a product of the number of nuclear and electromagnetic states per energy interval at E_f .

4.1 The spin of the photon

As we know in a system with spherical symmetry the angular momentum is a conserved quantity which is proved in **Appendix**. From here we deduced that the angular momentum commutes with the Hamiltonian. In the case of electromagnetism the old \mathbf{A} which, as shown in (10) determines the physical quantities, is a vector and, therefore, its rotation is a bit more complicated than in the scalar case of the wave function.

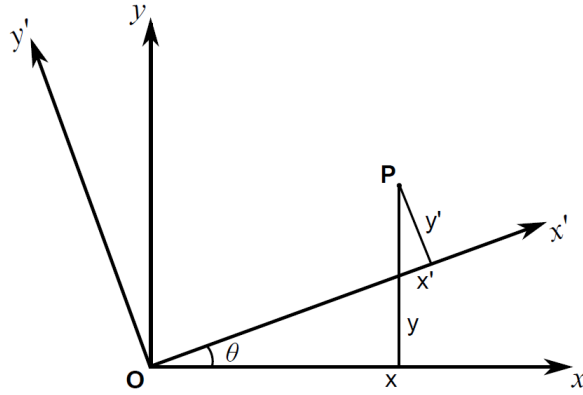


Figure 4: Relation between the systems of coordinates related by a rotation along the axis $z = z'$

We will rotate an angle θ along the z -axis. In the original system the coordinates of a point P are $P = (x, y, z)$ while in the rotated system we will use the notation $P = (x', y', z')$. As can be seen from the below figure, the relation between the two coordinates is,

$$\begin{aligned} x' &= \cos \theta x + \sin \theta y \\ y' &= -\sin \theta x + \cos \theta y \\ z' &= z \end{aligned}$$

In the same fashion the components of the vector \mathbf{A} transform as

$$\begin{aligned} A'_x(x', y', z') &= \cos \theta A_x(\cos \theta x + \sin \theta y, -\sin \theta x + \cos \theta y, z) \\ &\quad + \sin \theta A_y(\cos \theta x + \sin \theta y, -\sin \theta x + \cos \theta y, z) \\ A'_y(x', y', z') &= -\sin \theta A_x(\cos \theta x + \sin \theta y, -\sin \theta x + \cos \theta y, z) \\ &\quad + \cos \theta A_y(\cos \theta x + \sin \theta y, -\sin \theta x + \cos \theta y, z) \\ A'_z(x', y', z') &= A_z(\cos \theta x + \sin \theta y, -\sin \theta x + \cos \theta y, z) \end{aligned}$$

performing an infinitesimal rotation ($\cos \theta \approx 1, \sin \theta \approx \theta$) one gets,

$$A_x(\cos \theta x + \sin \theta y, -\sin \theta x + \cos \theta y, z) \approx A_x(x, y, z) - i\theta L_z A_x$$

repeating the same for the components A'_y and A'_z one gets, that

$$\mathbf{A}' = \mathbf{A} - i\theta(L_z + S_z)\mathbf{A}$$

where

$$S_z \begin{pmatrix} A_x \\ A_y \\ A_z \end{pmatrix} = \begin{pmatrix} -iA_y \\ iA_x \\ 0 \end{pmatrix}$$

The eigenvalues of S_z are $-1, 0$ and $+1$. In the same fashion one can define S_x and S_y by rotating along the axis x and y , respectively. We thus see that the generator of rotations for a vector field is $\mathbf{J} = \mathbf{L} + \mathbf{S}$, where \mathbf{S} is the intrinsic spin of the vector field with eigenvector $S = 1$. This implies that the photon carries a spin $S = 1$.

4.2 Coupling to electromagnetic fields

If we separate H' into two operators, one acting on the nuclear wave function and the other on the external electromagnetic field. External electromagnetic field needs to be quantized and decomposed by a multipole expansion into components with definite spherical tensor ranks. Both quantization and multipole expansion of the electromagnetic field involve tedious procedures, one can refer to Blatt and Weisskopf[16].

Electromagnetic perturbation in a nucleus can be visualized in the following way. If we consider a point particle with charge q , In the absence of any external electromagnetic field, the Hamiltonian is $H_0 = \frac{1}{2m}\mathbf{p}^2$. In the presence of an electromagnetic field, the momentum is modified from that for a free particle by the following transformation: $\mathbf{p} \rightarrow \mathbf{p} + \frac{q}{c}\mathbf{A}$. So, the Hamiltonian becomes:

$$H = \frac{1}{2m} \left(\mathbf{p} + \frac{q}{c} \mathbf{A} \right)^2 = H_0 + \mathbf{H}'$$

So, the perturbed Hamiltonian becomes:

$$\begin{aligned} \mathbf{H}' &= -\frac{q}{2mc}(\mathbf{p} \cdot \mathbf{A} + \mathbf{A} \cdot \mathbf{p}) + \frac{q^2}{2mc^2}\mathbf{A} \cdot \mathbf{A} \\ &= -\frac{q}{mc}\mathbf{A} \cdot \mathbf{p} + \frac{q^2}{2mc^2}\mathbf{A} \cdot \mathbf{A} \longrightarrow -\frac{q}{mc}\mathbf{A} \cdot \mathbf{p} \quad (\text{as } \mathbf{p} = -i\hbar\nabla \text{ and } \nabla \cdot \mathbf{A} = 0) \end{aligned} \quad (32)$$

As we know $\mathcal{J} = q\mathbf{v} = q\frac{\mathbf{p}}{m}$ So, we have:

$$\boxed{\mathbf{H}' = -\frac{1}{c}\mathbf{A} \cdot \mathbf{J}} \quad (33)$$

In this we didn't consider the dipole moment of the nucleon which can also interact with the external electromagnetic field. We have already seen than the intrinsic magnetic dipole moment of a nucleon can be expressed in terms of current.

$$\mathbf{H}' = -\frac{1}{c} \sum_{\mu=1}^4 \mathbf{A}_\mu \mathbf{J}_\mu$$

where $A_\mu = (\mathbf{A}, i\phi)$ and $J_\mu = (\mathcal{J}, i\rho c)$. So, the general form of Hamiltonian becomes:

$$H = H_{\text{nuc}} + H_{\text{field}} + H_{\text{int}}$$

H_{nuc} is some nuclear model Hamiltonian with eigenfunctions $\psi_i(1 \dots \mathbf{A})$ such that $H_{\text{nuc}}\psi_i(1 \dots \mathbf{A}) = E_i\psi_i(1 \dots \mathbf{A})$. H_{field} is given by:

$$H_{\text{field}} = \frac{1}{8\pi} \int (\mathbf{E}^2(r, t) + \mathbf{B}^2(r, t)) d^3r$$

As we know energy stored in the electric field per unit volume is

$$\frac{1}{2}\epsilon_0 \mathbf{E}^2 \text{ (in SI units)} = \frac{E^2}{8\pi} \text{ (in CGS units)}$$

and energy stored in the magnetic field per unit volume is

$$\frac{1}{2\mu_0} \mathbf{B}^2 \text{(in SI units)} = \frac{\mathbf{B}^2}{8\pi} \text{(in CGS units)}$$

So, $H_{\text{field}} = \mathbf{E}_{\text{field}} = \mathbf{E}_{\text{elec}} + \mathbf{E}_{\text{mag}}$. The interaction between the external field and the nucleus is

$$H_{\text{int}} = -\frac{1}{c} \int j_\mu A^\mu d^3r = \int \left(\rho(\mathbf{r}, t) \Phi(\mathbf{r}, t) - \frac{1}{c} J(\mathbf{r}, t) \cdot \mathbf{A}(\mathbf{r}, t) \right) d^3r.$$

As we know in CGS units the maxwells equations are given by:

$$\nabla \cdot \mathbf{E} = 4\pi\rho \quad (34)$$

$$\nabla \cdot \mathbf{B} = 0 \quad (35)$$

$$\nabla \times \mathbf{E} = -\frac{1}{c} \frac{\partial \mathbf{B}}{\partial t} \quad (36)$$

$$\nabla \times \mathbf{B} = \frac{1}{c} \left(4\pi \mathbf{J} + \frac{\partial \mathbf{E}}{\partial t} \right) \quad (37)$$

From (35) we have

$$\mathbf{B} = \nabla \times \mathbf{A} \quad (38)$$

and putting it in (36) we have, $\nabla \times (\mathbf{E} + \frac{1}{c} \frac{\partial \mathbf{A}}{\partial t}) = 0$. So,

$$\mathbf{E} = -\nabla\phi - \frac{1}{c} \frac{\partial \mathbf{A}}{\partial t} \quad (39)$$

considering the scalar potential to be constant w.r.t space and time we have $\mathbf{E} = -\frac{1}{c} \frac{\partial \mathbf{A}}{\partial t}$ and inserting (38),(39) in (34) and (37) we get

$$\nabla \cdot \mathbf{E} = \nabla \cdot \left(-\nabla\phi - \frac{1}{c} \frac{\partial \mathbf{A}}{\partial t} \right) = 4\pi\rho \quad (40)$$

$$\nabla \times \nabla \times \mathbf{A} = \frac{1}{c} \left(4\pi \mathbf{J} + \frac{\partial}{\partial t} \left(-\nabla\phi - \frac{1}{c} \frac{\partial \mathbf{A}}{\partial t} \right) \right) \Rightarrow \left(\nabla^2 \mathbf{A} - \frac{1}{c^2} \frac{\partial^2 \mathbf{A}}{\partial t^2} \right) - \nabla \left(\nabla \cdot \mathbf{A} + \frac{1}{c} \frac{\partial \phi}{\partial t} \right) = \frac{4\pi \mathbf{J}}{c} \quad (41)$$

If we take the gauge condition $\nabla \cdot \mathbf{A} + \frac{1}{c} \frac{\partial \phi}{\partial t} = 0$ or $\nabla \cdot \mathbf{A} = 0$ (for ϕ independent of t). In a region outside any charge and current distributions, the four-potential is obtained from the time-dependent partial differential equation,

$$\left(\nabla^2 - \frac{1}{c^2} \frac{\partial^2}{\partial t^2} \right) \mathbf{A}_\mu(\mathbf{r}, t) = 0$$

To remove the time dependence we expand $\mathbf{A}_\mu(\mathbf{r}, t)$ as

$$\mathbf{A}_\mu(\mathbf{r}, t) = \sum_k \mathbf{A}_k(\mathbf{r}) e^{-i\omega t} \quad (42)$$

where $\omega = kc$ to get

$$(\nabla^2 + k^2) \mathbf{A}_k(\mathbf{r}) = 0 \implies \mathbf{A}_k(\mathbf{r}) = \mathbf{B}_k e^{i\mathbf{k} \cdot \mathbf{r}} + \mathbf{C}_k e^{i\mathbf{k} \cdot \mathbf{r}} \quad (43)$$

from (42) and (43) we have:

$$\boxed{\mathbf{A}(\mathbf{r}, t) = \frac{1}{N} \sum_k \sum_{\eta} \left\{ \mathbf{b}_{k\eta} \epsilon_{\eta} e^{i(\mathbf{k}\cdot\mathbf{r} - \omega t)} + \mathbf{b}_{k\eta}^{\dagger} \epsilon_{\eta} e^{-i(\mathbf{k}\cdot\mathbf{r} + \omega t)} \right\}} \quad (44)$$

where B_k and C_k are constants to be determined by boundary conditions and N is a normalization constant. Being the quantum of a vector field, each γ -ray carries one unit of angular momentum. $\nabla \cdot \mathbf{A} = 0$ means that only two components of \mathbf{A} are independent. These two components may be identified by two unit vectors ϵ_{η} with $\eta = 1$. Equation (43) is identical to the equation for a harmonic oscillator. So, we can think of the electromagnetic field as a **collection of harmonic oscillators**, one for each frequency (or wave number \mathbf{k}) and polarization direction η . The separation in energy between harmonic oscillator states is in units of $\hbar\omega$.

4.3 Multipole expansion of the electromagnetic fields

For applications to problems with rotational symmetry, it is more convenient to express $\mathbf{A}(r, t)$ in terms of operators having definite spherical tensor ranks, $\mathbf{A}(r, t) = \sum_{\lambda\mu} \mathbf{A}_{\lambda\mu}(r, t)$ where the vector function $\mathbf{A}(r, t)$ with spherical tensor rank (λ, μ) satisfies the following relations as the eigenfunction of angular momentum operators \mathbf{J}^2 and \mathbf{J}_0 :

$$J^2 A_{\lambda\mu}(r, t) = \lambda(\lambda + 1) A_{\lambda\mu}(r, t) \quad J_0 \mathbf{A}_{\lambda\mu}(r, t) = \mu A_{\lambda\mu}(r, t) \quad (45)$$

Dropping the time dependence from (42) to make it simple and writing in terms of vector spherical harmonics,

$$\mathbf{A}_{\lambda\mu}^E(k\mathbf{r}) = \frac{-i}{k} \nabla \times (\mathbf{r} \times \nabla) (j_{\lambda}(kr) Y_{\lambda\mu}(\theta\phi)) \quad (46)$$

$$\mathbf{A}_{\lambda\mu}^M(k\mathbf{r}) = (\mathbf{r} \times \nabla) (j_{\lambda}(kr) Y_{\lambda\mu}(\theta\phi)) \quad (47)$$

Here we consider two different types of multipole fields satisfying (43) rather than considering two polarization directions. we have now two different types of multipole fields satisfying Eq. (43). In both cases the photon carries angular momentum λ with z-projection μ . Therefore they are multipole components, with multipolarity λ , of the electromagnetic field. However for the case $\lambda = 0$ there is no angular dependence ($Y_{00}(\theta, \phi) = \frac{1}{\sqrt{4\pi}}$) and since for any angle independent function $\phi(r)$ it is $\nabla\phi(r) \propto r$, the electromagnetic field vanishes ($r \times r = 0$). In other words, there is **no monopole photon** in the electromagnetic field. We have,

$$\begin{aligned} \nabla \times (\mathbf{r} \times \nabla) &= -\nabla \frac{\partial}{\partial r} r + \mathbf{r} \nabla^2, \\ \nabla \cdot (\mathbf{r} \times \nabla) &= -(\nabla \times \nabla) \cdot \mathbf{r} = 0. \end{aligned}$$

As we have $\pi_O = (-1)^{\lambda}$ for Y^{λ} and $\pi_O = -1$ for the vectors \mathbf{r} , ∇ and \mathbf{p} and $\pi_O = +1$ for pseudo vector $\mathbf{l} = \mathbf{r} \times \mathbf{p}$. Thus the parity of the electromagnetic field is

$$\begin{aligned} &-(-1)^{\lambda} \text{for electric multipole} \\ &+(-1)^{\lambda} \text{for magnetic multipole} \end{aligned}$$

The two multipoles can be distinguished by the parity and are related to each other. We have

$$\mathbf{A}_{\lambda\mu}^E(k\mathbf{r}) = \frac{1}{k} \nabla \times \mathbf{A}_{\lambda\mu}^M(k\mathbf{r}) \quad (48)$$

By using (46) and (47) we can write the (λ, μ) multipole part of the perturbing Hamiltonian H' as scalar operators:

$$\mathcal{O}(E\lambda\mu) = \frac{-i(2\lambda+1)!!}{ck^{\lambda+1}(\lambda+1)} \int \mathbf{j}_E(r) \cdot \nabla \times (\mathbf{r} \times \nabla) (j_\lambda(kr) Y_{\lambda\mu}(\theta\phi)) dr \quad (49)$$

$$\mathcal{O}(M\lambda\mu) = \frac{-(2\lambda+1)!!}{ck^\lambda(\lambda+1)} \int \mathbf{j}_M(r) \cdot (\mathbf{r} \times \nabla) (j_\lambda(kr) Y_{\lambda\mu}(\theta\phi)) dr, \quad (50)$$

where $(2\lambda+1)!! = 1 \cdot 3 \cdot 5 \cdots (2\lambda+1)$. The normalization used in these operators are such that they reduce to those for the static moments of Eq. (17) in the limit $k \rightarrow 0$.

In nuclear electromagnetic processes it is convenient to take into account the range of the quantities involved. Thus nuclear photo transitions occur at large wavelengths of the photons as compared to the nuclear radius. Generally γ -rays involved in nuclear transitions have energies $E_\gamma < 10$ MeV i.e.

$$k = \frac{E_\gamma}{\hbar c} \approx 0.05 \text{ fm}^{-1}, \lambda = \frac{2\pi}{k} \approx 10^2 \text{ fm}$$

and the nuclear radius R , for even for a heavy nucleus, for example ^{207}Pb ($R \approx 7$ fm). Hence $kr < 1$ So, while expanding the bessel function $j_\lambda(kr)$ in (49) and (50) we only need to consider the first term as $kr < 1$.

Now to calculate contribution of each multipole to the transition probability as given in (107). Using (49),(50) and $\rho(E_f)$ we get the transition probability for multipole λ from an initial nuclear state $|J_i M_i \zeta\rangle$ to final nuclear state $|J_f M_f \xi\rangle$ as

$$\mathcal{W}(\lambda; J_i \zeta \rightarrow J_f \xi) = \frac{8\pi(\lambda+1)}{\lambda[(2\lambda+1)!!]^2} \frac{k^{2\lambda+1}}{\hbar} B(\lambda; J_i \zeta \rightarrow J_f \xi) \quad (51)$$

where the reduced transition probability $B(\lambda; J_i \zeta \rightarrow J_f \xi)$ is

$$B(\lambda; J_i \zeta \rightarrow J_f \xi) = \sum_{\mu M_l} |\langle J_f M_f \xi | \mathbf{O}_{\lambda\mu} | J_i M_i \zeta \rangle|^2 = \frac{1}{2J_i + 1} |\langle J_f \xi | \mathbf{O}_\lambda | J_i \zeta \rangle|^2 \quad (52)$$

Now if we look notice the dimension of reduced transition probability we have,
From (16) dimension of $\mathbf{O}_{\lambda\mu}(E)$ goes as er^λ which implies

$$B(E\lambda; J_i \zeta \rightarrow J_f \xi) \sim e^2 r^{2\lambda} \text{ (from (52)).} \quad (53)$$

Charge is measured in units of e and length in units of femtometer (fm). So, For Electric multipole $B(E\lambda) \sim e^2 \text{ fm}^{2\lambda}$. From (26) because of gradient operator, dimension of $\mathbf{O}_{\lambda\mu}(M)$ goes as $\mu_N \text{ fm}^{(\lambda-1)}$ which implies

$$B(M\lambda; J_i \zeta \rightarrow J_f \xi) \sim \mu_N^2 \text{ fm}^{(2\lambda-2)} \quad (54)$$

From (51) to find the dimension of transition probability (using $k \sim \frac{1}{r} \sim \text{fm}^{-1}$) we have,

$$\mathcal{W}(E\lambda) : \frac{[\text{fm}^{-1}]^{2\lambda+1}}{[\text{MeV} - \text{s}]} \times e^2 [\text{fm}]^{2\lambda} = \frac{[\text{fm}^{-1}]^{2\lambda+1}}{[\text{MeV} - \text{s}]} \times [\text{MeV} - \text{fm}] [\text{fm}]^{2\lambda} = [\text{s}]^{-1}$$

Similarly, for $\mathcal{W}(M\lambda)$ recalling that $\mu_N = \frac{e\hbar}{2M_p c} \sim e[\text{fm}]$ we have,

$$\mathcal{W}(M\lambda) : \frac{[\text{fm}^{-1}]^{2\lambda+1}}{[\text{MeV} - \text{s}]} \times e^2 [\text{fm}]^2 \text{fm}^{(2\lambda-2)} = \frac{[\text{fm}^{-1}]^{2\lambda+1}}{[\text{MeV} - \text{s}]} \times [\text{MeV} - \text{fm}] [\text{fm}]^{2\lambda} = [\text{s}]^{-1}$$

Both have dimensions of inverse time which is expected as transition rate \mathcal{W} is the number of decays per unit time. From (51), (53) and (54) using $k^{2\lambda+1} = \left(\frac{1}{\hbar c}\right)^{2\lambda+1} E_\gamma^{2\lambda+1}, e^2 = \alpha \hbar c$ (in CGS units) we have:

$$\mathcal{W}(\lambda) = \begin{cases} \alpha \hbar c \frac{8\pi(\lambda+1)}{\lambda[(2\lambda+1)!!]^2} \frac{1}{\hbar} \left(\frac{1}{\hbar c}\right)^{2\lambda+1} E_\gamma^{2\lambda+1} B(E\lambda \text{ in } e^2 \text{fm}^{2\lambda}) \\ \alpha \hbar c \left(\frac{\hbar c}{2M_p c^2}\right)^2 \frac{8\pi(\lambda+1)}{\lambda[(2\lambda+1)!!]^2} \frac{1}{\hbar} \left(\frac{1}{\hbar c}\right)^{2\lambda+1} E_\gamma^{2\lambda+1} B(M\lambda \text{ in } \mu_N^2 \text{fm}^{2\lambda-2}) \end{cases} \quad (55)$$

Electromagnetic transition probabilities for the lowest four multipoles are given in this table.

$\mathcal{W}(E1) = 1.59 \times 10^{15} E_\gamma^3 \times B(E1)$	$\mathcal{W}(M1) = 1.76 \times 10^{13} E_\gamma^3 \times B(M1)$
$\mathcal{W}(E2) = 1.23 \times 10^9 E_\gamma^5 \times B(E2)$	$\mathcal{W}(M2) = 1.35 \times 10^7 E_\gamma^5 \times B(M2)$
$\mathcal{W}(E3) = 5.71 \times 10^2 E_\gamma^7 \times B(E3)$	$\mathcal{W}(M3) = 6.31 \times 10^0 E_\gamma^7 \times B(M3)$
$\mathcal{W}(E4) = 1.70 \times 10^{-4} E_\gamma^9 \times B(E4)$	$\mathcal{W}(M4) = 1.88 \times 10^{-6} E_\gamma^9 \times B(M4)$

E_γ are in MeV, $B(E\lambda)$ in $e^2 \text{fm}^{2\lambda}$, and $B(M\lambda)$ in $\mu_N^2 \text{fm}^{(2\lambda-2)}$

4.3.1 Selection rules

Ratio between two multipole transitions λ and $\lambda + 1$ from (51) is $\mathcal{R} = \frac{\mathcal{W}(\lambda+1)}{\mathcal{W}(\lambda)} \sim (kr)^2$ (r is included so that the ratio remains dimensionless). For 1 MeV gamma ray taking r to be of the order of 1 fm hence we get \mathcal{R} to be around 3×10^{-5} which means that

$$\mathcal{W}(E\lambda) \gg \mathcal{W}(E(\lambda + 1)) \quad \mathcal{W}(M\lambda) \gg \mathcal{W}(M(\lambda + 1))$$

Hence the transition between an initial nuclear state with spin-parity $J_i^{\pi_i}$ and a final state $J_f^{\pi_f}$ is usually dominated by the lowest order allowed by angular momentum and parity selection rules. For transition of order λ , the operator carries λ units of angular momentum. Hence λ can take the value

$$|J_f - J_i| \leq \lambda \leq |J_f + J_i|$$

The operator for an $E\lambda$ -transition is proportional to $Y_{\lambda\mu}(\theta, \phi)$ (see 17). Under an inversion of the coordinate system, we get

$$O_{\lambda\mu}(E\lambda) \xrightarrow{P} (-1)^\lambda O_{\lambda\mu}(E\lambda) \quad (56)$$

The magnetic operator, on the other hand has an extra ∇ which gives another - sign So,

$$O_{\lambda\mu}(M\lambda) \xrightarrow{P} (-1)^{\lambda+1} O_{\lambda\mu}(M\lambda) \quad (57)$$

Selection rules are the results of conservation laws. For system under certain condition it shows symmetry. For instance, the invariance of a nuclear system as a whole under spatial rotations leads to the conservation of the total angular momentum. When a nucleus emits (absorbs) a photon, the initial (final) total nuclear angular momentum should be equal to the sum of the final (initial) total nuclear angular momentum and the angular momentum carried by the radiation. The operators for $E\lambda$ and $M\lambda$ can be classified according to their transformation under parity change: $P\mathcal{O}P^{-1} = \pi_{\mathcal{O}}\mathcal{O}$. The matrix element becomes

$$\langle \psi_f | \mathcal{O} | \psi_i \rangle = \langle \psi_f | P^{-1} P \mathcal{O} P^{-1} P | \psi_i \rangle = \pi_i \pi_f \pi_{\mathcal{O}} \langle \psi_f | \mathcal{O} | \psi_i \rangle \quad (58)$$

Unless $\pi_i \pi_f \pi_{\mathcal{O}} = +1$ the matrix element will vanish. Hence, transitions are divided into two classes,

- $\pi_{\mathcal{O}} = +1$ i.e. the ones which do not change parity $\pi_i \pi_f = +1$ for M1, E2, M3, E4...
- $\pi_{\mathcal{O}} = -1$ i.e. the ones which do change parity $\pi_i \pi_f = -1$ for E1, M2, E3, M4...

The lowest allowed multipolarity in the decay rate dominates over the next higher one (when more than one is allowed) by several orders of magnitude. The most common types of transitions are electric dipole (E1), magnetic dipole (M1), and electric quadrupole (E2). From 57 and 56 the parity selection rule becomes:

$$\pi_i \pi_f = (-1)^{\lambda} \text{ for } E\lambda \text{ and}$$

$$\pi_i \pi_f = (-1)^{\lambda+1} \text{ for } M\lambda$$

where π_i , and π_f are, respectively, the parities of the initial and final states. From the table it is clear that magnetic transitions are weaker than the electric ones. Because of the selection rules we can't compare the transition probabilities for same multipolarity as it can't occur between a pair of nuclear states. For a given pair of nuclear states if both $E\lambda$ and $M(\lambda+1)$ are allowed by angular momentum and parity selection rules, $E\lambda$ -mode dominates the transition by a large factor. But if both $M(\lambda)$ and $E(\lambda+1)$ transitions are allowed, we have to find transition probabilities of each of those transitions and then compare.

4.3.2 $E\lambda$ -transition

To calculate reduced transition probability we need to know both the initial and final wave functions. We have to make some assumptions about these wave functions without considering specific states involved in transition. We consider independent particle picture i.e. nuclear transitions take place by a nucleon moving from one state $|j_i m_i\rangle$ to another state $|j_f m_f\rangle$ without affecting the rest of the nucleus. So, Matrix element of $O_{\lambda\mu}(E\lambda)$ between many-body nuclear wave functions $|J_i M_i \zeta\rangle$ and $|J_f M_f \xi\rangle$ using 17 become

$$\left\langle J_f M_f \xi \left| \sum_{k=1}^A e(k) r_k^\lambda Y_{\lambda\mu}(\theta_k, \phi_k) \right| J_i M_i \zeta \right\rangle = \langle J_f m_f | e r^\lambda Y_{\lambda\mu}(\theta, \phi) | j_i m_i \rangle$$

A single-particle wave function can be expressed as the product of three components: a radial wave function $R_{\ell,t}(r)$, an orbital angular momentum part represented by spherical

harmonics $Y_{\ell,m}(\theta, \phi)$, and an intrinsic spin part $\chi_{1/2}$. When coupling $Y_{\ell,m}(\theta, \phi)$ with $\chi_{1/2}$ to angular momentum (j, m) , the resulting expression is:

$$|jm\rangle = R_{n\ell}(r) \{Y_\ell(\theta, \phi) \times \chi_{1/2}\}_{jm}$$

where n is the principal quantum number.

$$\begin{aligned} j_f m_f |er^\lambda Y_{\lambda\mu}| j_t m_1 \rangle &= \int_0^\infty R_{n_f \ell_f}^*(r) er^\lambda R_{n_i \ell_i}(r) r^2 dr \\ &\quad \times \left\langle (Y_{\ell_f}(\theta, \phi) \times \chi_{1/2})_{J_f m_f} |Y_{\lambda\mu}(\theta, \phi)| (Y_{\ell_i}(\theta, \phi) \times \chi_{1/2})_{J_i m_i} \right\rangle \end{aligned} \quad (59)$$

The radial dependence of Eq. 59 is contained in the integral

$$\langle r^\lambda \rangle = \int R_{n_f \ell_f}^*(r) r^\lambda R_{n_i \ell_i}(r) r^2 dr \quad (60)$$

where $R_{n_i \ell_i}$ and $R_{n_f \ell_f}$ are, respectively, the normalized radial wave functions of the initial and final single-particle states. For estimate purpose we can estimate this expectation value by assuming nucleus to be a sphere of uniform density with $R = r_0 A^{1/3}$ to get $\langle r^\lambda \rangle = \frac{3}{\lambda+3} r_0^\lambda A^{\lambda/3}$ (where r_0 is 1.2 fm)

From 52 Reduced transition probability is

$$\begin{aligned} B(\lambda; J_1 \zeta \rightarrow J_f \xi) &= \sum_{\mu M_f} |\langle J_f M_f \xi | \mathbf{O}_{\lambda\mu} | J_i M_i \zeta \rangle|^2 \\ &= e^2 \langle r^\lambda \rangle^2 \sum_{m_f \mu} \left\langle (Y_{\ell_f}(\theta, \phi) \times \chi_{1/2})_{J_f m_f} |Y_{\lambda\mu}(\theta, \phi)| (Y_{\ell_i}(\theta, \phi) \times \chi_{1/2})_{J_i m_i} \right\rangle^2 \end{aligned} \quad (61)$$

As we know the total solid angle about a point is 4π steradians, an average of any angular dependence must be around the value $\frac{1}{4\pi}$. So, estimated reduced transition probability becomes

$$B_{\text{est.}}(E\lambda) = e^2 \langle r^\lambda \rangle^2 \frac{1}{4\pi} \quad (62)$$

Now using $\langle r^\lambda \rangle = \frac{3}{\lambda+3} r_0^\lambda A^{\lambda/3}$ and $r_0 = 1.2$ fm in 62 we obtain the **Weisskopf single-particle estimate** for the λ th multipole reduced electric transition probability,

$$B_W(E\lambda) = \frac{1}{4\pi} \left(\frac{3}{\lambda+3} \right)^2 (1.2)^{2\lambda} A^{2\lambda/3} e^2 \text{fm}^{2\lambda} \quad (63)$$

This value is used as the unit for $E\lambda$ -transition and called the **Weisskopf unit** for reduced transition probability.

4.3.3 $M\lambda$ -transition

Estimating magnetic transitions involves some added complexity, considering contributions from both the intrinsic spin of nucleons and the orbital motion of protons. Taking the

magnetic multipole operator of arbitrary order given in 26 and similar to the electric case as given in 61 we get:

$$\begin{aligned}
B(\lambda; J_1 \zeta \rightarrow J_f \xi) &= \sum_{\mu M_f} |\langle J_f M_f \xi | \mathbf{O}_{\lambda\mu}(M\lambda) | J_i M_i \zeta \rangle|^2 \\
&= \lambda(2\lambda+1) \langle r^{(\lambda-1)} \rangle^2 \\
&\times \sum_{m_j \mu} \left\{ \left(g_s - \frac{2g_\ell}{\lambda+1} \right) \right. \\
&\times \left\langle (Y_{\ell_l}(\theta, \phi) \times \chi_{1/2})_{j_f m_f} \left| (Y_{(\lambda-1)}(\theta, \phi) \times s)_{\lambda\mu} \right| (Y_{\ell_i}(\theta, \phi) \times \chi_{1/2})_{j_i m_i} \right\rangle \\
&+ \left. \frac{2g_\varepsilon}{\lambda+1} \left\langle (Y_{\ell_f}(\theta, \phi) \times \chi_{1/2})_{j_f m_f} \left| (Y_{(\lambda-1)}(\theta, \phi) \times j)_{\lambda\mu} \right| (Y_{\ell_1}(\theta, \phi) \times \chi_{1/2})_{j_i m_i} \right\rangle \right\}^2
\end{aligned} \tag{64}$$

Similar to the previous case taking nucleus to be a sphere of uniform density with $R = r_0 A^{1/3}$ to get $\langle r^{(\lambda-1)} \rangle = \frac{3}{\lambda+3} r_0^{(\lambda-1)} A^{(\lambda-1)/3}$ (where r_0 is 1.2 fm). The first term, which involves the gyromagnetic ratios, may have factors replaced by a reasonable average value. This is typically considered to be

$$\lambda(2\lambda+1) \left(g_s - \frac{2g_\ell}{\lambda+1} \right)^2 \approx 10$$

For the average of the square of the angular part, we can once again adopt the previously used value for $E\lambda$ -transitions i.e. $\frac{1}{4\pi}$. This yields the following result:

$$B_W(M\lambda) = \frac{10}{\pi} \left(\frac{3}{\lambda+3} \right)^2 (1.2)^{2\lambda-2} A^{(2\lambda-2)/3} \mu_N^2 \text{fm}^{2\lambda-2} \tag{65}$$

as the final expression for the **Weisskopf estimate of the reduced magnetic multipole transition probability**.

Using the calculated values of reduced transition probability for both electric and magnetic transitions in 63 and 65 in Eq. 55 yields the **Weisskopf units for transition probability**:

$$\mathcal{W}_W(E\lambda) = \alpha \hbar c \frac{8\pi(\lambda+1)}{\lambda[(2\lambda+1)!!]^2} \frac{1}{\hbar} \left(\frac{1}{\hbar c} \right)^{2\lambda+1} \frac{1}{4\pi} \left(\frac{3}{\lambda+3} \right)^2 (1.2)^{2\lambda} A^{2\lambda/3} E^{2\lambda+1}$$

$$\mathcal{W}_W(M\lambda) = \alpha \hbar c \left(\frac{\hbar}{2M_p c} \right)^2 \frac{8\pi(\lambda+1)}{\lambda[(2\lambda+1)!!]^2} \frac{1}{\hbar} \left(\frac{1}{\hbar c} \right)^{2\lambda+1} \frac{10}{\pi} \left(\frac{3}{\lambda+3} \right)^2 (1.2)^{2\lambda-2} A^{(2\lambda-2)/3} E^{2\lambda+1}$$

Explicit values in terms of nucleon number A and transition energy E are provided in the following Table.

Order λ	$E\lambda$			$M\lambda$		
	$\mathcal{W}(\text{s}^{-1})$	$\Gamma(\text{MeV})$	$A^{2/3}E_\gamma^3$	$\mathcal{W}(\text{s}^{-1})$	$\Gamma(\text{MeV})$	E_γ^3
1	1.02×10^{14}	6.75×10^{-8}	$A^{2/3}E_\gamma^3$	3.15×10^{13}	2.07×10^{-8}	E_γ^3
2	3.28×10^7	4.79×10^{-14}	$A^{4/3}E_\gamma^5$	2.24×10^7	1.47×10^{-14}	$A^{2/3}E_\gamma^5$
3	1.07×10^{-5}	7.02×10^{-27}	$A^{8/3}E_\gamma^9$	3.27×10^{-6}	2.16×10^{-27}	$A^2E_\gamma^9$
4	2.40×10^{-12}	1.58×10^{-33}	$A^{10/3}E_\gamma^{11}$	7.36×10^{-13}	4.84×10^{-34}	$A^{8/3}E_\gamma^{11}$

E_γ in MeV. The E_γ - and A – dependent factors are common to both \mathcal{W} and Γ .

For a transition to exhibit an enhancement of an order of magnitude or more compared to the estimated single-particle values, a collective behavior of many nucleons must come into play. This concept is manifested in the form of collective motion, such as nuclear vibrations and rotations.

5 Angular Distribution of Multipole Radiation

5.1 Fields and Radiation of a Localized Oscillating Source

For a system involving charges and currents that change over time, we can perform a Fourier analysis of the temporal variations and address each Fourier component individually. Therefore, it is not restrictive to examine the potentials, fields, and radiation arising from a localized system of charges and currents undergoing sinusoidal time variations[19].

$$\begin{aligned}\rho(\mathbf{x}, t) &= \rho(\mathbf{x})e^{-i\omega t} \\ \mathbf{J}(\mathbf{x}, t) &= \mathbf{J}(\mathbf{x})e^{-i\omega t}\end{aligned}$$

From 41 invoking the gauge condition we get (In SI Units):

$$\left(\nabla^2 \mathbf{A} - \frac{1}{c^2} \frac{\partial^2 \mathbf{A}}{\partial t^2} \right) = -\mu_0 \mathbf{J}$$

To solve this non-homogeneous wave equation for \mathbf{A} we have

$$\Psi(\mathbf{x}, t) = \Psi_{\text{homog.}}(\mathbf{x}, t) + \iint G^{(\pm)}(\mathbf{x}, t; \mathbf{x}', t') f(\mathbf{x}', t') d^3x' dt'$$

as the solution for the equation of type $\left(\nabla_x^2 - \frac{1}{c^2} \frac{\partial^2}{\partial t^2} \right) \Psi(\mathbf{x}, t) = -4\pi\delta(\mathbf{x}, t)$

Hence comparing both and leaving the homogeneous part we get:

$$\mathbf{A}(\mathbf{x}, t) = \frac{\mu_0}{4\pi} \int d^3x' \int dt' \frac{\mathbf{J}(\mathbf{x}', t')}{|\mathbf{x} - \mathbf{x}'|} \delta\left(t' + \frac{|\mathbf{x} - \mathbf{x}'|}{c} - t\right) \quad (66)$$

$$\text{where } f(\mathbf{x}', t') = \frac{\mu_0}{4\pi} \mathbf{J} \text{ and } G^{(\pm)}(\mathbf{x}, t; \mathbf{x}', t') = \frac{\delta\left(t' - \left[t \mp \frac{|\mathbf{x} - \mathbf{x}'|}{c}\right]\right)}{|\mathbf{x} - \mathbf{x}'|} \quad (67)$$

Using the current distribution of a system $\mathbf{A}(\mathbf{x}, t)$ can be calculated. From it $\vec{\mathbf{B}}$ can be calculated from it $\vec{\mathbf{E}}$ and eventually poynting vector also can be calculated using the following expressions

$$\vec{\mathbf{B}} = \nabla \times \mathbf{A}(\mathbf{x}, t) = \mu \vec{\mathbf{H}} \implies \boxed{\vec{\mathbf{H}} = \frac{\nabla \times \mathbf{A}}{\mu_0}} \quad (68)$$

$$\nabla \times \vec{\mathbf{H}} = \mathbf{J} + \epsilon_0 \frac{\partial \mathbf{E}}{\partial t} = i\omega \epsilon_0 \mathbf{E} \text{ (as } J = 0 \text{ at the point of observation } (\mathbf{x}, t) \text{ and } \frac{\partial}{\partial t} = -i\omega)$$

$$\implies \boxed{E = \frac{i(\nabla \times \mathbf{H})}{\epsilon_0(kc)} = i \frac{Z_0}{k} \nabla \times \mathbf{H}} \text{ (where } Z_0 \text{ is the impedance of free space)} \quad (69)$$

From 66 we get:

$$\mathbf{A}(\mathbf{x}, t) = \frac{\mu_0}{4\pi} \int d^3x' \frac{\mathbf{J}(\mathbf{x}')}{|\mathbf{x} - \mathbf{x}'|} e^{ik|\mathbf{x} - \mathbf{x}'|} e^{-i\omega t} = \mathbf{A}(\mathbf{x}) e^{-i\omega t} \quad (70)$$

If the source dimensions are of order d and the wavelength is $\lambda = 2\pi c/\omega$, and if $d \ll \lambda$, then there are three spatial regions of interest:

1. The near (static) zone: $d \ll r \ll \lambda$
2. The intermediate (induction) zone: $d \ll r \sim \lambda$
3. The far (radiation) zone: $d \ll \lambda \ll r$

Consider $\int_V \nabla_x \cdot (x'_i \mathbf{J}(\mathbf{x}')) d^3x' = \int_S (x'_i \mathbf{J}(\mathbf{x}')) \cdot \hat{n} da' = 0$ (as at $\infty \mathbf{J}(\mathbf{x}') = 0$)
Hence,

$$\begin{aligned} \int_V \nabla_x \cdot (x'_i \mathbf{J}(\mathbf{x}')) d^3x' &= \int_V \nabla_x x'_i \cdot (\mathbf{J}(\mathbf{x}')) d^3x' + \int_V x'_i (\nabla_x \cdot \mathbf{J}(\mathbf{x}')) d^3x' \\ &= \int_V \hat{n}'_i \cdot (\mathbf{J}(\mathbf{x}')) d^3x' + \int_V x'_i (i\omega\rho) d^3x' \text{ (using } \nabla_x \cdot \mathbf{J}(\mathbf{x}') = -\frac{\partial \rho}{\partial t} = i\omega\rho) \\ \implies \boxed{\int (\mathbf{J}_i(\mathbf{x}')) d^3x' = -i\omega \vec{p}} \end{aligned} \quad (71)$$

where $\vec{p} = \int_V x'_i \rho d^3x'$ is the dipole moment oscillating in time but is a constant vector $|\mathbf{x} - \mathbf{x}'| \approx r - \hat{n} \cdot \vec{x}'$ and $|\mathbf{x}| = r$ So, we have,

• For far Field Zone

From 70 the spatial part of $\mathbf{A}(\mathbf{x}, t)$ becomes

$$\begin{aligned} \mathbf{A}(\mathbf{x}) &= \frac{\mu_0}{4\pi} \int d^3x' \frac{\mathbf{J}(\mathbf{x}')}{|r - \hat{n} \cdot \vec{x}'|} e^{ik|r - \hat{n} \cdot \vec{x}'|} = \frac{\mu_0}{4\pi} \frac{e^{ikr}}{r} \int d^3x' \mathbf{J}(\mathbf{x}') e^{-ik(\hat{n} \cdot \vec{x}')} \\ &= \frac{\mu_0}{4\pi} \frac{e^{ikr}}{r} \int d^3x' \mathbf{J}(\mathbf{x}') \left(\sum_{k=0}^{\infty} \frac{(-ik)^n}{n!} (\hat{n} \cdot \vec{x}')^n \right) \end{aligned} \quad (72)$$

If we take only the first term i.e. $n = 0$ of 72 we get:

$$\mathbf{A}(\mathbf{x}) = \frac{\mu_0}{4\pi} \frac{e^{ikr}}{r} (-i\omega \vec{p})$$

Hence using 68 we have

$$\begin{aligned} \vec{\mathbf{H}} &= \frac{\nabla \times \mathbf{A}}{\mu_0} = \frac{-i\omega}{4\pi} \left[\vec{\nabla} \left(\frac{e^{ikr}}{r} \right) \times (\vec{p}) + \left(\frac{e^{ikr}}{r} \right) \vec{\nabla} \times \vec{p} \right] \\ &= \frac{-i\omega}{4\pi} \left[ik \left(\frac{e^{ikr}}{r} \right) - \left(\frac{e^{ikr}}{r^2} \right) \right] (\hat{n} \times \vec{p}) \quad (\text{as } \vec{p} \text{ is const. } \vec{\nabla} \times \vec{p} = 0 = \vec{\nabla} \cdot \vec{p}) \\ \implies \boxed{\vec{\mathbf{H}} = \frac{ck^2 e^{ikr}}{4\pi r} \left(1 - \frac{1}{ikr} \right) \hat{n} \times \vec{p}} \end{aligned} \quad (73)$$

$$\begin{aligned} E &= i \frac{Z_0}{k} \nabla \times \mathbf{H} = i \sqrt{\frac{\mu_0}{\epsilon_0}} \cdot \frac{1}{k} \cdot \frac{ck^2}{4\pi} \times \left(\frac{e^{ikr}}{r} \left(1 - \frac{1}{ikr} \right) \hat{n} \times \vec{p} \right) \\ &= \frac{ik}{4\pi\epsilon_0} \nabla \times \left[(\hat{n} \times \vec{p}) \frac{e^{ikr}}{r} \left(1 - \frac{1}{ikr} \right) \right] \\ &= \frac{ik}{4\pi\epsilon_0} \left(\nabla \left[\frac{e^{ikr}}{r} \left(1 - \frac{1}{ikr} \right) \right] \times (\hat{n} \times \vec{p}) + \left[\frac{e^{ikr}}{r} \left(1 - \frac{1}{ikr} \right) \right] \nabla \times (\hat{n} \times \vec{p}) \right) \\ &= \frac{ik}{4\pi\epsilon_0} \left(\left[\frac{ike^{ikr}}{r} - \frac{2e^{ikr}}{r^2} + \frac{2e^{ikr}}{ikr^3} \right] [(\hat{n} \cdot \vec{p}) \hat{n} - \vec{p}] - \left[\frac{e^{ikr}}{r} \left(1 - \frac{1}{ikr} \right) \right] \left[\frac{\vec{p}}{r} + \frac{(\vec{p} \cdot \hat{n}) \hat{n}}{r} \right] \right) \end{aligned}$$

$$\boxed{\vec{\mathbf{E}} = \frac{1}{4\pi\epsilon_0} \left[k^2 (\hat{n} \times \vec{p}) \times \hat{n} \frac{e^{ikr}}{r} + (3(\hat{n} \cdot \vec{p}) \hat{n} - \vec{p}) \left(\frac{1}{r^3} - \frac{ik}{r^2} \right) e^{ikr} \right]} \quad (74)$$

It is observed that the magnetic field is always perpendicular to the radius vector at any distance. On the contrary, the electric field has components both parallel and perpendicular to \mathbf{n} .

- In the radiation zone/far field zone (i.e. $kr \gg 1$), the fields assume their limiting forms.

$$\mathbf{H} = \frac{ck^2}{4\pi} (\mathbf{n} \times \mathbf{p}) \frac{e^{ikr}}{r} \quad (75)$$

$$\mathbf{E} = Z_0 \mathbf{H} \times \mathbf{n} \quad (76)$$

illustrating the typical behavior of radiation fields.

- In the near zone ($kr \ll 1$ or $r \ll \lambda$) we have,

$$\begin{aligned} \mathbf{H} &= \frac{i\omega}{4\pi} (\mathbf{n} \times \mathbf{p}) \frac{1}{r^2} \\ \mathbf{E} &= \frac{1}{4\pi\epsilon_0} [3\mathbf{n}(\mathbf{n} \cdot \mathbf{p}) - \mathbf{p}] \frac{1}{r^3} \end{aligned}$$

- The product of the magnetic field and the impedance Z_0 is a factor (kr) smaller than the electric field in the region where $kr \ll 1$. Thus, the fields in the near zone are predominantly electric in nature.

The power radiated per unit solid angle by the oscillating dipole moment \mathbf{p} , averaged over time, is given by

$$\frac{dP}{d\Omega} = \frac{1}{2} \operatorname{Re} [r^2 \mathbf{n} \cdot \mathbf{E} \times \mathbf{H}^*] \quad (77)$$

where \mathbf{E} and \mathbf{H} are given by 75 and 76. So, putting 76 in 77 we get

$$\begin{aligned} \frac{dP}{d\Omega} &= \frac{Z_0}{2} \operatorname{Re} [r^2 \mathbf{n} \cdot (|\mathbf{H}|^2 \mathbf{n} - \mathbf{H}^* \cdot \mathbf{n})] = \frac{Z_0}{2} r^2 |\mathbf{H}|^2 \\ &= \frac{c^2 Z_0}{32\pi^2} k^4 |(\mathbf{n} \times \mathbf{p})|^2 = \frac{c^2 Z_0}{32\pi^2} k^4 |\mathbf{p}|^2 \sin^2 \theta \end{aligned} \quad (78)$$

The total power radiated, is

$$P = \int \frac{dP}{d\Omega} d\Omega = \frac{c^2 Z_0 k^4}{12\pi} |\mathbf{p}|^2$$

5.2 Multipole Expansion of the Electromagnetic Fields

Assuming a time dependence $e^{-i\omega t}$, the Maxwell equations in a source-free region of empty space can be expressed as,

$$\begin{aligned} \nabla \times \mathbf{E} &= ik Z_0 \mathbf{H}, \quad \nabla \times \mathbf{H} = -ik \mathbf{E}/Z_0 \\ \nabla \cdot \mathbf{E} &= 0 \quad \nabla \cdot \mathbf{H} = 0 \end{aligned}$$

where $k = \frac{\omega}{c}$. If \mathbf{E} is eliminated by combining the two curl equations, we obtain for \mathbf{H} ,

$$(\nabla^2 + k^2) \mathbf{H} = 0, \quad \nabla \cdot \mathbf{H} = 0 \quad (79)$$

and \mathbf{E} is given by

$$\mathbf{E} = \frac{i Z_0}{k} \nabla \times \mathbf{H} \quad (80)$$

Similarly, \mathbf{H} can be eliminated to give,

$$(\nabla^2 + k^2) \mathbf{E} = 0, \quad \nabla \cdot \mathbf{E} = 0 \quad (81)$$

and \mathbf{H} is given by

$$\mathbf{H} = -\frac{i}{k Z_0} \nabla \times \mathbf{E} \quad (82)$$

We want to find multipole solutions for 79,80 and 81,82. From these equations it is clear that the Cartesian component of \mathbf{H} and \mathbf{E} satisfies the Helmholtz wave equation

$$(\nabla^2 + k^2) \psi(\mathbf{x}, \omega) = 0$$

whose solution in cylindrical coordinates can be written as

$$\psi(\mathbf{x}) = \sum_{l,m} \left[A_{lm}^{(1)} h_l^{(1)}(kr) + A_{lm}^{(2)} h_l^{(2)}(kr) \right] Y_{lm}(\theta, \phi) = \sum_{l,m} [g_l(kr)] Y_{lm}(\theta, \phi) \quad (83)$$

where the coefficients $A_{lm}^{(1)}$ and $A_{lm}^{(2)}$ will be determined by the boundary conditions.

Studying the angular functions to introduce concepts useful in analyzing the vector wave equation.

The basic angular functions are the spherical harmonics $Y_{lm}(\theta, \phi)$, which are the solutions of the equation,

$$-\left[\frac{1}{\sin \theta} \frac{\partial}{\partial \theta} \left(\sin \theta \frac{\partial}{\partial \theta} \right) + \frac{1}{\sin^2 \theta} \frac{\partial^2}{\partial \phi^2} \right] Y_{lm} = l(l+1) Y_{lm} \quad (84)$$

This equation can be written as in QM as $L^2 Y_{lm} = l(l+1) Y_{lm}$ where, $L^2 = L_x^2 + L_y^2 + L_z^2$ and \mathbf{L} operator is

$$\mathbf{L} = \frac{1}{i} (\mathbf{r} \times \nabla) \implies \mathbf{r} \cdot \mathbf{L} = 0 \quad (85)$$

. The components of \mathbf{L} are,

$$\begin{aligned} L_+ &= L_x + i L_y = e^{i\phi} \left(\frac{\partial}{\partial \theta} + i \cot \theta \frac{\partial}{\partial \phi} \right) \\ L_- &= L_x - i L_y = e^{-i\phi} \left(-\frac{\partial}{\partial \theta} + i \cot \theta \frac{\partial}{\partial \phi} \right) \\ L_z &= -i \frac{\partial}{\partial \phi} \end{aligned} \quad (86)$$

\mathbf{L} operator operates only on angular variables and is independent of \mathbf{r} . From 86 we can verify that

$$L^2 = - \left[\frac{1}{\sin \theta} \frac{\partial}{\partial \theta} \left(\sin \theta \frac{\partial}{\partial \theta} \right) + \frac{1}{\sin^2 \theta} \frac{\partial^2}{\partial \phi^2} \right]$$

As we know from QM we have

$$\begin{aligned} L_+ Y_{lm} &= \sqrt{(l-m)(l+m+1)} Y_{l,m+1} \\ L_- Y_{lm} &= \sqrt{(l+m)(l-m+1)} Y_{l,m-1} \\ L_z Y_{lm} &= m Y_{lm} \end{aligned} \quad (87)$$

Finally, we observe the following operator equations regarding the commutation properties of \mathbf{L} , L^2 , and ∇^2 :

$$\left. \begin{array}{l} L^2 \mathbf{L} = \mathbf{L} L^2 \\ \mathbf{L} \times \mathbf{L} = i \mathbf{L} \\ L_j \nabla^2 = \nabla^2 L_j \end{array} \right\} \text{ where } \nabla^2 = \frac{1}{r} \frac{\partial^2}{\partial r^2}(r) - \frac{L^2}{r^2} \quad (88)$$

Examining the scalar quantity $\mathbf{r} \cdot \mathbf{A}$, where \mathbf{A} is a well-behaved vector field, it is straightforward to confirm that the Laplacian operator acting on this scalar results in

$$\nabla^2(\mathbf{r} \cdot \mathbf{A}) = \mathbf{r} \cdot (\nabla^2 \mathbf{A}) + 2 \nabla \cdot \mathbf{A}$$

From 79,80 and 81,82 it follows that the scalars $\mathbf{r} \cdot \mathbf{E}$ and $\mathbf{r} \cdot \mathbf{H}$ both satisfy Helmholtz wave equation:

$$(\nabla^2 + k^2)(\mathbf{r} \cdot \mathbf{E}) = 0, \quad (\nabla^2 + k^2)(\mathbf{r} \cdot \mathbf{H}) = 0$$

Taking $(\nabla^2 + k^2)(\mathbf{r} \cdot \mathbf{E}) = 0$ the general solution for $\mathbf{r} \cdot \mathbf{E}$ is given by 83. Now we define a **magnetic multipole field of order** (l, m) by the conditions

$$\mathbf{r} \cdot \mathbf{H}_{lm}^{(M)} = \frac{l(l+1)}{k} g_l(kr) Y_{lm}(\theta, \phi) \quad (89)$$

$$\mathbf{r} \cdot \mathbf{E}_{lm}^{(M)} = 0 \quad (90)$$

where,

$$g_l(kr) = A_l^{(1)} h_l^{(1)}(kr) + A_l^{(2)} h_l^{(2)}(kr) \quad (91)$$

Using 82 and 85 gives

$$\begin{aligned} \mathbf{r} \cdot \mathbf{H} &= \mathbf{r} \cdot \left(-\frac{i}{kZ_0} \boldsymbol{\nabla} \times \mathbf{E} \right) \\ \implies Z_0 kr \cdot \mathbf{H} &= \frac{1}{i} \mathbf{r} \cdot (\boldsymbol{\nabla} \times \mathbf{E}) = \frac{1}{i} (\mathbf{r} \times \boldsymbol{\nabla}) \cdot \mathbf{E} = \mathbf{L} \cdot \mathbf{E} \end{aligned} \quad (92)$$

From 89,90 and 92 we have:

$$\mathbf{L} \cdot \mathbf{E}_{lm}^{(M)}(r, \theta, \phi) = l(l+1) Z_0 g_l(kr) Y_{lm}(\theta, \phi) \quad \mathbf{r} \cdot \mathbf{E}_{lm}^{(M)} = 0 \quad (93)$$

To obtain the purely transverse electric field from equation 93, it is noteworthy that the operator \mathbf{L} acts solely on the angular variables (θ, ϕ) . This implies that the radial dependence of $\mathbf{E}_{lm}^{(M)}$ must be expressed as $g_l(kr)$.

Secondly, when the operator \mathbf{L} acts on Y_{lm} , it transforms the m value according to 87 but does not alter the l value. Consequently, the components of $\mathbf{E}_{lm}^{(M)}$ can, at most, be linear combinations of Y_{lm} 's with different m values and a common l value, equal to the l value on the right-hand side of 93. Upon further consideration, it becomes apparent that for $\mathbf{L} \cdot \mathbf{E}_{lm}^{(M)}$ to yield a single Y_{lm} , the components of $\mathbf{E}_{lm}^{(M)}$ must be prepared beforehand to compensate for whatever raising or lowering of m values is performed by \mathbf{L} . In the case of the term $\mathbf{L} \cdot \mathbf{E}_+$, for instance, it must be that \mathbf{E}_+ is proportional to $\mathbf{L}_+ Y_{lm}$. This essentially implies that the electric field should be

$$\mathbf{E}_{lm}^{(M)} = Z_0 g_l(kr) \mathbf{L} Y_{lm}(\theta, \phi) \quad \mathbf{H}_{lm}^{(M)} = -\frac{i}{kZ_0} \boldsymbol{\nabla} \times \mathbf{E}_{lm}^{(M)} \quad (94)$$

This is the electromagnetic fields of a magnetic multipole of order (l, m) . $\mathbf{E}_{lm}^{(M)}$ is transverse to the radius vector, these multipole fields are sometimes called transverse electric (TE) rather than magnetic.

Similarly solving the equation $(\nabla^2 + k^2)(\mathbf{r} \cdot \mathbf{H}) = 0$ gives in a similar fashion the fields of an electric or transverse magnetic (TM) multipole of order (l, m) are :

$$\begin{aligned} \mathbf{r} \cdot \mathbf{E}_{lm}^{(E)} &= -Z_0 \frac{l(l+1)}{k} f_l(kr) Y_{lm}(\theta, \phi) \\ \mathbf{r} \cdot \mathbf{H}_{lm}^{(E)} &= 0 \end{aligned}$$

Solving this in a similar manner gives:

$$\mathbf{H}_{lm}^{(E)} = f_l(kr) \mathbf{L} Y_{lm}(\theta, \phi) \quad \mathbf{E}_{lm}^{(E)} = \frac{i Z_0}{k} \nabla \times \mathbf{H}_{lm}^{(E)} \quad (95)$$

$f_l(kr)$ is given by an expression like 91. Since the vector spherical harmonic, $\mathbf{L} Y_{lm}$. Given its significant role, introducing the normalized form becomes convenient.

$$\mathbf{X}_{lm}(\theta, \phi) = \frac{1}{\sqrt{l(l+1)}} \mathbf{L} Y_{lm}(\theta, \phi)$$

$$\begin{aligned} \int \mathbf{X}_{l'm'}^* \cdot \mathbf{X}_{lm} d\Omega &= \int \frac{1}{l(l+1)} (\mathbf{L} Y_{lm}(\theta, \phi))^* (\mathbf{L} Y_{lm}(\theta, \phi)) d\Omega \\ &= \int \frac{1}{l(l+1)} (Y_{lm}^*(\theta, \phi) \mathbf{L}^2 Y_{lm}(\theta, \phi)) d\Omega \\ &= \int \delta_{ll'} \delta_{mm'} d\Omega \text{ (as } \mathbf{L}^2 Y_{lm} = l(l+1) Y_{lm} \text{ & } Y_{lm}^* Y_{lm} = \delta_{ll'} \delta_{mm'}) \\ &= 1 \end{aligned} \quad (96)$$

By combining the two types of fields, we can express the general solution to the Maxwell equations as (using 94 and 95):

$$\begin{aligned} \mathbf{E} &= \sum_{l,m} \left(\mathbf{E}_{lm}^{(E)} + \mathbf{E}_{lm}^{(M)} \right) \\ &= \sum_{l,m} \left(a_E(l, m) \frac{i Z_0}{k} \nabla \times (f_l(kr) \mathbf{L} Y_{lm}(\theta, \phi)) + a_M(l, m) Z_0 g_l(kr) \mathbf{L} Y_{lm}(\theta, \phi) \right) \\ &= Z_0 \sum_{l,m} \left[\frac{i}{k} a_E(l, m) \nabla \times f_l(kr) \mathbf{X}_{lm} + a_M(l, m) g_l(kr) \mathbf{X}_{lm} \right] \end{aligned} \quad (97)$$

$$\begin{aligned} \mathbf{H} &= \sum_{l,m} \left(\mathbf{H}_{lm}^{(E)} + \mathbf{H}_{lm}^{(M)} \right) \\ &= \sum_{l,m} \left(a_E(l, m) f_l(kr) \mathbf{L} Y_{lm}(\theta, \phi) + a_M(l, m) \left(-\frac{i}{k Z_0} \nabla \times (Z_0 g_l(kr) \mathbf{L} Y_{lm}(\theta, \phi)) \right) \right) \\ &= \sum_{l,m} \left[a_E(l, m) f_l(kr) \mathbf{X}_{lm} - \frac{i}{k} a_M(l, m) \nabla \times g_l(kr) \mathbf{X}_{lm} \right] \end{aligned} \quad (98)$$

where the coefficients $a_E(l, m)$ and $a_M(l, m)$ specify the amounts of electric (l, m) multipole and magnetic (l, m) multipole fields. Now to find these coefficients let's take:

$$\begin{aligned} \int \mathbf{X}_{l'm'}^* \cdot \mathbf{E} d\Omega &= Z_0 \sum_{l,m} \left[\frac{i}{k} a_E(l, m) \int \mathbf{X}_{l'm'}^* \cdot (\nabla \times f_l(kr) \mathbf{X}_{lm}) d\Omega + a_M(l, m) g_l(kr) \int \mathbf{X}_{l'm'}^* \cdot \mathbf{X}_{lm} d\Omega \right] \\ &\Rightarrow \int \frac{1}{\sqrt{l(l+1)}} \mathbf{L}^* Y_{lm}^*(\theta, \phi) \cdot \mathbf{E} d\Omega = Z_0 \sum_{l,m} a_M(l, m) g_l(kr) \delta_{ll'} \delta_{mm'} \\ &\int \frac{Z_0 k \mathbf{r} \cdot \mathbf{H}}{\sqrt{l(l+1)}} Y_{lm}^*(\theta, \phi) d\Omega = Z_0 a_M(l'm') g_{l'}(kr) \text{ (using 92)} \end{aligned}$$

So, we get

$$a_M(l, m)g_l(kr) = \frac{k}{\sqrt{l(l+1)}} \int Y_{lm}^* \mathbf{r} \cdot \mathbf{H} d\Omega$$

Similarly,

$$Z_0 a_E(l, m)f_l(kr) = -\frac{k}{\sqrt{l(l+1)}} \int Y_{lm}^* \mathbf{r} \cdot \mathbf{E} d\Omega$$

Knowledge of $\mathbf{r} \cdot \mathbf{H}$ and $\mathbf{r} \cdot \mathbf{E}$ at two different radii, r_1 and r_2 , in a source-free region will therefore permit a complete specification of the fields.

5.3 Angular Distribution of Multipole Radiation

For a general localized source distribution, the fields in the radiation zone ($kr \gg 1$) using 98 by taking $g_l(kr) = f_l(kr) = \frac{(-i)^{l+1} e^{ikr}}{kr}$ and introducing time dependence $e^{i\omega t}$ are given by

$$\begin{aligned} \mathbf{H} &\rightarrow \frac{e^{ikr-i\omega t}}{kr} \sum_{l,m} (-i)^{l+1} [a_E(l, m) \mathbf{X}_{lm} + a_M(l, m) \mathbf{n} \times \mathbf{X}_{lm}] \\ \mathbf{E} &\rightarrow Z_0 \mathbf{H} \times \mathbf{n} \end{aligned}$$

The coefficients $a_E(l, m)$ and $a_M(l, m)$ will be related to the properties of the source. As we already derived in 78 for radiation zone total power emitted per solid angle is given by:

$$\begin{aligned} \frac{dP}{d\Omega} &= \frac{Z_0}{2} r^2 |\mathbf{H}|^2 \\ &= \frac{Z_0}{2k^2} \left| \sum_{l,m} (-i)^{l+1} [a_M(l, m) (\mathbf{X}_{lm} \times \mathbf{n}) + a_E(l, m) \mathbf{X}_{lm}] \right|^2 \end{aligned} \quad (99)$$

The polarization of the radiation is determined by the orientations of the vectors. It is noteworthy that electric and magnetic multipoles of a given (l, m) share the same angular dependence but exhibit polarizations perpendicular to each other. As a result, the multipole order can be identified by measuring the angular distribution of radiated power, while the nature of the radiation (electric or magnetic) can be discerned only through polarization measurements.

For a pure multipole of order (l, m) the angular distribution 99 reduces to a single term,

$$\frac{dP(l, m)}{d\Omega} = \frac{Z_0}{2k^2} |a(l, m)|^2 |\mathbf{X}_{lm}|^2 \quad (100)$$

$$\begin{aligned}
|\mathbf{X}_{lm}|^2 &= \mathbf{X}_{x_{lm}}^2 + \mathbf{X}_{y_{lm}}^2 + \mathbf{X}_{z_{lm}}^2 \\
&= \frac{1}{l(l+1)} [(L_x Y_{lm})^2 + (L_y Y_{lm})^2 + (L_z Y_{lm})^2] \\
&= \frac{1}{l(l+1)} \left[\left(\frac{L_+ + L_-}{2} Y_{lm} \right)^2 + \left(\frac{L_+ - L_-}{2} Y_{lm} \right)^2 + (m Y_{lm})^2 \right] \text{(using } L_{\pm} = L_x \pm i L_y) \\
&= \frac{1}{l(l+1)} \left[\frac{1}{2} (L_+ Y_{lm})^2 + \frac{1}{2} (L_- Y_{lm})^2 + (m Y_{lm})^2 \right] \text{(using 87)} \\
&= \left\{ \frac{1}{2}(l-m)(l+m+1) |Y_{l,m+1}|^2 + \frac{1}{2}(l+m)(l-m+1) |Y_{l,m-1}|^2 + m^2 |Y_{lm}|^2 \right\}
\end{aligned}$$

Hence, 100 becomes

$$\boxed{\frac{dP(l, m)}{d\Omega} = \frac{Z_0 |a(l, m)|^2}{2k^2 l(l+1)} \left\{ \frac{1}{2}(l-m)(l+m+1) |Y_{l,m+1}|^2 + \frac{1}{2}(l+m)(l-m+1) |Y_{l,m-1}|^2 + m^2 |Y_{lm}|^2 \right\}} \quad (101)$$

The dipole distributions are observed to correspond to a dipole oscillating parallel to the z-axis ($m = 0$) and two dipoles, one along the x-axis and one along the y-axis, 90° out of phase ($m = \pm 1$). The dipole and quadrupole angular distributions are depicted as polar intensity diagrams in Fig. 5. These diagrams are illustrative of $l = 1$ and $l = 2$ multipole angular distributions, while a general multipole distribution of order l will entail a coherent superposition of the $(2l+1)$ amplitudes for different m , as depicted in the previous equation.

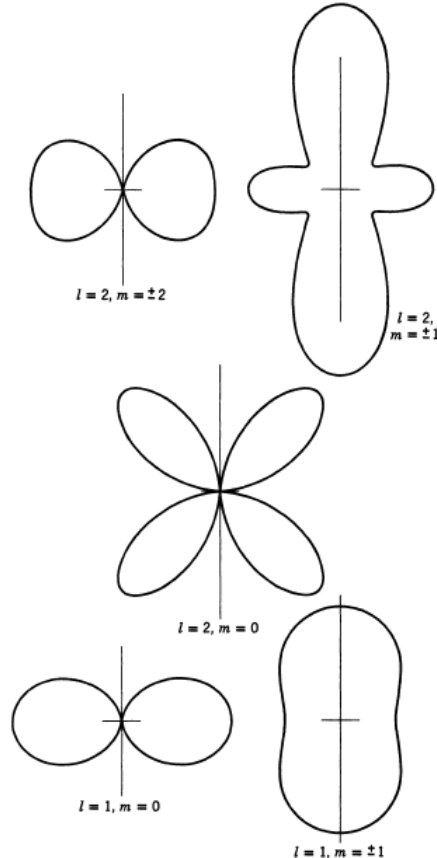


Figure 5: Dipole and quadrupole radiation patterns for pure (l, m) multipoles.

Some Angular Distributions: $|\mathbf{X}_{lm}(\theta, \phi)|^2$

l	0	m	
		± 1	± 2
1 Dipole	$\frac{3}{8\pi} \sin^2 \theta$	$\frac{3}{16\pi} (1 + \cos^2 \theta)$	
Quadrupole	$\frac{15}{8\pi} \sin^2 \theta \cos^2 \theta$	$\frac{5}{16\pi} (1 - 3 \cos^2 \theta + 4 \cos^4 \theta)$	$\frac{5}{16\pi} (1 - \cos^4 \theta)$

The total power radiated by a pure multipole of order (l, m) is determined by integrating 100 across all angles. Given that the \mathbf{X}_{lm} functions are normalized to unity, the radiated power can be expressed as

$$P = \int \frac{dP}{d\Omega} d\Omega = \int \frac{Z_0}{2k^2} |a(l, m)|^2 |\mathbf{X}_{lm}|^2 d\Omega = \frac{Z_0}{2k^2} |a(l, m)|^2 \text{(using 96)}$$

For a general source, the angular distribution is described by the coherent sum 99. Upon integration over angles, it can be demonstrated that the interference terms do not contribute. Consequently, the total power radiated is simply an incoherent sum of contributions from the different multipoles.

$$P = \frac{Z_0}{2k^2} \sum_{l,m} [|a_E(l, m)|^2 + |a_M(l, m)|^2]$$

While a complete exploration of radiative transitions in atoms and nuclei necessitates a quantum-mechanical approach, we can gain insights into the qualitative aspects through semi-classical arguments and straightforward estimates of the effective multipole moments using classical formulas. Blatt and Weisskopf[19], Chapter XII, provides a comprehensive quantum-mechanical treatment of multipole radiation.

6 Lifetimes of excited states

In order to measure the lifetime of an excited state, it has to be populated using a nuclear reaction chosen to optimize the conditions required for accurate measurement. Once populated, the state will remain excited for a mean lifetime τ which is related to its intrinsic width Γ by the Heisenberg uncertainty principle such that $\Gamma\tau \geq \hbar$. As the state is an excited one there is a finite probability of decay to some state of lower energy. The probability of decay is proportional to Γ and is determined by the matrix element of the decay operator[5, 3]

$$\Gamma \propto |\langle \psi_f | \hat{O}_{\text{decay}} | \psi_i \rangle|^2$$

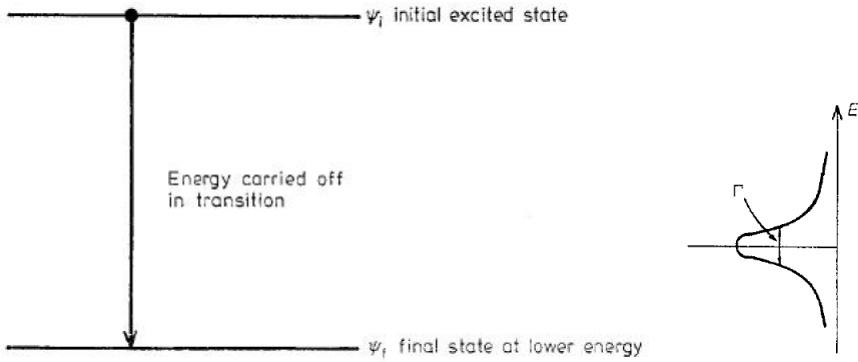


Figure 6: Schematic diagram of a decay of an excited state of a nucleus having a decay width Γ . The mean lifetime of the level $\tau = \hbar/\Gamma$ and $\hat{O}_{\text{decay}} = \sum_{L,\mu} \{\hat{O}(EL)_\mu + \hat{O}(ML)_\mu\}$

From lifetimes of a nuclear state we can get decay probabilities of that transition. The lifetimes of the decay thus reveal information on the nature of the states. The lifetime can be compared with Weisskopf single particle estimates to help constrain the spin difference between the initial and final states, or if this is already known (from for example angular correlation data) it can be used to deduce other properties such as determining nuclear quadrupole deformation from lifetimes of E2 transitions.

6.1 Historical Background

In 1921, Hahn made the pioneering discovery of the first instance of nuclear isomerism. Prior knowledge indicated that ^{234}Th underwent beta-ray decay to produce ^{234}Pa with a half-life of 1.14 minutes. However, Hahn observed an additional beta-ray activity with a 6.7-hour half-life that coincided with the decay of ^{234}Th . Intriguingly, this second substance shared identical atomic number and atomic mass with ^{234}Pa . Despite this observation, no explanation was provided for such behavior at that time.

In 1936, von Weizsäcker proposed the initial explanation for isomeric states. He posited that nuclei could exist in excited states characterized by different angular momenta. When the angular momentum of an excited nuclear state significantly differed from those of lower-energy states, the nucleus would undergo a relatively challenging transition involving a substantial change in angular momentum. Von Weizsäcker demonstrated that angular momentum changes of one or two units led to lifetimes on the order of 10^{-13} seconds. Additionally, he illustrated that each additional unit of angular momentum change could result in a lifetime extension by approximately a factor of 10^6 .

Von Weizsäcker's explanation spurred experimentalists to seek out additional isomeric states, aiming to establish further properties of these states. However, it became evident that determining the angular momenta and parities of these states solely based on measured lifetimes might be challenging. This difficulty arose because lifetime calculations necessitated detailed knowledge or assumptions about nuclear structure. Early endeavors to compute lifetimes involved employing various nuclear models, such as one featuring a radiating proton in an average field or the liquid drop model, where radiation was assumed to result from vibrations of the drop. Unfortunately, these initial calculations faced limited success due to the inadequacy of experimental evidence supporting the models.

The first notably successful nuclear model, known as the shell model, emerged in 1950 through the work of Mayer and Haxel, Jensen, and Suess. Isomeric transition data played a

crucial role in providing experimental evidence that supported the foundation of this model.

6.2 Experimental Methods of Measuring Lifetimes of Isomeric States

Given the broad spectrum of lifetimes exhibited by nuclear states, various techniques are essential for their measurement. Numerous methods have been devised for gauging the lifetimes of isomeric states, categorized into two primary groups: those directly measuring the lifetime and those employing indirect measurements. In indirect methods, other quantities, such as the Coulomb excitation cross-section or the level width, are measured, and the lifetime is subsequently calculated. Figure 7 illustrates the range of lifetimes addressed by different experimental methods.

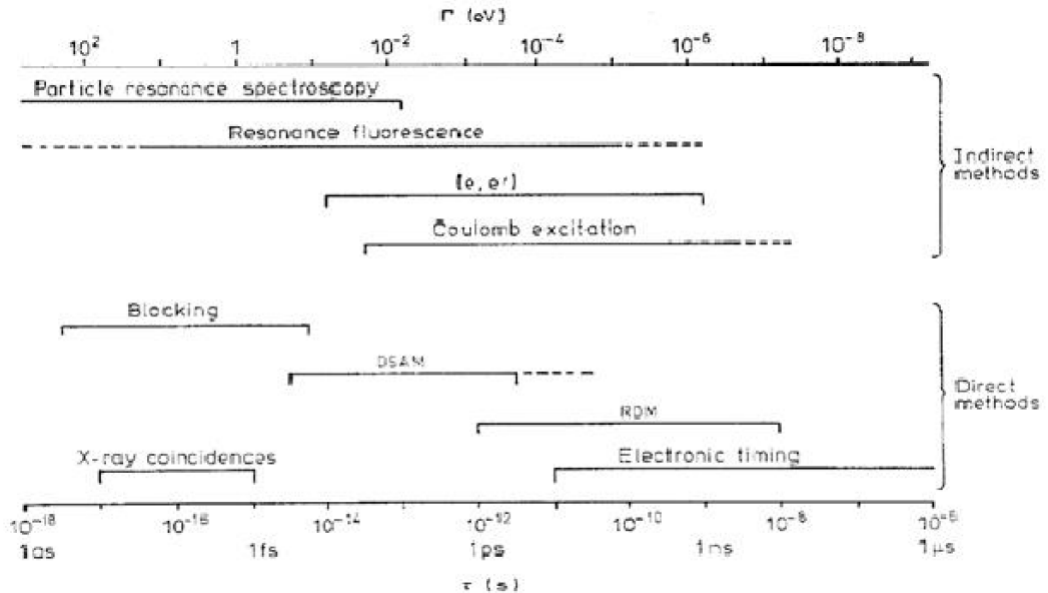


Figure 7: A graphical representation delineating different techniques for measuring lifetimes across various regimes. The chart is segmented into direct methods, which measure τ directly, and indirect methods, measuring Γ .

The utilization of γ -ray Doppler shift techniques relies on the premise that, following a nuclear reaction, the velocity of a recoiling nucleus in an excited state can be determined, at the moment of the γ -ray decay of the state, by measuring the Doppler energy shift of the γ -ray. Subsequent enhancements in these techniques emerged with the advent of high-resolution γ -ray detectors. In the Doppler shift attenuation method (DSAM), the lifetime of the level emitting a γ -ray is juxtaposed with the slowing down time of a recoiling nucleus in a solid. This slowing down/stopping time must be experimentally known or calculated. It results from two physical processes: electronic stopping, involving the excitation and exchange of electrons as the ionized atom of the recoil nucleus traverses the stopping material, and nuclear stopping, characterized by the scattering of the moving atom by the screened Coulomb fields of the nuclei in the stopping material. Electronic stopping prevails for recoil velocities v for which $v/c > 2\%$ (where c is the velocity of light), while nuclear

stopping gains significance at recoil velocities for which $v/c < 0.5\%$. Elliott and Bell (1948) pioneered the measurement of a nuclear lifetime using attenuated Doppler shifts.

Additional indirect methods include inelastic electron scattering and Coulomb excitation. In the latter scenario, multi-step processes are viable due to the extended duration taken by two colliding heavy ions during the collision. The cross-section in this context is linked to the products of multiple matrix elements and, consequently, the products of the widths of various excited states. These indirect methods are constrained to states that can be accessed beginning with a final state, which is the ground state of a stable nucleus.

In our case, our primary focus revolves around direct electronic fast timing technique. The range of lifetimes achievable through an electronic technique involving gamma-ray detection effectively spans from 10^{-11} to 10^{-6} seconds. While these boundaries may have some flexibility, our work primarily confines itself to this range, particularly emphasizing the shorter lifetime limit, typically within the range of a few nanoseconds. Among the various methods for directly measuring lifetimes through electronic timing, the approach utilizing delayed coincidences stands out as one of the most widely employed.

6.3 Delayed Coincidence Techniques

The emissions from an isomeric state exhibit a delay compared to the prompt transitions feeding into that isomeric state. The delayed coincidence method involves detecting radiations that both populate and depopulate the state whose lifetime needs determination. This method entails assessing the time differences in pulses from radiation detectors observing the source and correlating this distribution with the nuclear lifetime. In early studies, the time distribution was determined by counting coincidence rates at fixed artificial delays using a coincidence unit with finite resolving time. In contemporary delayed coincidence work, a time-to-amplitude converter is commonly employed, translating the time difference of two pulses into a signal whose amplitude is proportionate to the time difference. Subsequently, the distribution is histogrammed. This system necessitates a time resolution function termed the "prompt curve," derived from a nuclear cascade involving a state with an extremely short lifetime (approximately 1 ns). Additionally, from the isomeric state of interest, another time distribution function called the "delayed curve" is obtained.

The analysis of the delayed curve obtained from delayed coincidence experiments has been approached through various methods, some of which will be explored below. Subsequently, in this section, these techniques will be compared and discussed.

6.3.1 Centroid Shift Method

When employing the delayed coincidence method to measure lifetimes, the standard procedure involves measuring the time resolution curve (also known as the time spectrum) for the specific transition under consideration. This approach utilizes two detectors, denoted as 1 and 2 in Figure 8. Detector 1 captures the radiation associated with a transition that populates the isomeric state of interest, while detector 2 detects the radiation involved in depopulating the state. Subsequently, a delayed coincidence distribution is generated by introducing various time delays to the pulses from detector 2 in relation to the pulses from detector 1.

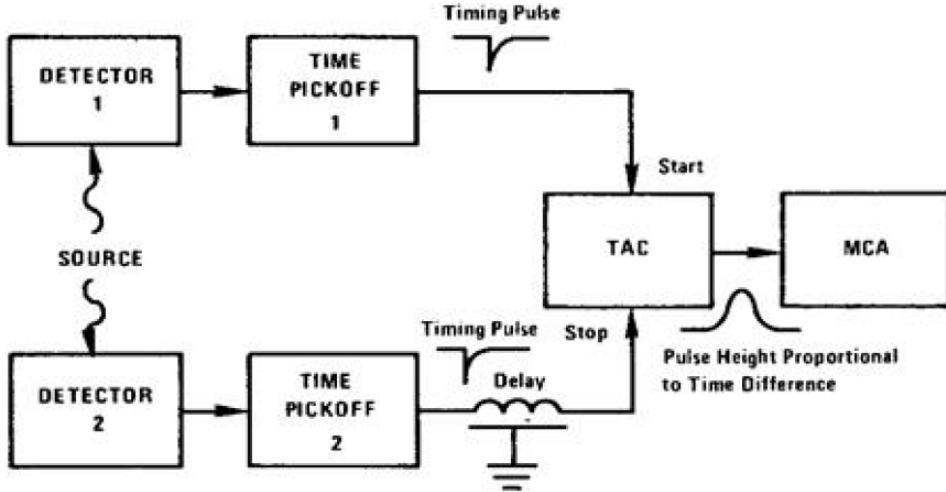


Figure 8: Schematic diagram of a simple time spectrometer

In an in-beam measurement using a large array of detectors, the process undergoes a change. Simultaneous detection of numerous gamma rays occurs across the array of detectors, making it impractical to ascertain the timing information for a single transition. In this scenario, the data from all detectors is recorded with specific time parameters. Subsequently, the data is organized into an energy-time matrix, enabling the generation of the time distribution curve for the transition of interest, referred to as the delayed curve.

The prompt curve is derived from a cascade that exhibits the same radiation energies as the two radiations employed in obtaining the delayed coincidence distribution. Ideally, the prompt curve should be measured with a source that is identical in all aspects to the delayed source, except for the lifetime, though such a source is seldom available. Additionally, the lifetime of the intermediate level in the prompt radiations should be negligible compared to the lifetime of the isomeric state. The centroid of the prompt curve is established as the zero of time, and the lifetime of the isomeric state can then be determined by the shift of the delayed coincidence curve relative to the prompt curve. This approach, known as the centroid shift method, is utilized when the lifetime to be measured is short or comparable to the full width at half maximum (FWHM) of the prompt time resolution curve.

In the analysis of delayed data, a 673 keV transition in ^{113}In was identified as a delayed transition. The excitation of many low-lying states of ^{113}In occurred through the ^{113}Cd (p, n) ^{113}In reaction conducted by H. J. Kim and W. T. Milner[16]. Gamma-rays were detected using a coaxial Ge(Li) detector. The centroid shift method was employed to determine a 0.62 ns isomer, from which the decay of the 673 keV transition originates. Another 680 keV transition served as the prompt curve, exhibiting a full width at half maximum (FWHM) of 86.8 ns. The results obtained are illustrated in Figure 9.

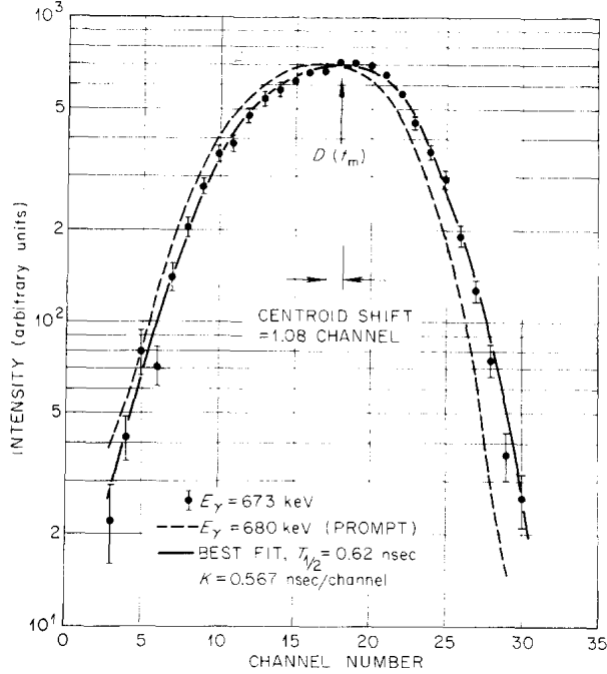


Figure 9: H. J. Kim et al.[16]utilized the centroid shift technique to fit and plot the delayed intensity curve of a 673 keV transition along with a prompt curve for a 680 keV transition. This analysis enabled the determination of a 0.62 ns half-life for the isomer in ^{113}In .

The effectiveness of the centroid shift method for measuring nuclear lifetimes is notably influenced by the selection of the prompt curve and is susceptible to instrumental variations. The accuracy of this method is constrained by factors impacting the prompt curve:

1. Variation in the interaction location of the radiation.
2. Energy of the detected gamma-ray.
3. Finite decay time of light-emitting states in the scintillator or, in the case of a semiconductor detector, variations in the time taken for electrons and holes to reach the electrodes.
4. Jitter and uncertainties in the triggering times of associated electronics.

Optimal use of small detectors and appropriate geometry can minimize the impact of the first factor. The consideration of the second factor involves determining an efficiency curve for a detector, while the next two are fixed and finite for a given arrangement.

6.3.2 Slope method

The direct and uncomplicated approach to determine the lifetime involves employing the slope method. For longer lifetimes, the observed delayed curve tends to exhibit a skewed profile, representing a convolution of a prompt (Gaussian) component and a slope generated by the state's lifetime (exponential). This skewed portion can be subjected to exponential fitting to extract and ascertain the lifetime. This is the method I implemented to find the lifetime of a state.

An illustration of this approach is evident in an in-beam γ -ray spectroscopy study on the excited states of ^{207}Po conducted by V. Rahkonen et al.[15]. The levels in ^{207}Po were excited through the ^{207}Pb ($^3\text{He}, 3n$) ^{207}Po and (α, xn) reactions, utilizing the ^3He beam from the Jyvaskyla cyclotron and the α beam from the Stockholm cyclotron. The three parameter $\gamma - \gamma - t$ measurements were done using coaxial Ge(Li) detectors and Gamma-ray spectra and time spectra in nano-second region were recorded. The study validated the previously established level scheme and introduced a new $40(2)$ ns $25/2^+$ isomer at 2379.3 keV for ^{207}Po . The outcomes are depicted in Figure 10.

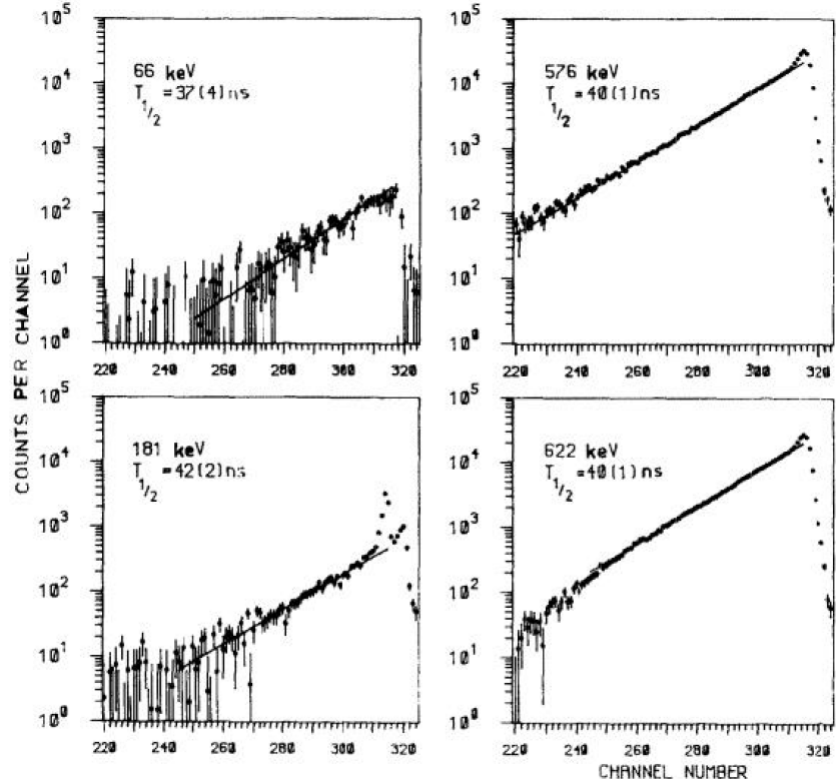


Figure 10: Rahkonen et al.[15] applied the slope method to analyze the time spectra of certain transitions in ^{207}Po , revealing a half-life of 40 ns for a $25/2^+$ state.

6.3.3 Moment relations

In numerous scenarios, while the delayed curve is accurately measured, obtaining a comparable prompt curve can be challenging. Consequently, the centroid shift method is inapplicable due to the unknown zero of time. The moment method requires a basic understanding of the prompt curve's shape to estimate the lifetime. If $P(x)$ represents the unobserved true prompt curve and $F(x)$ is the measured delay curve, the following relation holds among the moments of the two curves:

$$M_r(F) = \sum_{k=0}^r \frac{r!}{k!(r-k)!} M_{r-k}(P) M_r(\omega)$$

where, $M_r(F)$ is the r th moment of $F(x)$ defined as:

$$M_r(F) = \int_{-\infty}^{\infty} x^r F(x) dx$$

And, The radioactive decay law for radiation of mean life τ is expressed as follows:

$$\omega(x) = \tau^{-1} \exp(-x/\tau)$$

In the above equation, integration gives:

$$M_n(\omega) = n! \tau^n$$

Considering the definition of the zero of time and assuming a Gaussian prompt curve, we also establish:

$$M_1(P) = 0 \quad M_2(P) = \sigma^2 \quad M_1(P) = \epsilon$$

For the three moments of the delayed curve about the centroid τ , the moment N is calculated as follows:

$$N_r(F) = \int_{-\infty}^{\infty} (x - \tau)^r F(x) dx$$

Hence,

$$N_1(F) = 0 \quad N(F) = \sigma^2 + \tau^2 \quad N_1(F) = 2\tau^3 + \epsilon$$

The lifetime τ comes out in terms of the third moment of the delayed curve and the prompt cube.

$$\tau = \left(\frac{N_3(F) - M_3(P)}{2} \right)^{\frac{1}{3}}$$

The lifetime τ , expressed in terms of the second and first moments, looks like:

$$\tau = (M_2(F) - M_2(P))^{\frac{1}{2}}$$

And,

$$\tau = (M_1(F) - M_1(P))$$

Weaver and Bell[6] performed this calculation for data obtained from the measurement of the half-life of the 1507 keV excited state of ^{156}Gd . They successfully verified the half-life of that state to be 0.188 ns using the third-moment technique.

6.3.4 Numerical Convolution

The experimental delayed curve $F(t)$ is modeled as the convolution of the prompt curve $P(t)$ with an exponential curve and is then fitted to the experimental data. $F(t) = Ne^{-\lambda t} \times P(t)$

Iterations are performed, and a numerically convoluted fit is determined. In this case, errors primarily depend on the sensitivity of the numerical interpolation.

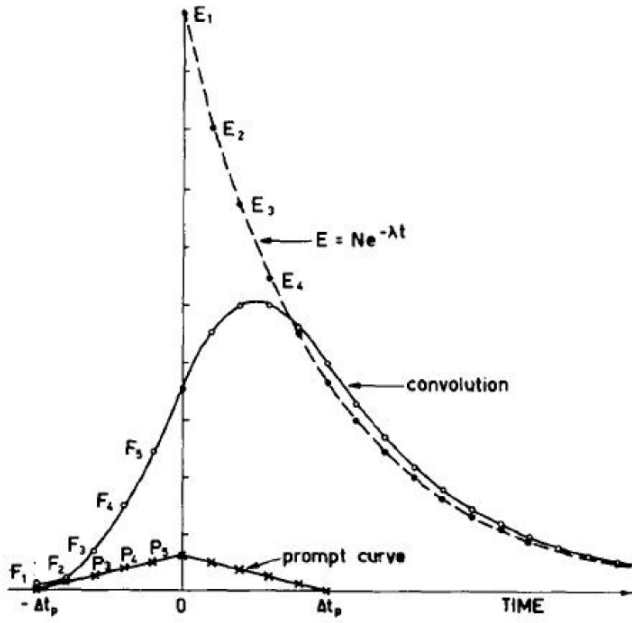


Figure 11: This represents the delayed curve $F(t)$ as a convolution of a prompt curve $P(t)$ and an exponential curve $E(t) = Ne^{-\lambda t}$.

The lifetime of the state is directly extracted by fitting the time difference spectrum by the convolution function (if the time difference spectrum shows an exponential tail). The convolution function associated with the single exponential decay can be written as

$$y = y_0 + \frac{A}{t_0} \exp \left(0.5 \left(\frac{w}{t_0} \right)^2 - \frac{x - x_c}{t_0} \right) \left(\frac{\operatorname{erf} \left(\frac{z}{\sqrt{2}} + 1 \right)}{2} \right)$$

$$\text{where } z = \frac{(x-x_c)}{w} - \frac{w}{t_0}$$

I have written a code to fit the time difference spectrum obtained by the experiment to this above function. The code is provided in the appendix for reference.

6.3.5 Comparison and Applications

Olsen and Bostrom[16] conducted a comparative analysis between the outcomes derived from a convolution method and those obtained through the slope method and the moment method. Their investigation, summarized below, involves a decay lifetime of " τ " and a time resolution of $2\tau_0$ for the equipment.

1. Both the convolution method and moment methods are influenced by the cutoff of the number of channels considered for measurement, indicating sensitivity to the time range.
2. For short lifetimes, the convolution methods and the moment method yield smaller statistical errors compared to other methods. The slope method is not recommended in such scenarios.
3. The moments method is highly sensitive to drifts between the prompt curve and the delayed curve.

4. When $\tau > 2\tau_0$, statistical errors play a minor role. However, if $\tau \leq 2\tau_0$, statistical errors become significant due to uncertainties and non-linearity in time calibration.
5. For $\tau > 2\tau_0$, the slope and convolution methods exhibit comparable and superior performance compared to the moments methods.

6.4 Delayed coincidence method

In this approach, an energy-time matrix is constructed, and for the specific state under investigation for which the lifetime is to be determined, gating is applied to isolate the decaying transition from that state, resulting in its time distribution (delayed curve). If the lifetime (τ) of the excited state is greater than the time resolution (τ_0) of the detector, the skew in the time resolution becomes evident. The delayed curve can be considered as a convolution of a prompt curve and an exponential decay. The mean lifetime can be obtained by fitting an exponential function to the skewed portion. However, if τ is comparable to τ_0 , a comparison is made between the delayed curve and the prompt curve (time distribution of a prompt transition) with similar or equal energy (if possible). This enables the determination of the time difference between the centroids of the prompt and delayed curves, providing the mean lifetime τ .

Andrejtscheff et al.[17] employed the delayed coincidence method in a study where they conducted in-beam measurements for heavy-ion reactions. Their approach involved determining the centroid of the delayed transitions of interest in relation to the centroids of known neighboring prompt transitions. Subsequently, they created a centroid diagram depicting centroid positions versus gamma energy. This diagram unveiled the centroid shift of the delayed transition concerning the zero-time line established by the prompt transitions in the centroid diagram. For instance, in the case of a 1256 keV transition in ^{109}Sn formed by the $^{16}\text{O}(^{95}\text{Mo}, \text{pn})^{109}\text{Sn}$ reaction, the centroid diagram indicated a $T_{1/2} = 2.0(3)\text{ns}$, as depicted in Figure 12.

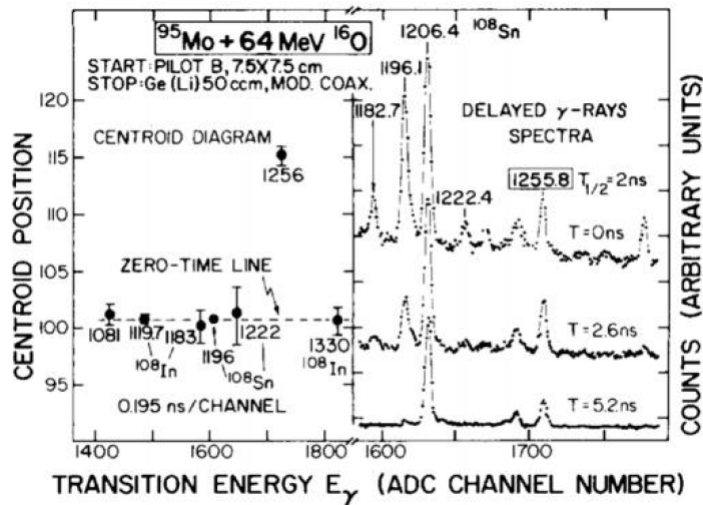


Figure 12: The centroid diagram[17] illustrates the centroid shift of the 1256 keV transition in ^{109}Sn concerning the 1196 keV prompt transition of ^{108}Sn along the zero-time line. The validation of the half-life is further confirmed by observing changes in intensity in the delayed gamma-ray spectra.

Given that the transitions of the nuclei under examination are influenced by various contaminants, the subtraction of background becomes an essential and integral aspect of this technique during the generation of the time difference spectrum. To achieve this, we choose channels corresponding to the peaks, and for background subtraction, an equal number of channels are selected from the troughs near the peaks in the total projection. The proximity to the peaks is crucial as detector efficiency is dependent on energy. Our objective is to derive the time difference from the peak counts of our transitions, and we adopt the approach depicted in Figure 13 to accomplish this.

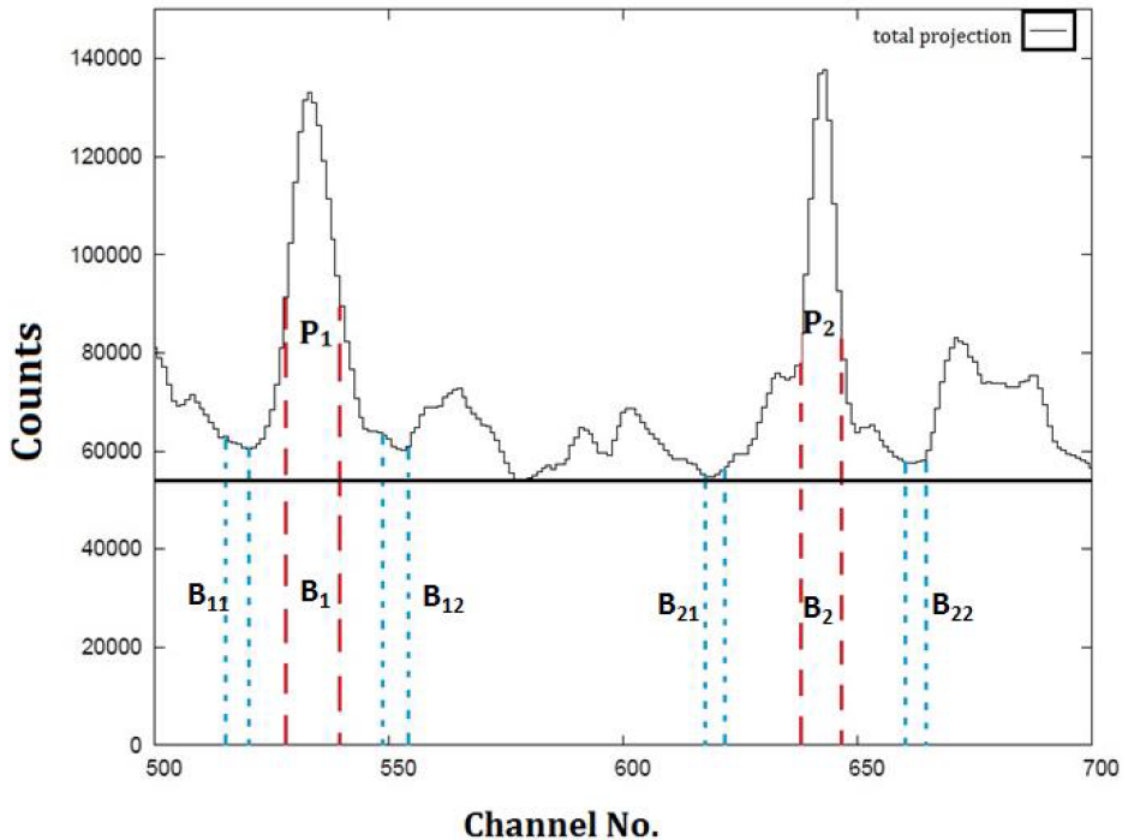


Figure 13: A segment of the overall projection is presented to showcase the background selection and the subsequent background subtraction procedure. This process is implemented to mitigate the impact of substantial background interference when determining the time difference between the two peak energies.

In this we can observe that $T_1 = P_1 + B_1$ and, $T_2 = P_2 + B_2$

The number of background channels selected is equal to the number of channels for peaks such that,

$$B_1 = B_{11} + B_{12}, \text{ and } B_2 = B_{21} + B_{22}$$

For time difference, we need to calculate $P_1 * P_2$ Hence,

$$\begin{aligned}
T_1 * T_2 &= (P_1 + B_1) * (P_2 + B_2) \\
&= (P_1 + B_{11} + B_{12}) * (P_2 + B_{21} + B_{22}) \\
&= P_1 * P_2 + P_1 * B_{21} + P_1 * B_{22} \\
&\quad + B_{11} * P_2 + B_{11} * B_{21} + B_{11} * B_{22} \\
&\quad + B_{12} * P_2 + B_{12} * B_{21} + B_{12} * B_{22}
\end{aligned}$$

$$\begin{aligned}
T_1 * B_2 &= (P_1 + B_1) * (B_2) \\
&= P_1 * B_{21} + P_1 * B_{22} + B_{11} * B_{21} + B_{11} * B_{22} + B_{12} * B_{21} + B_{12} * B_{22}
\end{aligned}$$

$$\begin{aligned}
B_1 * T_2 &= (B_1) * (P_2 + B_2) \\
&= B_{11} * P_2 + B_{11} * B_{21} + B_{11} * B_{22} + B_{12} * P_2 + B_{12} * B_{21} + B_{12} * B_{22} \\
B_1 * B_2 &= (B_1) * (B_2) \\
&= B_{11} * B_{21} + B_{11} * B_{22} + B_{12} * B_{21} + B_{12} * B_{22}
\end{aligned}$$

Now, $P_1 * P_2 = T_1 * T_2 - T_1 * B_2 - B_1 * T_2 + B_1 * B_2$ (102)

Thus, by employing this spectral arithmetic, we obtain the peak counts corresponding to our transitions. Here, $P_1 * P_2$ signifies the timing information between the peak energies P_1 and P_2 , observed when gating on P_2 and examining P_1 .

Using this delayed coincidence method and following the above steps, the known lifetimes of the isomeric states in ^{152}Eu and ^{133}Ba populated in our Gammasphere data were determined. The γ -coincidences within a $1 \mu\text{s}$ coincidence window were histogrammed into energy-gated energy-time matrices for the transitions feeding and de-exciting the isomeric state of our interest.

6.5 Experimental setup and Data acquisition system

The experiments were performed at the TIFR-BARC Pelletron LINAC Facility at TIFR-Mumbai. A hybrid array composed of 12 Compton suppressed high purity germanium (HPGe) clover detectors arranged in spherical manner to cover all spatial angles[15] and 14 $\text{LaBr}_3(\text{Ce})$ (shown in figure 14a) scintillator detectors were used for the experiment.



(a) $\text{LaBr}_3(\text{Ce})$ detector



(b) Indian National Gamma Array (INGA)

Figure 14: Image depicting the Indian National Gamma Array featuring Compton-suppressed clover detectors, situated in Hall-2 of the TIFR-BARC Pelletron-LINAC facility in Mumbai.

Three clover detectors were positioned at 140° , three at 157° , four at 90° , and one at 115° relative to the beam direction. To enhance the peak-to-background ratio, the HPGe clover detector was shielded with a BGO scintillator. Data collection involved the use of a 2 or higher fold coincidence condition employing an XIA-based digital data acquisition system. Two crate synchronizations were employed, where one crate (master) housed 6 modules with a sampling frequency of 100 MHz (for HPGe), and the other crate contained 1 module with a sampling frequency of 250 MHz (for $\text{LaBr}_3(\text{Ce})$). A mixed radioactive source comprising ^{152}Eu and ^{133}Ba was utilized for energy calibration.

The Fast Timing Technique utilizes the output signal from one detector as a start signal and another as a stop signal to acquire the time difference spectrum. The start signal corresponds to the population of the state for which the lifetime is to be calculated. As depicted in Figure 15, the two Constant Fraction Discriminator (CFD) signals are compared in a Time to Amplitude Converter (TAC) to extract the time difference.

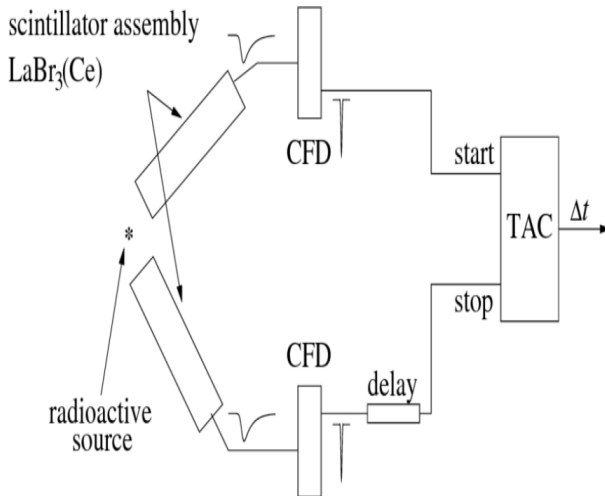


Figure 15: Schematic of the detector setup for fast timing adapted from reference[16].

The data were sorted using “MultipARameter time-stamp-based COincidence Search program” to form NTuple containing time difference between two detectors and coincidence of gamma rays.[17] Typically, numerous excited states of nuclei exhibit lifetimes on the order of picoseconds or femtoseconds, which is shorter than the time resolution of the setup. In the absence of any gating condition, the time difference spectrum will resemble a Gaussian (prompt) function. A time coincidence window of $2 \mu\text{s}$, along with energy and time offset parameters for each detector, was input into the MARCOS system to generate gamma-gated spectra (for both types of detectors) and time difference spectra. Various gamma-gated conditions were applied to the total time difference spectrum of $\text{LaBr}_3(\text{Ce})$, with or without gamma gating on HPGe, to obtain the time difference spectrum for a specific state. The final time difference spectrum was obtained by following the formula[16]

$$T(i) = T_{\text{p1,p2}}(i) - T_{\text{p1,bg2}}(i) - T_{\text{bg1,p2}}(i) + T_{\text{bg1,bg2}}(i)$$

The reason of using this formula is already explained in 102. Four conditional time difference spectra ($T_{\text{p1,p2}}, T_{\text{p1,bg2}}, T_{\text{bg1,p2}}, T_{\text{bg1,bg2}}$) were created using time-stamped data. Here, $T_{\text{p1,p2}}$ denotes the time difference spectrum with a start at the energy gate around the E_{γ_1} peak and a stop at the energy gate around the E_{γ_2} peak, while $T_{\text{p1,bg2}}$ represents the start at the energy gate around E_{γ_1} and stop at the background near the E_{γ_2} peak. Similarly, $T_{\text{bg1,p2}}$ and $T_{\text{bg1,bg2}}$ represent the background-peak and background-background time difference spectra, respectively.

6 Data Analysis Procedure

The data underwent sorting through the "MultipARameter time-stamp-based COincidence Search program" to generate an NTuple comprising the time difference between two detectors and the coincidence of gamma rays.[12]

6.1 Energy Calibration

The detector's output signal doesn't directly represent energy; instead, it's initially recorded as a channel number. To calibrate the energy, a mixed standard source containing ^{152}Eu and ^{133}Ba was utilized. A nonlinear equation was employed to establish the correspondence between channel number and energy.

$$E(x) = a + bx + cx^2 + dx^3 \quad (4)$$

Due to temperature dependence of electronics, voltage fluctuation may occur and gain of each detector may changes with time so the calibration for all the 14 detectors were carried out for about 6 runs, where each run correspond to collected counts for 30 minutes. The calibration is carried out by using the following peaks as shown in the figure below. Few detectors required to be calibrated by more than 10 peaks to minimize the chi-square per degrees of freedom. The program used for calibration is attached in appendix. DAMM software is used for carrying out the calibration.

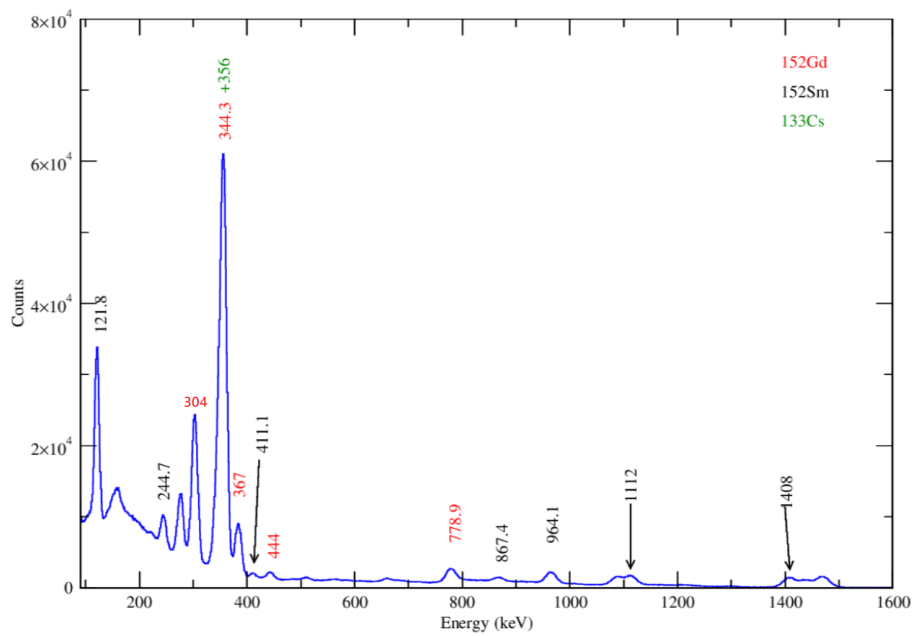


Figure 9: Identification of peaks from $\text{LaBr}_3(\text{Ce})$ detector

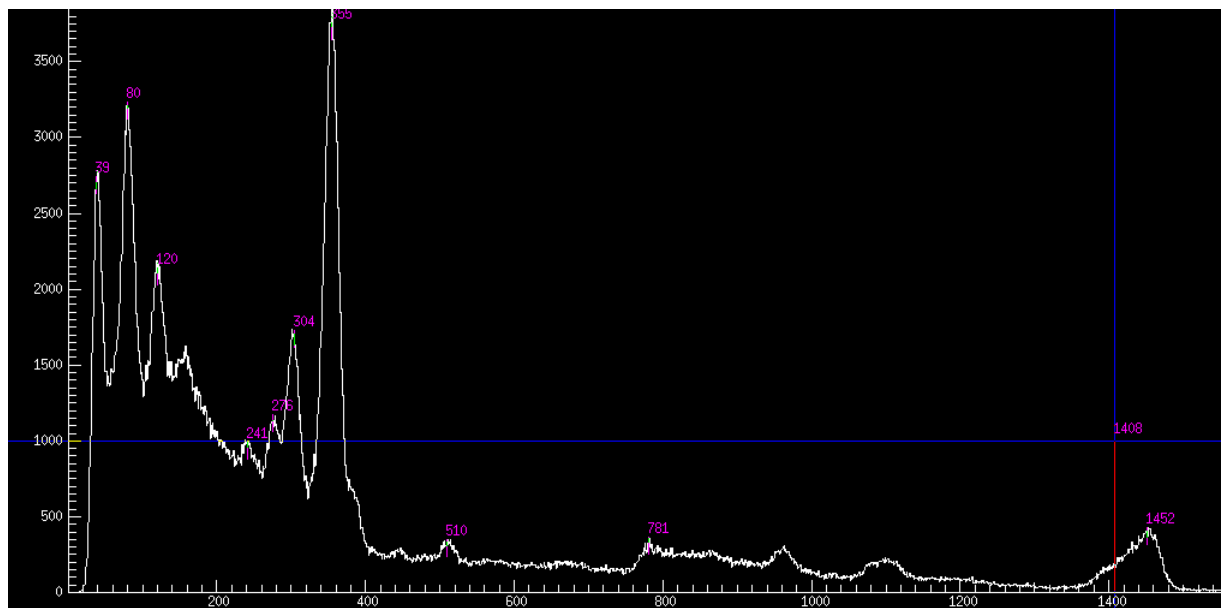


Figure 10: Energy spectrum from $\text{LaBr}_3(\text{Ce})$ detector after calibration

Superimposing all the calibrated spectras for all 14 detectors we get:

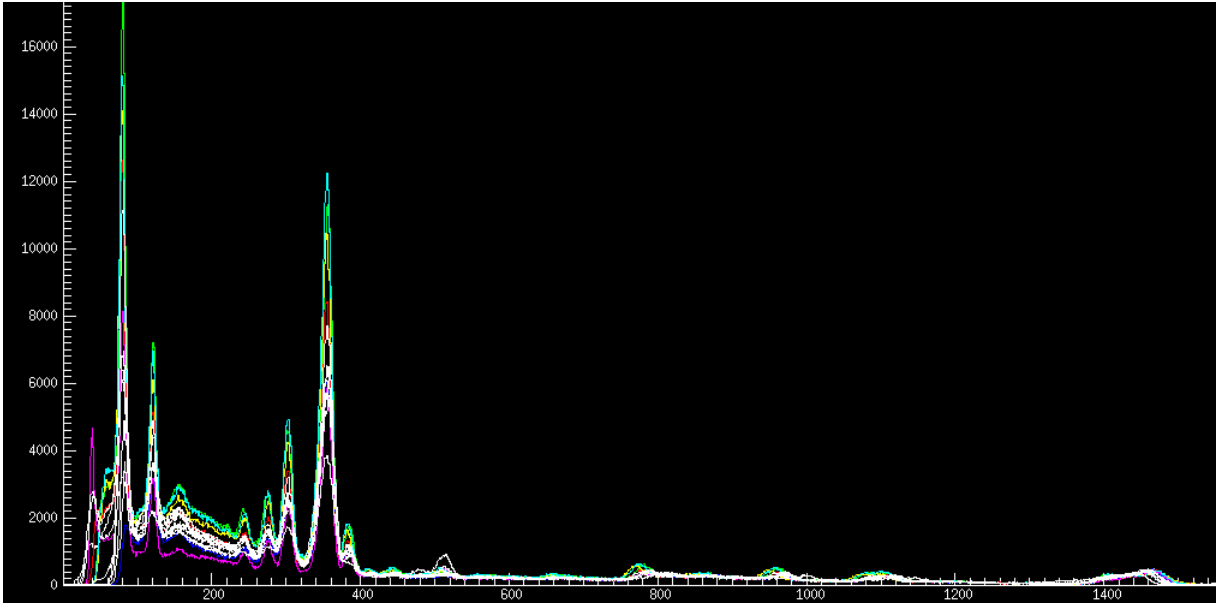


Figure 11: Energy spectrum from all 14 $\text{LaBr}_3(\text{Ce})$ detectors after calibration

From this figure we can clearly observe that in certain detectors the peak around 39 keV is missing in some $\text{LaBr}_3(\text{Ce})$ detectors which can be explained by the fact that such low keV energies are easily absorbed by the detector housing.

6.2 Time offset

In general, many excited states of nuclei have lifetimes on the order of picoseconds or femtoseconds, which are shorter than the time resolution of the experimental setup. Without any gating conditions, the time difference spectrum typically appears as a Gaussian (prompt) function. Due to physical parameters of the detector and additional decay introduced by connecting wires, the peak of the time distribution for each detector may vary, necessitating correction. MARCOS utilized a center of 2000 channel number (1ch = 200ps) for the time difference spectrum. The time offset for each detector was calculated as $T_0 - 2000$, where T_0 represents the channel number corresponding to the peak position of the raw time difference spectrum. The time resolution of a scintillator-based detection system relies on the rate of photoelectrons at the detection threshold, which is influenced by the time distribution of photons undergoing conversion in the photodetector.

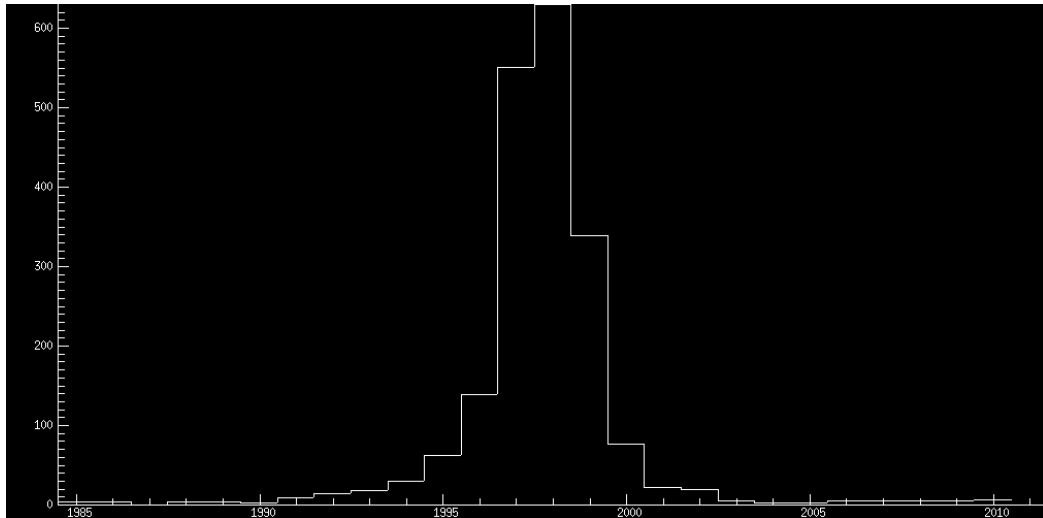


Figure 12: Time offset of a detector (note that it is not exactly at channel number 2000)

7 Observations and Results

7.1 Lifetime Measurement

The half-life measurements for the first excited state with the spin parity $\frac{5}{2}^+$ of the ^{133}Cs at the excitation energy of 81 KeV with an established half-life of 6.28 ns. Coincidence window of $2\mu\text{s}$ is used for this experiment. The electron capture decay of ^{133}Ba with a half life of 10.55 years leads into the excited states of ^{133}Cs followed by its de-excitation and eventually coming to the ground state. A decay scheme was proposed by Stewart and Lu (1960) and analysis for the spin parity assignments was done by K.C. Mann et al[17].

Based on predictions from the single-particle shell model, the spin-parity of the ground state of ^{133}Cs is determined to be $\frac{7}{2}^+$, indicating that it resides in the $g_{7/2}$ state. The 81-keV transition is identified as a mixed M1 transition with a small amount of E2 mixing. Similarly, the 53-keV transition, which also exhibits M1 + E2 transition characteristics and has a lower branching ratio than the 81-keV transition, is not clearly observed in the spectrum.

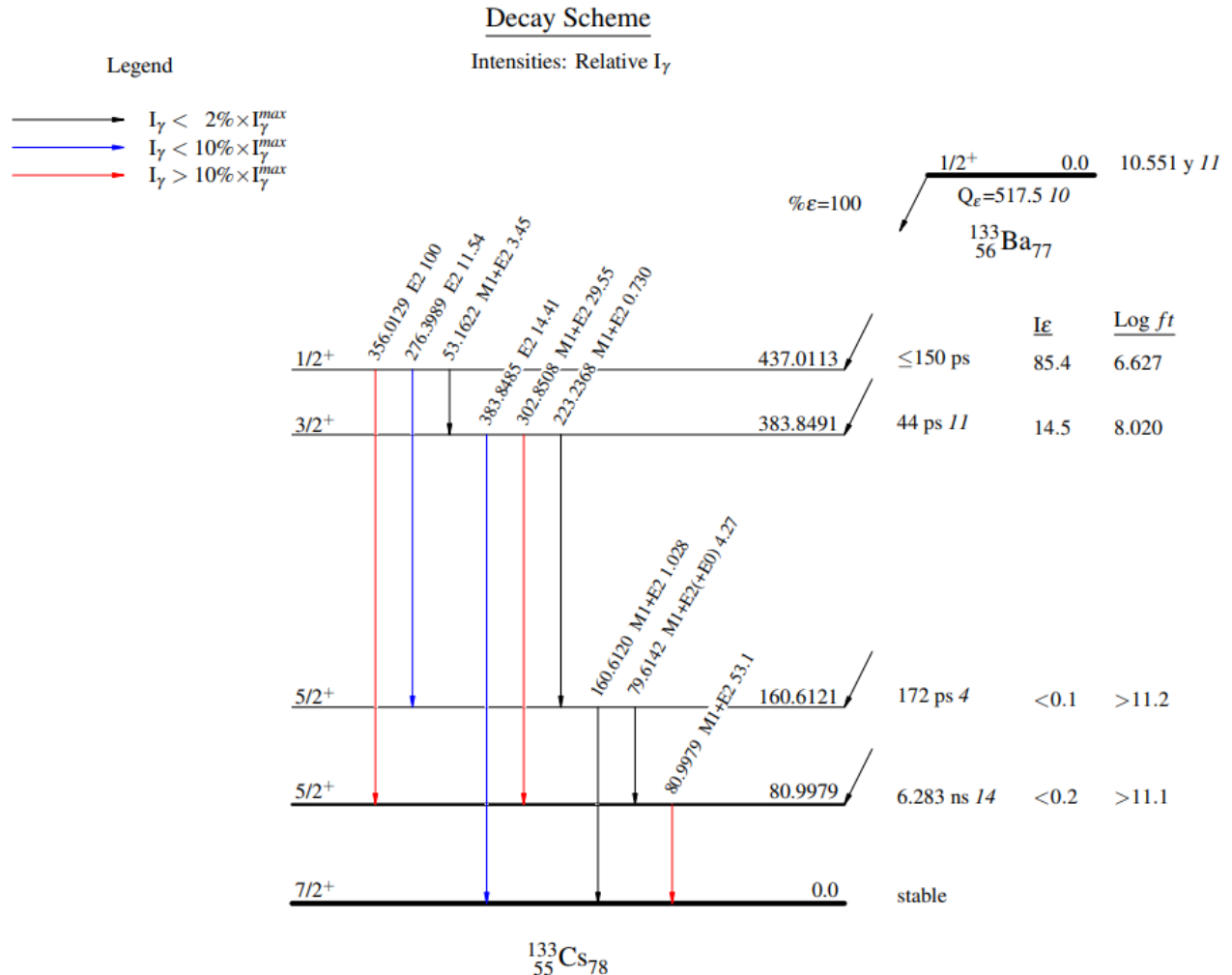


Figure 16: Decay Scheme of ^{133}Ba taken from NNDC Website[18]

The time difference spectrum is obtained to find the lifetime of the state $\frac{5}{2}^+$ of ^{133}Cs . It is then fitted with the convolution function associated with the single exponential decay can be written as

$$y = y_0 + \frac{A}{t_0} \exp \left(0.5 \left(\frac{w}{t_0} \right)^2 - \frac{x - x_c}{t_0} \right) \left(\frac{\operatorname{erf} \left(\frac{z}{\sqrt{2}} + 1 \right)}{2} \right)$$

where $z = \frac{(x-x_c)}{w} - \frac{w}{t_0}$ and the parameters y_0, A, x_c, w, t_0 represent the following:

y_0 = offset, A = area, x_c = center, w = width, t_0 = unknown

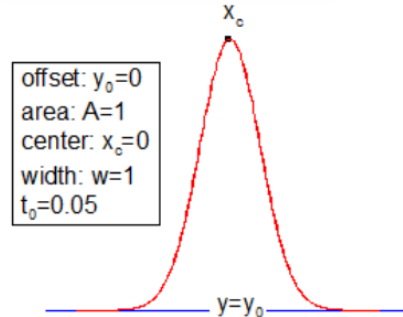


Figure 17: Sample Curve depicting the parameters

I have written a code to fit the time difference spectrum obtained by the experiment to this above function. The code is provided in the appendix for reference. The fitted plot obtained is shown in the figure 18.

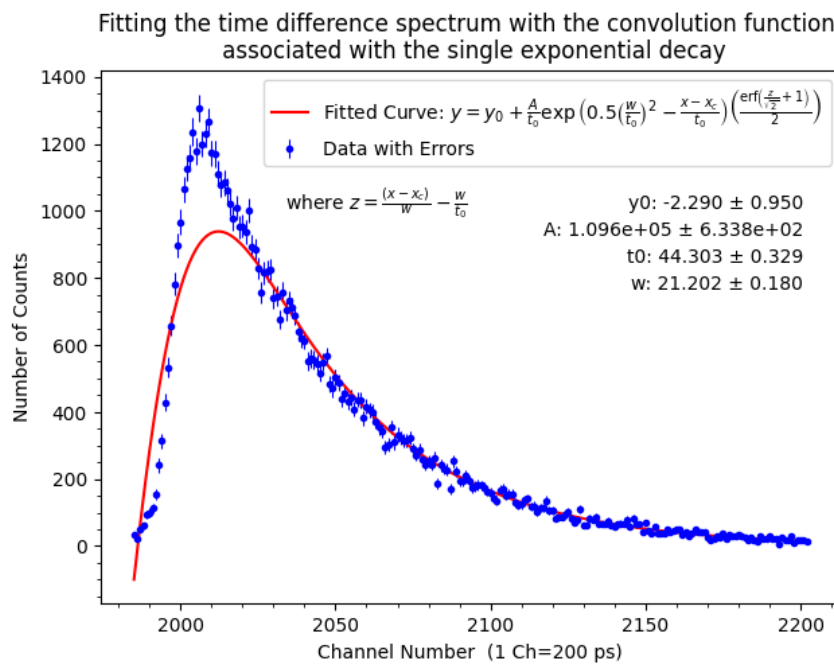


Figure 18: The time difference spectrum is fitted to the curve

$$y = y_0 + \frac{A}{t_0} \exp \left(0.5 \left(\frac{w}{t_0} \right)^2 - \frac{x - x_c}{t_0} \right) \left(\frac{\operatorname{erf} \left(\frac{z}{\sqrt{2}} + 1 \right)}{2} \right)$$

by keeping $x_c = 2006$ to be a constant and varying the other parameters y_0, A, w and t_0 to minimise chi square. The program I wrote for this is attached in Appendix A.4

We can observe that The Gaussian part of the curve is not fitted perfectly. This is due to the reason that the data points in the Gaussian part of the curve is much smaller as compared the data points in the exponential decay part of the curve. From the fitting we get $t_0 = 44.303 \pm 0.329 = (44.303 \pm 0.329) \times 200 \text{ ps}$

Hence $T_{1/2}$ calculated using this method is

$$\ln(2) \times (44.303 \pm 0.329) \times 0.2 \text{ ns} = 6.14 \pm 0.15 \text{ ns}$$

Now we can find the half life of the state by using second method i.e. by removing the data points of the Gauss part and fitting the rest data points to a exponential decay. The decay of the isomeric state is observed by measuring intensity distribution of a delayed transition in the subsequent time cuts. When this intensity distribution is fitted exponentially:

$$y = y_0 + Ae^{-x/t_0}$$

gives, t_0 the mean lifetime and $T_{1/2} = 0.693 \times t_0$ gives the half-life of the state. I have written a code to fit the time difference spectrum obtained by the experiment to this above function. The code is provided in the appendix for reference. The fitted plot obtained is shown in the figure 19.

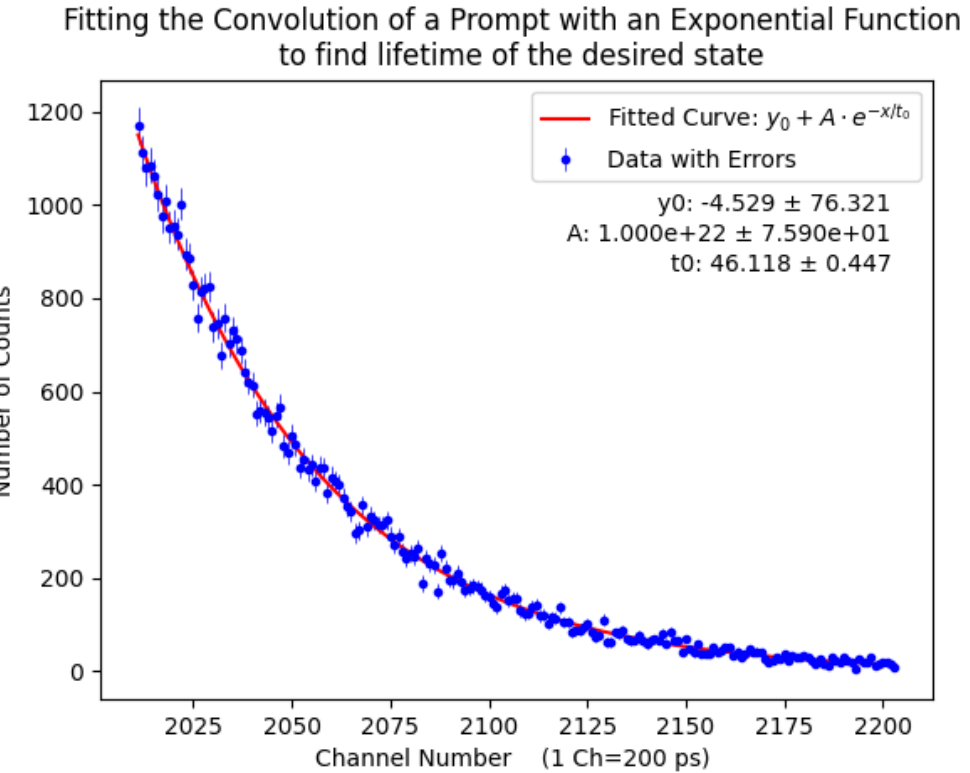


Figure 19: The time difference spectrum after removing the Gaussian part is fitted to the curve

$$y = y_0 + Ae^{-x/t_0}$$

by varying the parameters y_0, A and t_0 to minimize chi square. The program I wrote for this is attached in Appendix A.5

From the fitting we get $t_0 = 46.118 \pm 0.447 = (46.118 \pm 0.447) \times 200 \text{ ps}$
Hence $T_{1/2}$ calculated using this method (using 1) is $\ln(2) \times (46.118 \pm 0.447) \times 0.2 \text{ ns} = 6.39 \pm 0.092 \text{ ns}$

If we take the average of the $T_{1/2}$ calculated using two methods we get $(T_{1/2})_{\text{avg.}} = 6.27 \pm 0.12 \text{ ns}$

The half life of the state $\frac{5}{2}^+$ of ^{133}Cs as reported in literature is 6.283 ns [18]. The percentage error of the calculated result from the accepted value is 0.2%.

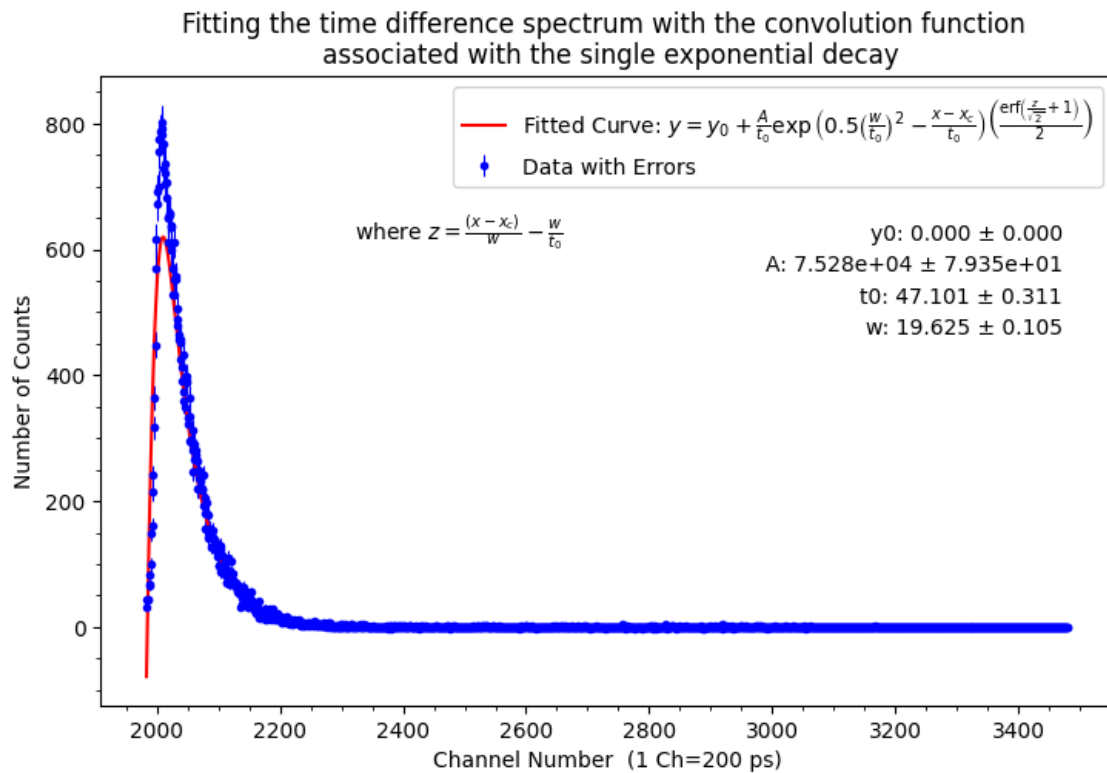


Figure 15: The time difference spectrum obtained by gating around 81 keV in one detector and 356 keV in another detector. Then it is fitted to the curve

$$y = y_0 + \frac{A}{t_0} \exp \left(0.5 \left(\frac{w}{t_0} \right)^2 - \frac{x - x_c}{t_0} \right) \left(\frac{\operatorname{erf} \left(\frac{z_c}{\sqrt{2}} + 1 \right)}{2} \right)$$

by keeping $x_c = 2006$ to be a constant and varying the other parameters y_0, A, w and t_0 to minimise chi square. The program I wrote for this is attached in Appendix A

Now we take different ranges of intervals and plot how lifetime changes by taking different intervals resulting in different values of chi-square.

Plot to observe how lifetime changes by taking different intervals
resulting in different values of chi-square

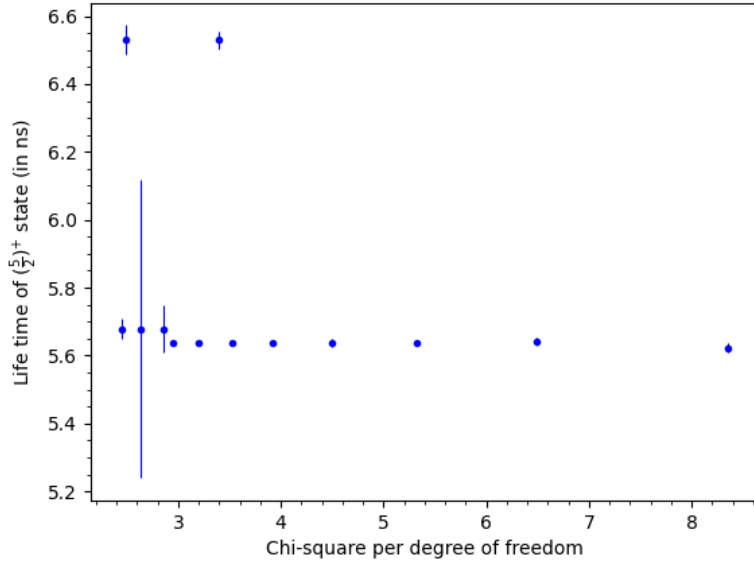


Figure 16: From this plot we can find the average of $T_{1/2}$ calculated by taking different intervals to be 5.98 ± 0.04 ns ($T_{1/2} = \ln(2) \times (t_0) \times 0.2$ ns)

Fitting the time difference spectrum with the convolution function associated with the single exponential decay

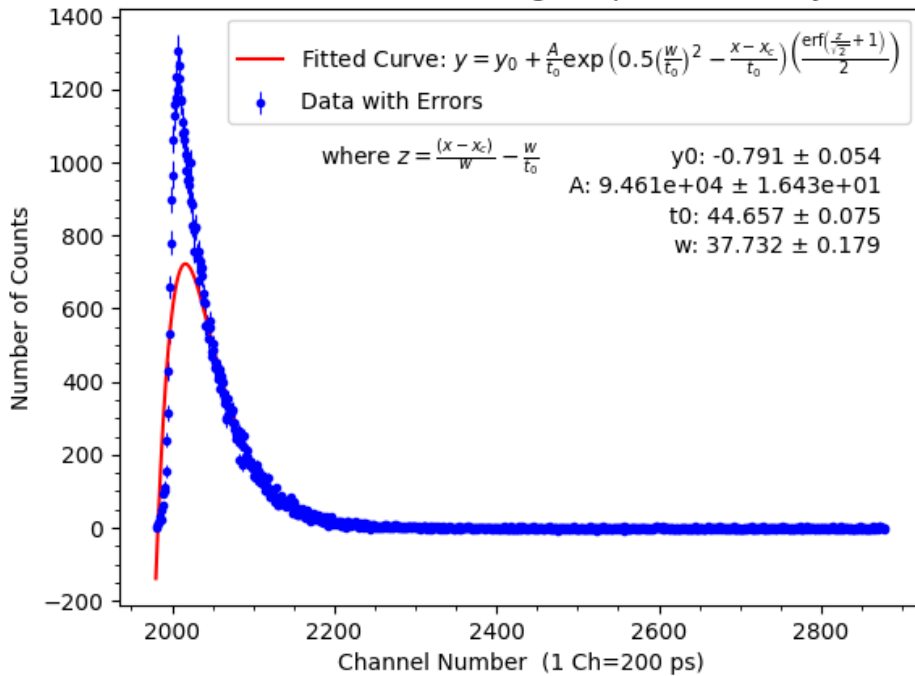


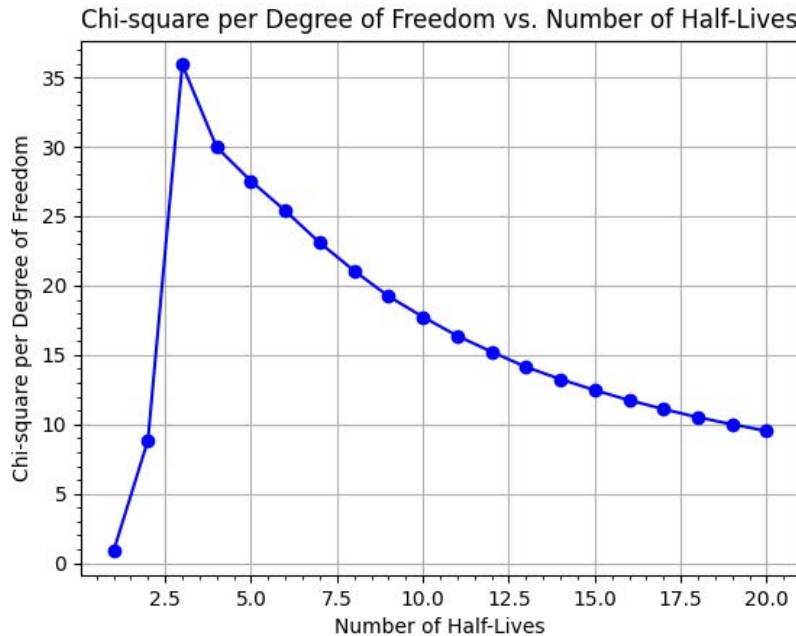
Figure 17: The time difference spectrum obtained by gating around 81 keV in one detector and 304 keV in another detector. Then it is fitted to the curve

$$y = y_0 + \frac{A}{t_0} \exp \left(0.5 \left(\frac{w}{t_0} \right)^2 - \frac{x - x_c}{t_0} \right) \left(\frac{\operatorname{erf} \left(\frac{z}{\sqrt{2}} + 1 \right)}{2} \right)$$

by keeping $x_c = 2006$ to be a constant and varying the other parameters y_0 , A , w and t_0 to minimise chi square.

From the fitting we get $t_0 = 44.657 \pm 0.075 = (44.657 \pm 0.075) \times 200$ ps

Hence $T_{1/2}$ calculated using this method(using $T_{1/2} = 0.693 \times \langle T \rangle$) is $\ln(2) \times (44.657 \pm 0.075) \times 0.2$ ns = 6.19 ± 0.02 ns



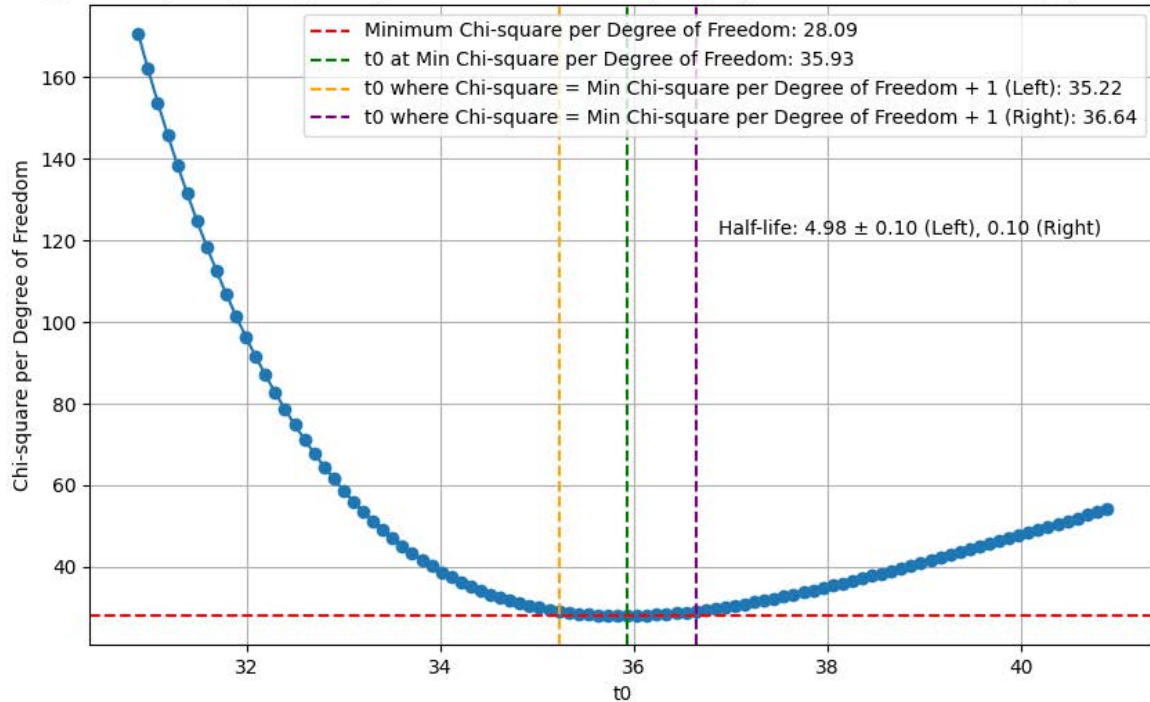
From the figure we observe that the fit for the first two half-lives does not follow the Gaussian plus exponential model resulting in a lower chi-square per degree of freedom. After this interval the fit improves and the chi-square per degree of freedom decreases as the data points increase.

So plotting the fitted parameters beta in different intervals to observe how each parameter is converging resulting in convergence of half-life.

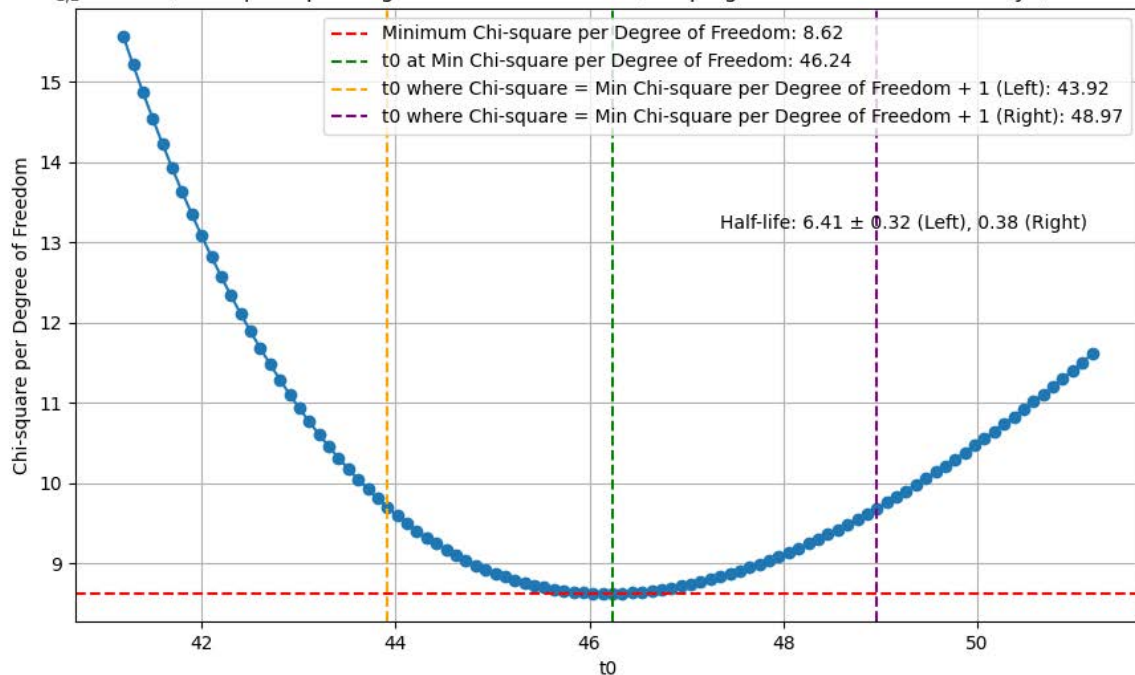
Interval (In terms of Half-Lives)	Chi-square per DoF	y0	A	t0	w	Half-Life
1	0.8573804533	455.12	7.75E+04	110.91	4.24	15.37475205
2	8.838181148	446.3	2.20E+04	42.72	4.05	5.922673726
3	35.9125452	-1664.01	8.15E+05	145.73	49.76	20.20265632
4	29.9722088	-660.89	4.09E+05	143.51	30.14	19.89523209
5	27.52780567	-288.14	2.18E+05	113.43	23.1	15.72502954
6	25.38428829	-95.89	1.21E+05	80.66	19.74	11.18173508
7	23.08493426	-40.39	9.42E+04	67.24	19.18	9.320767397
8	21.06404243	-18.02	8.30E+04	60.14	19.3	8.337729477
9	19.22573261	-9.22	7.80E+04	56.48	19.57	7.829476234
10	17.74627211	-4.94	7.53E+04	54.14	19.87	7.504941315
11	16.37648954	-2.62	7.36E+04	52.56	20.14	7.286615909
12	15.22663672	-1.53	7.27E+04	51.65	20.33	7.159562669
13	14.13082025	-1.14	7.23E+04	51.26	20.43	7.105629289
14	13.25544902	-0.7	7.19E+04	50.78	20.55	7.039789228
15	12.4625237	-0.39	7.16E+04	50.42	20.64	6.989365839
16	11.73738481	-0.18	7.14E+04	50.16	20.72	6.953063953
17	11.1001455	-0.1	7.13E+04	50.06	20.75	6.939229131
18	10.50631273	-0.06	7.12E+04	50.01	20.76	6.932715459
19	10.00001816	0.1	7.11E+04	49.79	20.83	6.902456693
20	9.521763359	0.13	7.10E+04	49.75	20.84	6.897092305

Then to observe how chi-square per degree of freedom changes with t_0 by keeping other fitted parameters constant we get the following plots for 3 distinct intervals and we can observe that the concavity of chi-square increases as the interval or the number of data points increases.

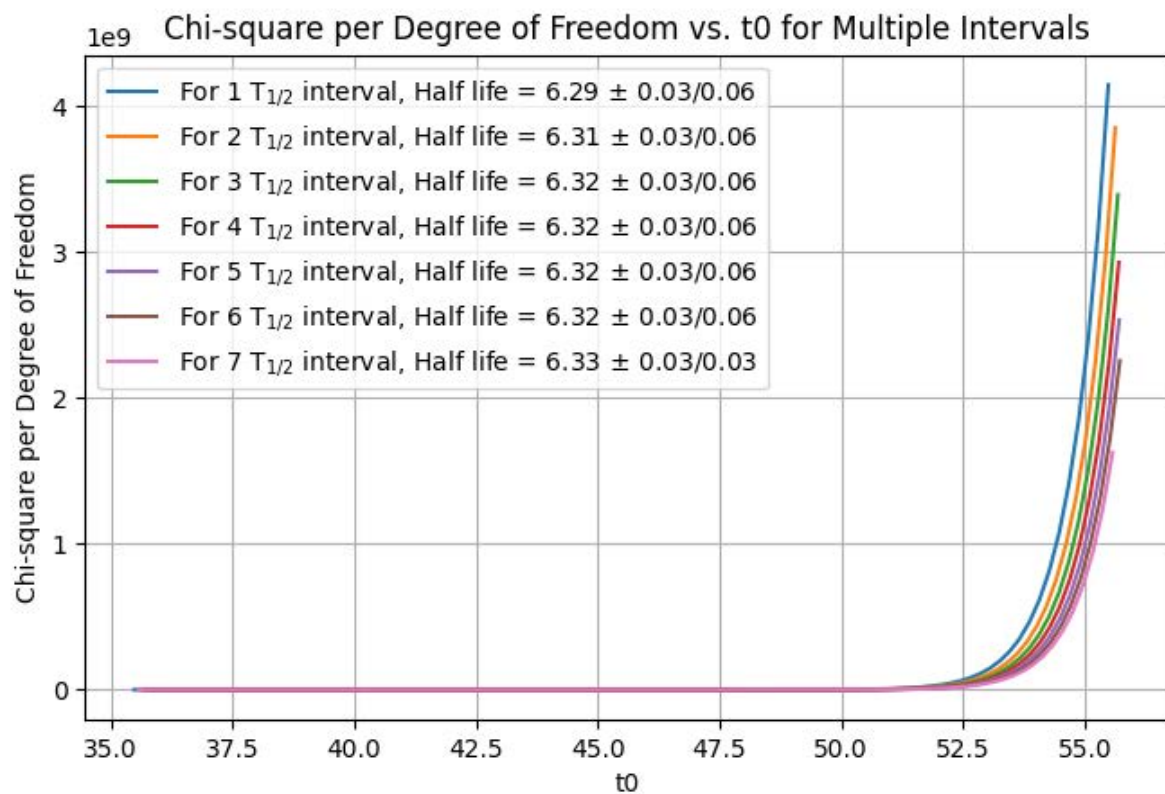
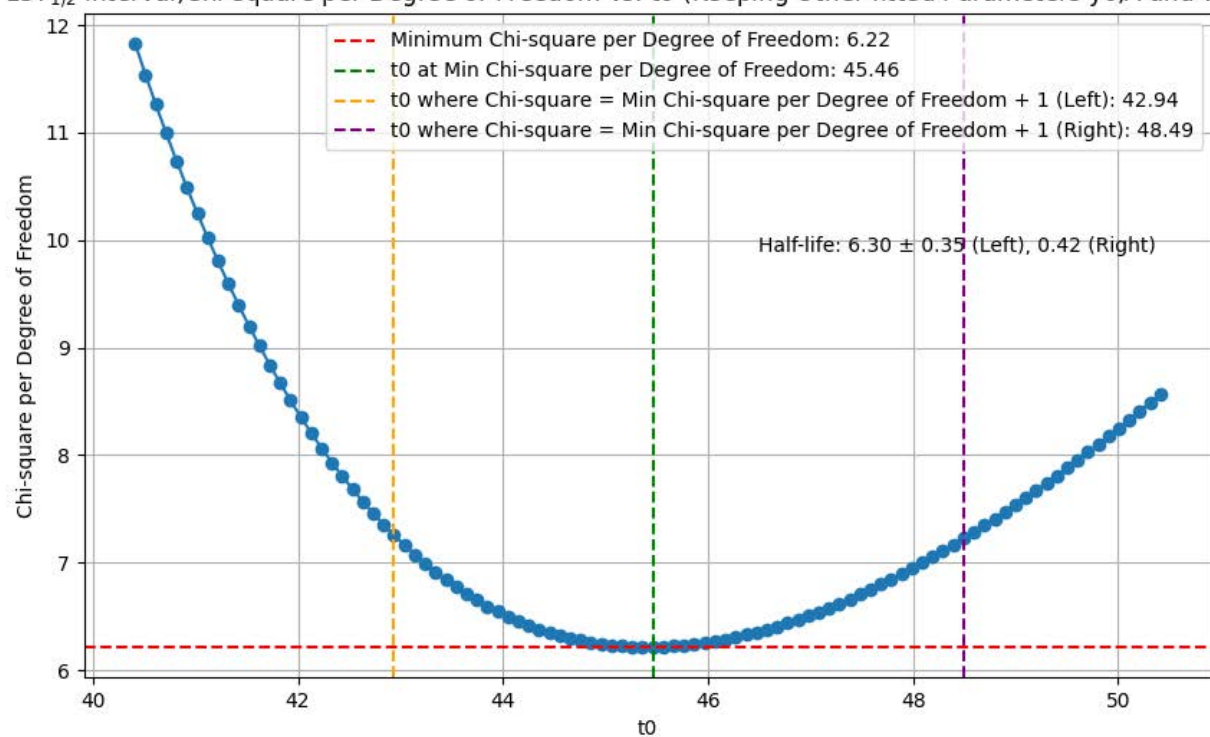
(For $3T_{1/2}$ interval) Chi-square per Degree of Freedom vs. t_0 (Keeping Other fitted Parameters y_0, A and w Constant)



(For $10T_{1/2}$ interval) Chi-square per Degree of Freedom vs. t_0 (Keeping Other fitted Parameters y_0, A and w Constant)



(For 15 $T_{1/2}$ interval) Chi-square per Degree of Freedom vs. t_0 (Keeping Other fitted Parameters y_0, A and w Constant)



The time difference spectrum after removing the Gaussian part is fitted to the curve

$$y = y_0 + Ae^{-x/t_0}$$

by varying the parameters y_0 , A and t_0 to minimize chi square. Keeping y_0 and A constant, t_0 is varied, and a chi-square plot is obtained for different intervals ranging from 1 half-life to 7 half-lives. Similar to the chi-square plots obtained for the Gaussian plus exponential fit, we observe that the concavity of the chi-square plot increases as the interval or the number of data points increases.

Several factors influence the applicability of this technique:

- **Statistical considerations:** As the state decays, the counts in the subsequent time cuts decrease. To ensure there are enough counts for intensity determination in the later part of the decay curve, the transition being measured should have a high enough count rate. This implies that the nuclei of interest should be well populated, and the peak-to-background ratio should be high.
- **Bin size of the time cuts:** The bin size should be significantly smaller than the half-life to ensure an adequate number of points for the exponential fit. If the bin size is comparable to the half-life, there may be insufficient points for a reliable fit. Additionally, a sufficient number of time cuts is necessary to cover three to four half-lives of the isomeric state for an accurate fit.
- **Detector response time:** Each detector has a processing time that depends on the interaction position of the gamma and the energy of the gamma. It is essential to ensure that the time cuts are not smaller than the detector response time. Attempting to determine lifetimes of isomeric states lower than the detector response time is not achievable using this method.

7.2 Common Timing Electronic Modules

Ensuring precise and consistent marking of the arrival time of detected events is the primary function of a timing spectrometer. The achievement of optimal time resolution is crucial, whether the application involves time spectroscopy or the determination of simultaneous events from two different detectors. The approach to achieving the best time resolution depends on the type of detector and the selection of an appropriate timing discriminator based on detector characteristics and the intended application. The electronic components include various modules such as the Timing Filter Amplifier (TFA), Constant Fraction Discriminator (CFD), Delay Unit (DU), Coincidence Unit (CU), Delay Gate Generator (DGG), Time to Amplitude Converter (TAC), and Multi-Channel Analyzer (MCA), each with its own working principles, outlined as follows:

- **ConstantFractionDiscriminator(CFD):**The CFD produces an output logic pulse if its input signal exceeds a preset threshold level. It operates in three modes: leading edge (LE), constant fraction (CF), and slow rise time reject (SRT). In leading-edge mode, a voltage comparator with a preset threshold generates a logic pulse when the leading edge of the analog pulse crosses the threshold. The logic pulse ends when the trailing edge of the analog pulse crosses the threshold in the opposite direction. In CFD mode, the input signal is split into two parts. One part is attenuated to a fraction f corresponding to the desired timing fraction of full amplitude, and the other part is delayed and inverted. These two signals are added to form the constant-fraction timing signal. The sum waveform yields a bipolar pulse with a zero crossing time independent of the pulse amplitude. The CFD provides excellent time resolution for all commonly used detectors, surpassing the performance of the leading edge discriminator. It accepts input pulses in the range of 0 to -5 V and generates a NIM fast negative output and a slow positive output.
- **Timing Filter Amplifier (TFA):** The TFA is a wideband, pulse-shaping amplifier designed to optimize timing analysis. It allows users to adjust time constant settings for optimizing pulse shape and signal-to-noise ratio during timing measurements. Course gain and fine gain settings offer control for continuous coverage. The TFA module includes integrator and differentiator components, allowing adjustment of rise time and decay time for the signal. Time constants between 20 to 500 ns can be selected. The TFA features pole/zero adjustment to ensure a quick return to baseline after each pulse, optimizing overload recovery and high count rate performance. A toggle switch is provided for selecting inverted or non-inverted output polarity.
- **Multi-Channel Analyzer (MCA):** The MCA is an analog-to-digital converter capable of measuring distributions of input signals in the form of pulses. Input pulses are sorted into bins (channels) based on their amplitude. The MCA provides a visual display of the resulting distributions and typically outputs the data to a computer for further analysis. In this setup, the ORTEC software serves as the interface, allowing configuration of the MCA and setting preset values for measurement.
- **Delay Gate Generator (DGG):** The DGG accepts either positive or negative logic pulses and introduces a delay of up to 110 μ s. The output can have either positive or negative polarity with a selected pulse width ranging from 100 ns to 110 μ s.
- **Coincidence Unit (CU):** The CU allows the preparation of a desired gate range, either 10-100 ns or 0.1-1 μ s. It takes positive logic pulses from the discriminators to provide a NIM output to the MCA, serving as a gate for the pulse generated from the TAC.
- **Time to Amplitude Converter (TAC):** The ORTEC Model 566 TAC measures the time interval between its start and stop input pulses, generating an analog output pulse proportional to the measured time. It is suitable for timing experiments requiring usable time ranges of 50 ns to 2 ms, enabling the analysis of nuclear events within a selected time range.

8 Summary and Conclusion

The treatment of electromagnetic and weak interactions involves considering them as perturbations, resulting in transitions between various states. An analysis of the transition rates offers valuable insights into the characteristics of the atomic nucleus. The discussion encompasses different bulk properties of nuclei. The theory of Multipole expansion of electromagnetic fields is explored, placing emphasis on selection rules. The angular distribution of multipole radiation is also covered, elucidating dipole and quadrupole radiation patterns for pure (l, m) multipoles. The derivation of Weisskopf units for transition probability is presented for both electric and magnetic decay. Electromagnetic transitions are examined by establishing a connection between the transition probability \mathcal{W} and the nuclear matrix element M_{fi} through first-order time-dependent perturbation. Total power radiated due to contributions from the different multipoles is also discussed.

Various types of detectors and their properties are studied and utilized to get information about timing and energy information of the γ -ray . The achievement of optimal time resolution is crucial, whether the application involves time spectroscopy or the determination of simultaneous events from two different detectors. The approach to achieving the best time resolution depends on the type of detector and the selection of an appropriate timing discriminator based on detector characteristics and the intended application.

Various methods for finding life-time of a state are presented and compared. The half-life for the first excited state with the spin parity $\frac{5}{2}^+$ of the ^{133}Cs at the excitation energy of 81 KeV with an established half-life of 6.28 ns is measured in two different methods. In the first method the time difference spectrum is fitted with the convolution function associated with the single exponential decay. From this method the half-life is found to be 6.14 ± 0.15 ns. In the second method the revised time difference spectrum is obtained by removing the data points of the Gauss part and fitting the rest data points to a exponential decay. From this method the half-life is found to be 6.39 ± 0.092 ns. Taking the average of the two methods we get the half-life of the state to be 6.27 ± 0.12 ns. The percentage error of the calculated result from the accepted value is 0.2%. Several factors influencing the applicability of this technique is also discussed.

References

- J.M.Blattand V.F. Weisskopf. Theoretical Nuclear Physics. Wiley, New York, 1952.
- A. Bohr and B.R.Mottelson. Nuclear Structure, volume I. Benjamin, New York, 1969.
- Introductory Nuclear Physics, SAMUEL S.M.WONG, University of Toronto
- The Nuclear Many-Body Problem - Peter Ring, Peter Schuck
- P. J. Nolan and J.F. Sharpey-Schafer, The measurement of the lifetimes of excited nuclear states,Rep. Prog. Phys., Vol. 42, 1979.
- R. S. Weaver and R. E. Bell, Method of Evaluating Delayed Coincidence Experiments, Nuclear Instruments and Methods 9, 1960, 149-153.

H. J. Kim and W. T. Milner, Short Nuclear Lifetime Measurements via the Pulse Beam Delayed-Coincidence Technique, Nuclear Instruments and Methods 95, 1971, 429-434.

E. De Lima, H. Kawakami et al., Tests of the Methods of Analysis of Picosecond Lifetimes and Measurement of the Half-life of the 569.6 keV Level in ^{207}Pb , Nuclear Instruments and Methods 151, 1978, 221-225.

V. Rahkonen, An Investigation of the Yrast States in $^{205,207}\text{Po}$, Nuclear Physics A441, -32, 1985.

L. Boström, B. Olsen et al., Numerical Analysis of the Time Spectrum of Delayed Coincidences I and II, Nuclear Instruments and Methods 44, 1966, 61-64, 65-72.

W. Anderjtscheff M. Senba et al., Nanosecond Feeding Times: Evidence for High Spin Isomerism Near $A=75$ and 100, Physics Letters Vol. 113B, 3, 1982.

R. Palit, "Investigation of exotic shapes, correlations and isomers in nuclei with large compton suppressed clover array," in AIP Conference Proceedings, vol. 1336, pp. 573–575, American Institute of Physics, 2011.

J.-M. R'egis, Fast Timing with LaBr₃ (Ce) Scintillators and the Mirror Symmetric Centroid Difference Method. PhD thesis, 05 2011.

R. Palit and S. Saha, "Investigation of exotic modes of spinning nuclei near ^{90}Zr ," Pramana, vol. 82, no. 4, pp. 649–658, 2014.

M. S. Laskar, R. Palit, E. Ideguchi, T. Inakura, S. Mishra, F. Babra, S. Bhattacharya, . Choudhury , B. Das, B. Das, et al., "Enhanced B(E3)strength observed in ^{137}La ," Physical Review C, vol. 104, no. 1, p. L011301, 2021.

M. S. Laskar, R. Palit, E. Ideguchi, T. Inakura, S. Mishra, F. Babra, S. Bhattacharya, . Choudhury , B. Das, B. Das, et al., "Enhanced B(E3)strength observed in ^{137}La ," Physical Review C, vol. 104, no. 1, p. L011301, 2021.

K. C. Mann and R. P. Chaturvedi. The decay of ba133. Canadian Journal of Physics, 41(6):932–945,1963. doi: 10.1139/p63-099.URL <https://doi.org/10.1139/p63-099>.

[18] B. N. L. National Nuclear Data Center, "Nudat (nuclear structure and decay data)," 2008.

[19] Jackson, John David, 1925-2016. Classical Electrodynamics. New York :Wiley

A Appendix

A.1 Transition Probability in Time-Dependent Perturbation Theory

Transition probability and the transition matrix element can be connected by using time-dependent perturbation theory. Consider a time-dependent Hamiltonian,

$$H(t) = H_0 + H'(t) \quad (H_0 \text{ is independent of time})$$

$H'(t)$ is sufficiently weak so we can consider it to be a perturbation of H_0 . Let $\phi_n(r)$ represent the eigenfunction of H_0 such that they form a complete set of orthonormal functions. The eigenfunction $\psi(r, t)$ for H_0 alone is the solution of the time-dependent Schrodinger equation, $i\hbar \frac{\partial \psi(r, t)}{\partial t} = H_0 \psi(r, t)$ and expressing in terms of $\phi_n(r)$ we get

$$\psi(\mathbf{r}, t) = \sum_n c_n \phi_n(\mathbf{r}) e^{-iE_n t/\hbar} \implies c_n = \int \phi_n^*(\mathbf{r}) e^{iE_n t/\hbar} \psi(\mathbf{r}, t) dV \quad (103)$$

Hence the expansion coefficients are independent of time. In this case we have not included the perturbed hamiltonian. If we include it the expansion coefficients becomes time dependent

$$\Psi(\mathbf{r}, t) = \sum_n c_n(t) \phi_n(\mathbf{r}) e^{-tE_n/\hbar} \quad (104)$$

$c_n(t)$ denotes the probability amplitude for finding the system in the unperturbed state n at time t . Substituting (104) into the time-dependent Schrodinger equation for $H(t)$ to obtain $c_n(t)$ we get,

$$i\hbar \sum_n \left\{ \frac{dc_n(t)}{dt} - ic_n(t) \frac{E_n}{\hbar} \right\} \phi_n(r) e^{-iE_n t/\hbar} = \{H_0 + H'(t)\} \sum_n c_n(t) \phi_n(r) e^{-iE_n t/\hbar}$$

By taking products with $\phi_n^*(r) e^{iE_n t/\hbar}$ on both sides of the equation and integrating over all the independent variables except t , we obtain the result

$$\begin{aligned} & i\hbar \sum_n \left\{ \frac{dc_n(t)}{dt} - ic_n(t) \frac{E_n}{\hbar} \right\} e^{i(E_k - E_n)t/\hbar} \langle \phi_k(r) | \phi_n(r) \rangle \\ &= \sum_n c_n(t) \{ \langle \phi_k(r) | H_0 | \phi_n(r) \rangle + \langle \phi_k(r) | H'_0(t) | \phi_n(r) \rangle \} \phi_n(r) e^{i(E_k - E_n)t/\hbar} \end{aligned} \quad (105)$$

Now inserting $\langle \phi_k(r) | \phi_n(r) \rangle = \delta_{kn}$ and $\langle \phi_k(r) | H_0 | \phi_n(r) \rangle = E_n \delta_{kn}$ in (105) we have,

$$i\hbar \frac{dc_k(t)}{dt} = \sum_n \langle \phi_k | H'(t) | \phi_n(t) \rangle e^{i\omega_{kn} t} \quad (106)$$

where $\omega_{kn} = \frac{(E_k - E_n)}{\hbar}$. Take initial condition that at $t = 0$ the system is in state $\phi_0(r)$ i.e.

$$c_n(0) = \begin{cases} 1 & \text{for } n = 0 \\ 0 & \text{for } n \neq 0 \end{cases}$$

If the perturbation is weak we can expect for all time t of interest,

$$c_k(t) = \begin{cases} 1 & \text{for } k = 0 \\ 0 & \text{for } k \neq 0 \end{cases}$$

If we retain only the $n = 0$ term of (106) we get

$$i\hbar \frac{dc_k(t)}{dt} = \langle \phi_k | H'(t) | \phi_0(t) \rangle e^{i\omega_{k0}t}$$

If the time variation of $H'(t)$ is slow compared with $e^{i\omega_{k0}t}$, we can take H' to be a constant so solving the equation we get:

$$c_k(t) = \frac{\langle \phi_k | H' | \phi_0(t) \rangle}{E_k - E_0} (1 - e^{i\omega_{k0}t}) \implies |c_k(t)|^2 = 2 |\langle \phi_k(r) | H' | \phi_0(r) \rangle|^2 \frac{1 - \cos \omega_{k0}t}{(E_k - E_0)^2}$$

as the probability for finding the system in state k at time t if it started from state 0 at time $t = 0$. The total probability to a group of states within some interval labeled by f is given by a summation over all the final states k in the interval,

$$\sum_{k \in f} |c_k(t)|^2 = 2 \sum_{k \in f} |\langle \phi_k(r) | H' | \phi_0(r) \rangle|^2 \frac{(1 - \cos \omega_{k0}t)}{(E_k - E_0)^2}$$

Using $\omega_{kn} = \frac{(E_k - E_n)}{\hbar}$ and replacing the summation by integration over energy multiplied by the density of final states $\rho(E_k)$ we get,

$$\sum_{k \in f} |c_k(t)|^2 = \frac{2}{\hbar^2} \int |\langle \phi_k(r) | H' | \phi_0(r) \rangle|^2 \frac{(1 - \cos \omega_{k0}t)}{\omega_{k0}^2} \rho(E_k) dE_k$$

The transition probability per unit time, \mathcal{W} , corresponds to the rate of finding the system in the group of final states labeled by f and may be expressed as

$$\mathcal{W} = \frac{d}{dt} \sum_{k \in f} |c_k(t)|^2 = \frac{2}{\hbar^2} \int |\langle \phi_k(r) | H' | \phi_0(r) \rangle|^2 \frac{\sin \omega_{k0}t}{\omega_{k0}} \rho(E_k) dE_k$$

Since the function $\frac{\sin \omega_{k0}t}{\omega_{k0}}$ oscillates very quickly except where $\omega_{k0} \approx 0$, only a small region around $E_k = E_0$ can contribute to the integral. In this small energy interval we may regard the matrix element $\langle \phi_k(r) | H' | \phi_0(r) \rangle$ and the state density $\rho(E_k) = \rho(E_f)$ to be constant and also using $\int_{-\infty}^{+\infty} \frac{\sin \omega_{k0}t}{\omega_{k0}} d\omega_{k0} = \pi$ we have the **transition probability per unit time** as

$$\boxed{\mathcal{W} = \frac{2\pi}{\hbar} |\langle \phi_f(r) | H' | \phi_0(r) \rangle|^2 \rho(E_f)} \quad (107)$$

It is often referred to as **Fermi's golden rule**.

A.2 Parity and Angular Momentum

The parity operator $\hat{\pi}$ is defined as,

$$\hat{\pi}|x\rangle = |-x\rangle$$

The eigenvalues of the parity operator are obtained as,

$$\hat{\pi}|\psi_\lambda\rangle = \lambda|\psi_\lambda\rangle \implies \hat{\pi}^2|\psi_\lambda\rangle = \lambda^2|\psi_\lambda\rangle$$

Since,

$$\hat{\pi}^2|x\rangle = |x\rangle$$

one gets

$$\lambda^2|\psi_\lambda\rangle = |\psi_\lambda\rangle \implies \lambda = \pm 1$$

in x-space it is

$$\langle x|\hat{\pi}|\psi_\lambda\rangle = \langle -x|\psi_\lambda\rangle = \psi_\lambda(-x) = \lambda\psi_\lambda(x)$$

$$\psi_\lambda(x) = \begin{cases} \text{even} & \lambda = 1 \\ \text{odd} & \lambda = -1 \end{cases}$$

If $[H, \hat{\pi}] = 0$, as it happens with potentials with reflection symmetry, parity is conserved and λ is a good quantum number.

A.3 Unitary Operator: symmetries and conservation laws

A.3.1 Rotational symmetry

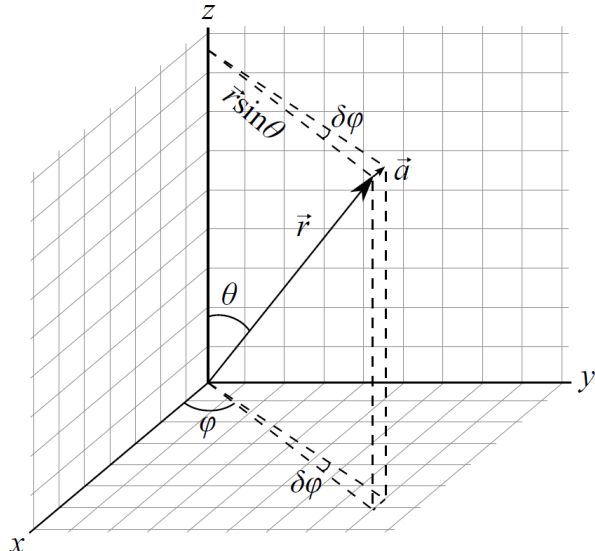


Figure 20: Relation between the vectors a , $\delta\varphi$ and r corresponding to the rotation of the system with angle $\delta\varphi$.

Performing a rotation of the system by an angle $\delta\varphi$, as shown in the figure, a function $\psi(r)$ is transformed to $\psi(r + a)$. As seen in the Figure, it is $a = \delta\varphi \mathbf{r} \sin \theta$ and the relation among the vectors $a, \delta\varphi$ and r is $a = \delta\varphi \times r$. Calling $F(r) = \psi(r + a)$ one gets

$$\Psi(r) = F(r - a) = F(r) - a \cdot \nabla F(r) + \dots$$

Performing a Taylor expansion as,

$$F(x + \Delta x, y + \Delta y, z + \Delta z) = F(x, y, z) + \frac{\partial F(x, y, z)}{\partial x} \Delta x + \frac{\partial F(x, y, z)}{\partial y} \Delta y + \frac{\partial F(x, y, z)}{\partial z} \Delta z + \dots$$

we get,

$$F(\mathbf{r} + \Delta \mathbf{r}) = F(\mathbf{r}) + \Delta \mathbf{r} \cdot \nabla F(\mathbf{r}) + \dots$$

With $\delta\varphi$ infinitesimal it is,

$$\Psi(\mathbf{r}) - F(\mathbf{r}) = -(\delta\varphi \times \mathbf{r}) \cdot \nabla F(\mathbf{r}) = -\delta\varphi \cdot (\mathbf{r} \times \nabla F(\mathbf{r}))$$

and replacing momenta by the corresponding operators one gets,

$$\mathbf{p} = \frac{i}{\hbar} \boldsymbol{\nabla} \implies \mathbf{r} \times \boldsymbol{\nabla} = \frac{i}{\hbar} \mathbf{r} \times \mathbf{p} = \frac{i}{\hbar} \mathbf{L}$$

Finally we have,

$$\Psi(\mathbf{r}) = F(\mathbf{r}) - \frac{i}{\hbar} \delta\varphi \cdot \mathbf{L} F(\mathbf{r}) = \left(1 - \frac{i}{\hbar} \delta\varphi \cdot \mathbf{L}\right) F(\mathbf{r})$$

For a finite angle φ one defines a small angle by using $\delta\varphi = \varphi/n$, where n is a large number. Rotating n times, i. e. applying the rotation operator n times, and in the limit of $n \rightarrow \infty$, one gets,

$$\Psi(\mathbf{r}) = \lim_{n \rightarrow \infty} \left(1 - \frac{i}{\hbar} \frac{\varphi \cdot \mathbf{L}}{n}\right)^n F(\mathbf{r})$$

As $e^t = \lim_{n \rightarrow \infty} (1 + \frac{t}{n})^n$ we have:

$$\Psi(\mathbf{r}) = e^{-\frac{i}{\hbar} \varphi \cdot \mathbf{L}} F(\mathbf{r}) = e^{-\frac{i}{\hbar} \varphi \cdot \mathbf{L}} \Psi(\mathbf{r} + \mathbf{a})$$

Therefore the rotation operator is $\mathbf{U}_R = e^{-\frac{i}{\hbar} \varphi \cdot \mathbf{L}}$ and we get $\Psi(\mathbf{r} + \mathbf{a}) = \mathbf{U}_R^{-1} \Psi(\mathbf{r})$
If the Hamiltonian is rotational invariant

$$H\Psi_n(\mathbf{r} + \mathbf{a}) = E_n \Psi(\mathbf{r} + \mathbf{a}) = E_n \mathbf{U}_R^{-1} \Psi(\mathbf{r}) = \mathbf{U}_R^{-1} H \Psi(\mathbf{r})$$

$$U_R H \Psi_n(\mathbf{r} + \mathbf{a}) = U_R H U_R^{-1} \Psi(\mathbf{r}) = H \Psi(\mathbf{r})$$

$$[\mathbf{H}, \mathbf{U}_R] = \mathbf{0} \implies [\mathbf{H}, \mathbf{L}] = \mathbf{0}$$

A.4 Code to Fit the all the data points with a convoluted function of a exponential decay

```

import numpy as np
import matplotlib.pyplot as plt
from scipy.optimize import minimize
from scipy.special import erf
from math import sqrt

from matplotlib.ticker import AutoMinorLocator

# Define the function to fit
def my_function(params, x, y_data, errors):
    y0, A, t0, w = params
    z = ((x - xc) / w) - w / t0
    arg = 0.5 * (w / t0)**2 - (x - xc) / t0
    erf_arg = z / sqrt(2) + 1
    y_fit = y0 + (A / t0) * np.exp(arg) * (erf(erf_arg) / 2)
    chi_sq = np.sum(((y_fit - y_data) / errors)**2)
    return chi_sq

# Load data from the file
data = np.loadtxt('133Cs_alldata.dat')
x_data = data[1985:2203, 0]
y_data = data[1985:2203, 1]
errors = data[1985:2203, 2]
xc = 2006
# Initial guess for parameters y0 A t0 w
initial_params = [-1.0, 100000, 15, 40]

# Perform chi-square minimization using the minimize function
result = minimize(my_function, initial_params, args=(x_data, y_data, errors))

# Extract the optimized parameters and covariance matrix
optimal_params = result.x
cov_matrix = result.hess_inv

# Calculate errors from the diagonal elements of the covariance matrix
errors_params = np.sqrt(np.diag(cov_matrix))

# Generate fitted data using the optimized parameters
z_opt = ((x_data - xc) / optimal_params[3]) - optimal_params[3] / optimal_params[2]
arg_opt = 0.5 * (optimal_params[3] / optimal_params[2])**2 - (x_data - xc) / optimal_params[2]
erf_arg_opt = z_opt / sqrt(2) + 1
y_fit = optimal_params[0] + (optimal_params[1] / optimal_params[2]) * np.exp(arg_opt) * (erf(erf_arg_opt) / 2)

# Plot the data points, fitted curve, and error bars
plt.errorbar(x_data, y_data, yerr=errors, fmt='o', label='Data with Errors', markersize=3, color='blue',
              capsize=2)
plt.plot(x_data, y_fit, label=f'Fitted Curve: $y = y_0 + \frac{A}{t_0} e^{-\frac{(x-x_c)}{w}}$')

# Add minor ticks on both x and y axes
plt.minorticks_on()

# Set the minor locator for both x and y axes
plt.gca().xaxis.set_minor_locator(AutoMinorLocator())
plt.gca().yaxis.set_minor_locator(AutoMinorLocator())

# Display the optimized parameters and their errors
plt.text(0.95, 0.75, f'y0: {optimal_params[0]:.3f} ± {errors_params[0]:.3f}', transform=plt.gca().transAxes)
plt.text(0.95, 0.70, f'A: {optimal_params[1]:.3e} ± {errors_params[1]:.3e}', transform=plt.gca().transAxes)
plt.text(0.95, 0.65, f't0: {optimal_params[2]:.3f} ± {errors_params[2]:.3f}', transform=plt.gca().transAxes)
plt.text(0.95, 0.60, f'w: {optimal_params[3]:.3f} ± {errors_params[3]:.3f}', transform=plt.gca().transAxes)

# Display the expression for z
plt.text(0.25, 0.75, f'where $z = \frac{(x - x_c)}{w} - \frac{t_0}{w}$', transform=plt.gca().transAxes)

plt.xlabel('Channel Number')
plt.ylabel('Number of Counts')
plt.title("Fitting the time difference spectrum with the convolution function \n associated with the sin")

```

```

plt.legend()

# Save the plot as a JPG file
plt.savefig('1.pdf', format='pdf')

plt.show()

# Display the optimized parameters
print("Optimized Parameters:")
print(f"y0: {optimal_params[0]} {errors_params[0]}")
print(f"A: {optimal_params[1]} {errors_params[1]}")
print(f"t0: {optimal_params[2]} {errors_params[2]}")

```

A.5 Code to Fit the convoluted part with a exponential function by removing gaussian part data points

```

import numpy as np
import matplotlib.pyplot as plt
from scipy.optimize import minimize

# Define the function to fit
def my_function(params, x):
    y0, A, t0 = params
    return y0 + A * np.exp(-x / t0)

# Define the chisquare
def chi_square(params, x, y_data, errors):
    y_fit = my_function(params, x)
    chi_sq = np.sum(((y_fit - y_data) / errors)**2)
    return chi_sq

# Numerical approximation of the Hessian matrix
def numerical_hessian(func, params, args, epsilon=1e-5):
    hessian_matrix = np.zeros((len(params), len(params)))
    for i in range(len(params)):
        for j in range(len(params)):
            params_plus_plus = np.copy(params)
            params_plus_plus[i] += epsilon
            params_plus_plus[j] += epsilon
            chi_plus_plus = func(params_plus_plus, *args)

            params_minus_plus = np.copy(params)
            params_minus_plus[i] -= epsilon
            params_minus_plus[j] += epsilon
            chi_minus_plus = func(params_minus_plus, *args)

            params_minus_minus = np.copy(params)
            params_minus_minus[i] -= epsilon
            params_minus_minus[j] -= epsilon
            chi_minus_minus = func(params_minus_minus, *args)

            params_minus_minus[j] += 2 * epsilon

            hessian_matrix[i, j] = (chi_plus_plus - chi_minus_plus - chi_minus_minus + func(params_minus_minus))

    return hessian_matrix

# Load data from the file
data = np.loadtxt('133Cs_only_exp.txt')
x_data = data[:, 0]
y_data = data[:, 1]
errors = data[:, 2] # Assuming the 3rd column contains errors

# Initial guess for parameters
initial_params = [-2.69, 1.0e22, 40.0]

# Perform chisquare minimization using the minimize function

```

```

result = minimize(chi_square, initial_params, args=(x_data, y_data, errors), method='L-BFGS-B')

# Extract the optimized parameters
y0_opt, A_opt, t0_opt = result.x

# Compute the Hessian matrix numerically
hessian_matrix = numerical_hessian(chi_square, result.x, args=(x_data, y_data, errors))

# Calculate errors from the diagonal elements of the covariance matrix
errors_params = np.sqrt(np.diag(np.linalg.inv(hessian_matrix)))

# Generate fitted data using the optimized parameters
y_fit = my_function([y0_opt, A_opt, t0_opt], x_data)

# Plot the data points, fitted curve, and error bars
plt.errorbar(x_data, y_data, yerr=errors, fmt='o', label='Data with Errors', markersize=3, color='blue')
plt.plot(x_data, y_fit, label=f'Fitted Curve: $y_0 + A \cdot e^{\{-x / t_0\}}$', color='red')

# Display the optimized parameters and their errors on the plot
plt.text(0.95, 0.8, f'y0: {y0_opt:.3f} ± {errors_params[0]:.3f}', transform=plt.gca().transAxes, ha='right')
plt.text(0.95, 0.75, f'A: {A_opt:.3e} ± {errors_params[1]:.3e}', transform=plt.gca().transAxes, ha='right')
plt.text(0.95, 0.7, f't0: {t0_opt:.3f} ± {errors_params[2]:.3f}', transform=plt.gca().transAxes, ha='right')

# Customize plot settings
plt.xlabel('Channel Number')
plt.ylabel('Number of Counts')
plt.title('Fitting the Convolution of a Prompt with an Exponential Function')
plt.legend()

# Save the plot as a JPG file
plt.savefig('fit_result_with_title.jpg', format='jpg')

# Display the optimized parameters and their errors
print("Optimized Parameters:")
print(f"y0: {y0_opt} ± {errors_params[0]}")
print(f"A: {A_opt} ± {errors_params[1]}")
print(f"t0: {t0_opt} ± {errors_params[2]}")

# Show the plot
plt.show()

```

A.6 Code to plot Chi-square per DoF vs Half-Life

```

import numpy as np
import matplotlib.pyplot as plt
from scipy.optimize import minimize
from scipy.special import erf
from math import sqrt, log

from matplotlib.ticker import AutoMinorLocator

# Define the function to fit
def my_function(params, x, y_data, errors):
    y0, A, t0, w = params
    z = ((x - xc) / w) - w / t0
    arg = 0.5 * (w / t0) ** 2 - (x - xc) / t0
    erf_arg = z / sqrt(2) + 1
    y_fit = y0 + (A / t0) * np.exp(arg) * (erf(erf_arg)) / 2
    chi_sq = np.sum(((y_fit - y_data) / errors) ** 2)
    return chi_sq

# Load data from the file
data = np.loadtxt('td_spectrum.txt')

# Initialize parameters

```

```

xc = 2007
initial_params = [0, 70000, 40, 20]

# Prepare arrays to store results
chi_square_per_dof = []
half_life_indices = []
half_lives = []
fitted_params_list = []

# Loop over each half-life interval
for i in range(1, 21):
    end_index = 1980 + 30 * i
    x_data = data[1980:end_index, 0]
    y_data = data[1980:end_index, 1]
    errors = data[1980:end_index, 2]

    # Check for zero values in errors and handle them
    errors[errors == 0] = np.inf # Replace zero errors with a large number to avoid division by zero

    # Perform chi-square minimization using the minimize function
    try:
        result = minimize(my_function, initial_params, args=(x_data, y_data, errors))
        chi_square_per_dof.append(result.fun / len(x_data))
        fitted_params = result.x
        fitted_params_list.append(fitted_params)
        half_life = fitted_params[2] * log(2) * 0.2
        half_lives.append(half_life)
    except Exception as e:
        chi_square_per_dof.append(np.nan)
        fitted_params_list.append([np.nan] * len(initial_params))
        half_lives.append(np.nan)
        print(f"Optimization failed for half-life {i}: {e}")

    half_life_indices.append(i)

# Print the table
print(f"\n{'Interval Taken':<20}{'Chi-square per DoF':<25}{'Half-Life':>25}")
for i in range(len(half_life_indices)):
    print(f"\n{half_life_indices[i]:<20}{chi_square_per_dof[i]:<25}{half_lives[i]}")

# Plot chi-square per degree of freedom vs half-life index
plt.figure()
plt.plot(half_life_indices, chi_square_per_dof, marker='o', linestyle='-', color='blue')
plt.xlabel('Number of Half-Lives')
plt.ylabel('Chi-square per Degree of Freedom')
plt.title('Chi-square per Degree of Freedom vs. Number of Half-Lives')
plt.grid(True)

# Add minor ticks on both x and y axes
plt.minorticks_on()
plt.gca().xaxis.set_minor_locator(AutoMinorLocator())
plt.gca().yaxis.set_minor_locator(AutoMinorLocator())

# Save the plot as a PDF file
plt.savefig('chi_square_vs_half_lives.pdf', format='pdf')

# Show the plot
plt.show()

# Display the fitted parameters, chi-square per degree of freedom, and half-life for each interval
print("\nDetailed Results:")
print(f"\n{'Interval':<10} {'Chi-square per DoF':<25} {'y0':<10} {'A':<15} {'t0':<10} {'w':<10} {'Half-Life':>25}")
for i, (params, chi_sq, half_life) in enumerate(zip(fitted_params_list, chi_square_per_dof, half_lives)):
    print(f"\n{i:<10} {chi_sq:<25} {params[0]:<10.2f} {params[1]:<15.2e} {params[2]:<10.2f} {params[3]:<10.2f}")

```

A.7 Code to plot Chi-square per DoF vs t0 for gauss+exponential fit

```

import numpy as np
import matplotlib.pyplot as plt
from scipy.optimize import minimize
from scipy.special import erf
from math import sqrt, log

# Define the function to fit
def my_function(params, x, y_data, errors):
    y0, A, t0, w = params
    z = ((x - xc) / w) - w / t0
    arg = 0.5 * (w / t0) ** 2 - (x - xc) / t0
    erf_arg = z / sqrt(2) + 1
    y_fit = y0 + (A / t0) * np.exp(arg) * (erf(erf_arg) / 2)

    # Add a small value to errors to prevent division by zero
    errors[errors == 0] = 1

    chi_sq = np.sum(((y_fit - y_data) / errors) ** 2)
    # Calculate degrees of freedom
    dof = len(x) - len(params)
    # Calculate chi-square per degree of freedom
    chi_sq_per_dof = chi_sq / dof
    return chi_sq_per_dof

# Load data from the file
data = np.loadtxt('td_spectrum.txt')
x_data = data[1983:2430, 0]
y_data = data[1983:2430, 1]
errors = data[1983:2430, 2]

xc = 2007
# Initial guess for parameters y0 A t0 w
initial_params = [0, 50000, 50, 6]

# Set bounds for optimization parameters
bounds = [(None, None), (0, None), (1, None), (0, None)] # y0 has no bounds, A > 0, t0 > 0, w > 0

# Perform chi-square minimization using the minimize function with bounds
result = minimize(my_function, initial_params, args=(x_data, y_data, errors), bounds=bounds)

# Extract the optimized parameters
optimal_params = result.x

# Calculate chi-square per degree of freedom for different t0 values while keeping other parameters constant
t0_range = np.linspace(optimal_params[2] - 5, optimal_params[2] + 5, 100)
chi_sq_per_dof_values_t0 = np.zeros_like(t0_range)
for k, t0 in enumerate(t0_range):
    params = [optimal_params[0], optimal_params[1], t0, optimal_params[3]]
    chi_sq_per_dof_values_t0[k] = my_function(params, x_data, y_data, errors)

# Find the minimum chi-square per degree of freedom and corresponding t0
min_chi_sq_per_dof = np.min(chi_sq_per_dof_values_t0)
min_chi_sq_per_dof_index = np.argmin(chi_sq_per_dof_values_t0)
t0_at_min_chi_sq_per_dof = t0_range[min_chi_sq_per_dof_index]

# Find t0 values on both sides of the minimum where chi-square per degree of freedom equals chi-square per dof
t0_chi_sq_plus_1_left = None
t0_chi_sq_plus_1_right = None
for i in range(min_chi_sq_per_dof_index - 1, -1, -1):
    if chi_sq_per_dof_values_t0[i] >= min_chi_sq_per_dof + 1:
        t0_chi_sq_plus_1_left = t0_range[i]
        break
for i in range(min_chi_sq_per_dof_index + 1, len(t0_range)):
    if chi_sq_per_dof_values_t0[i] >= min_chi_sq_per_dof + 1:
        t0_chi_sq_plus_1_right = t0_range[i]
        break

# Calculate half-life and its error

```

```

half_life = t0_at_min_chi_sq_per_dof * log(2) * 0.2
if t0_chi_sq_plus_1_left is not None:
    error_left = (t0_at_min_chi_sq_per_dof - t0_chi_sq_plus_1_left) * log(2) * 0.2
else:
    error_left = np.nan

if t0_chi_sq_plus_1_right is not None:
    error_right = (t0_chi_sq_plus_1_right - t0_at_min_chi_sq_per_dof) * log(2) * 0.2
else:
    error_right = np.nan

# Plot chi-square per degree of freedom vs. t0 while keeping other parameters constant
plt.figure(figsize=(8, 6))
plt.plot(t0_range, chi_sq_per_dof_values_t0, marker='o', linestyle='--')
plt.xlabel('t0')
plt.ylabel('Chi-square per Degree of Freedom')
plt.title(
    '(For $15T_{1/2}$ interval) Chi-square per Degree of Freedom vs. t0 (Keeping Other fitted Parameters'
)
plt.grid(True)

# Plot the minimum chi-square per degree of freedom point
plt.axhline(min_chi_sq_per_dof, color='red', linestyle='--',
            label=f'Minimum Chi-square per Degree of Freedom: {min_chi_sq_per_dof:.2f}')
plt.axvline(t0_at_min_chi_sq_per_dof, color='green', linestyle='--',
            label=f't0 at Min Chi-square per Degree of Freedom: {t0_at_min_chi_sq_per_dof:.2f}')

if t0_chi_sq_plus_1_left is not None:
    plt.axvline(t0_chi_sq_plus_1_left, color='orange', linestyle='--',
                label=f't0 where Chi-square = Min Chi-square per Degree of Freedom + 1 (Left): {t0_chi_sq_plus_1_left:.2f}')
if t0_chi_sq_plus_1_right is not None:
    plt.axvline(t0_chi_sq_plus_1_right, color='purple', linestyle='--',
                label=f't0 where Chi-square = Min Chi-square per Degree of Freedom + 1 (Right): {t0_chi_sq_plus_1_right:.2f}')

plt.legend()

# Plot half-life and its error
plt.text(0.95, 0.65, f'Half-life: {half_life:.2f} {error_left:.2f} (Left), {error_right:.2f} (Right)',
         transform=plt.gca().transAxes, ha='right', va='center', color='black', fontsize=10)

plt.show()

# Print the results
print(f"Minimum Chi-square per Degree of Freedom: {min_chi_sq_per_dof}")
print(f"Fitted Parameters at Minimum Chi-square per Degree of Freedom: {optimal_params}")
print(f"t0 (Half-life) at Minimum Chi-square per Degree of Freedom: {t0_at_min_chi_sq_per_dof}")
print(f"Half-life: {half_life}")
print(f"Error in Half-life (Left): {error_left}")
print(f"Error in Half-life (Right): {error_right}")

```

A.8 Code to plot Chi-square per DoF vs t0 for exponential fit only

```

import numpy as np
import matplotlib.pyplot as plt
from scipy.optimize import minimize
from math import log

# Define the function to fit
def my_function(params, x):
    y0, A, t0 = params
    return y0 + A * np.exp(-x / t0)

# Define the chi-square function
def chi_square(params, x, y_data, errors):
    y_fit = my_function(params, x)
    chi_sq = np.sum(((y_fit - y_data) / errors)**2)
    return chi_sq

```

```

# Numerical approximation of the Hessian matrix
def numerical_hessian(func, params, args, epsilon=1e-5):
    hessian_matrix = np.zeros((len(params), len(params)))
    for i in range(len(params)):
        for j in range(len(params)):
            params_plus_plus = np.copy(params)
            params_plus_plus[i] += epsilon
            params_plus_plus[j] += epsilon
            chi_plus_plus = func(params_plus_plus, *args)

            params_minus_plus = np.copy(params)
            params_minus_plus[i] -= epsilon
            params_minus_plus[j] += epsilon
            chi_minus_plus = func(params_minus_plus, *args)

            params_minus_minus = np.copy(params)
            params_minus_minus[i] -= epsilon
            params_minus_minus[j] -= epsilon
            chi_minus_minus = func(params_minus_minus, *args)

            params_minus_minus[j] += 2 * epsilon

            hessian_matrix[i, j] = (chi_plus_plus - chi_minus_plus - chi_minus_minus + func(params_minus_minus)) / (4 * epsilon)

    return hessian_matrix

# Load data from the file
data = np.loadtxt('td_spectrum.txt') # Replace 'your_data_file.txt' with your actual data file

# Initial guess for parameters
initial_params = [-2.69, 1.0e22, 40.0]

# Iterate through the intervals and calculate half-lives
intervals = [(2005, 2005 + 30*(i+1)) for i in range(7)]
half_lives = []
errors_left = []
errors_right = []

for i, (start, end) in enumerate(intervals):
    x_data = data[start:end, 0]
    y_data = data[start:end, 1]
    errors = data[start:end, 2]

    # Perform chi-square minimization using the minimize function
    result = minimize(chi_square, initial_params, args=(x_data, y_data, errors), method='L-BFGS-B')

    # Extract the optimized parameters
    y0_opt, A_opt, t0_opt = result.x

    # Compute the Hessian matrix numerically
    hessian_matrix = numerical_hessian(chi_square, result.x, args=(x_data, y_data, errors))

    # Check if the Hessian matrix is invertible
    try:
        covariance_matrix = np.linalg.inv(hessian_matrix)
        errors_params = np.sqrt(np.diag(covariance_matrix))
    except np.linalg.LinAlgError:
        errors_params = np.full(len(initial_params), np.nan)

    # Calculate chi-square per degree of freedom for different t0 values while keeping other parameters
    t0_range = np.linspace(t0_opt - 10, t0_opt + 10, 100)
    chi_sq_per_dof_values_t0 = np.zeros_like(t0_range)
    for k, t0 in enumerate(t0_range):
        params = [y0_opt, A_opt, t0]
        chi_sq_per_dof_values_t0[k] = chi_square(params, x_data, y_data, errors) / (len(x_data) - len(params))

    # Find the minimum chi-square per degree of freedom and corresponding t0
    min_chi_sq_per_dof = np.min(chi_sq_per_dof_values_t0)
    min_chi_sq_per_dof_index = np.argmin(chi_sq_per_dof_values_t0)
    t0_at_min_chi_sq_per_dof = t0_range[min_chi_sq_per_dof_index]

```

```

# Find t0 values on both sides of the minimum where chi-square per degree of freedom equals chi-square per dof
t0_chi_sq_plus_1_left = None
t0_chi_sq_plus_1_right = None
for j in range(min_chi_sq_per_dof_index - 1, -1, -1):
    if chi_sq_per_dof_values_t0[j] >= min_chi_sq_per_dof + 1:
        t0_chi_sq_plus_1_left = t0_range[j]
        break

for j in range(min_chi_sq_per_dof_index + 1, len(t0_range)):
    if chi_sq_per_dof_values_t0[j] >= min_chi_sq_per_dof + 1:
        t0_chi_sq_plus_1_right = t0_range[j]
        break

# Calculate half-life and its error
half_life = t0_at_min_chi_sq_per_dof * log(2) * 0.2
error_left = (t0_at_min_chi_sq_per_dof - t0_chi_sq_plus_1_left) * log(2) * 0.2 if t0_chi_sq_plus_1_left is not None else 0
error_right = (t0_chi_sq_plus_1_right - t0_at_min_chi_sq_per_dof) * log(2) * 0.2 if t0_chi_sq_plus_1_right is not None else 0

half_lives.append(half_life)
errors_left.append(error_left)
errors_right.append(error_right)

# Plot chi-square per degree of freedom vs. t0 for the current interval
plt.plot(t0_range, chi_sq_per_dof_values_t0, label=f'For {i+1} T$_{{{1/2}}}$ interval, Half life = {half_life:.2f}/{error_left:.2f}/{error_right:.2f}')
# plt.annotate(f'{half_life:.2f} +/- {error_left:.2f}/{error_right:.2f}', xy=(t0_at_min_chi_sq_per_dof, min_chi_sq_per_dof),
#             xytext=(t0_at_min_chi_sq_per_dof, min_chi_sq_per_dof + 1.5 + 0.5 * i),
#             arrowprops=dict(facecolor='black', arrowstyle='->'),
#             fontsize=8, ha='center')

# Customize and save the final plot
plt.xlabel('t0')
plt.ylabel('Chi-square per Degree of Freedom')
plt.title('Chi-square per Degree of Freedom vs. t0 for Multiple Intervals')
plt.legend()
plt.grid(True)
plt.savefig('chi_sq_multiple_intervals.pdf', format='pdf')
plt.show()

# Print half-lives and their errors for each interval
for i, (half_life, error_left, error_right) in enumerate(zip(half_lives, errors_left, errors_right)):
    print(f"Interval {intervals[i][0]}-{intervals[i][1]}: Half-life = {half_life:.2f} {error_left:.2f} (Left), {error_right:.2f} (Right)")

```